MECHANICAL AND BIOCOMPATIBILITY ANALYSES OF METABIOMATERIALS COBALT CHROME MOLYBDENUM MANUFACTURED BY SELECTIVE LASER MELTING FOR LOAD BEARING IMPLANT

SITI ROHAIDA BINTI MOHAMED

Master of Science

UNIVERSITI MALAYSIA PAHANG

UNIVERSITI MALAYSIA PAHANG

DECLARATION OF THESIS AND COPYRIGHT

Author's Full Name : SITI ROHAIDA BINTI MOHAMED

Date of Birth : 06 MARCH 1988

Title : MECHANICAL AND BIOCOMPATIBILITY ANALYSES OF METABIOMATERIALS COBALT CHROME MOLYBDENUM MANUFACTURED BY SELECTIVE LASER MELTING FOR LOAD BEARING IMPLANT

Academic Session : 2017/2018

I declare that this thesis is classified as:

☐	CONFIDENTIAL	(Contains confidential information under the Official Secret Act 1997)*
☐	RESTRICTED	(Contains restricted information as specified by the organization where research was done)*
☑	OPEN ACCESS	I agree that my thesis to be published as online open access (Full Text)

I acknowledge that Universiti Malaysia Pahang reserve the right as follows:

1. The Thesis is the Property of Universiti Malaysia Pahang
2. The Library of Universiti Malaysia Pahang has the right to make copies for the purpose of research only.
3. The Library has the right to make copies of the thesis for academic exchange.

Certified by:

_____ (Student's Signature)

SITI ROHAIDA BINTI MOHAMED
New IC Number: 880306-29-5090
Date:

_____ (Supervisor's Signature)

DR. SAIFUL ANWAR BIN CHE GHANI
Name of Supervisor
Date:

NOTE : * If the thesis is CONFIDENTIAL or RESTRICTED, please attach a thesis declaration letter.

SUPERVISOR'S DECLARATION

We hereby declare that we have checked this thesis and in our opinion, this thesis is adequate in terms of scope and quality for the award of the degree of Master of Science in Mechanical Engineering.

_____

(Supervisor's Signature)

Full Name : DR. SAIFUL ANWAR BIN CHE GHANI

Position : SENIOR LECTURER

Date :

_____

(Co-supervisor's Signature)

Full Name : DR. WAN SHARUZI BIN WAN HARUN

Position : SENIOR LECTURER

Date :

STUDENT'S DECLARATION

I hereby declare that the work in this thesis is based on my original work except for quotations and citations which have been duly acknowledged. I also declare that it has not been previously or concurrently submitted for any other degree at Universiti Malaysia Pahang or any other institutions.

_____

(Student's Signature)

Full Name : SITI ROHAIDA BINTI MOHAMED

ID Number : MMM14042

Date :

MECHANICAL AND BIOCOMPATIBILITY ANALYSES OF METABIOMATERIALS COBALT CHROME MOLYBDENUM MANUFACTURED BY SELECTIVE LASER MELTING FOR LOAD BEARING IMPLANT

SITI ROHAIDA BINTI MOHAMED

Thesis submitted in fulfillment of the requirements
for the award of the degree of
Master of Science

Faculty of Mechanical Engineering
UNIVERSITI MALAYSIA PAHANG

SEPTEMBER 2017

ACKNOWLEDGEMENTS

Firstly, I would like to express my special gratitude to my main supervisor, Dr. Saiful Anwar bin Che Ghani and my co-supervisor, Dr. Wan Sharuzi bin Wan Harun for their supervision, valuable advice, guidance, support and motivation that they offered throughout the journey of this research study. Their encouragement and expertise in additive manufacturing for orthopaedic application was the key and essential upon successful completion of this dissertation.

Truly thanks for all my team members and colleagues of GramsLab (Green Research for Advance Materials Laboratory) for moral supports and helps. Special thanks to Contraves Advanced Devices Sdn Bhd for the critical discussion during the fabrication of metabiomaterials and also Dr. Munirah binti Sha'ban and her team at Tissue Engineering Lab, Biomedical Department International Islamic University Malaysia for the preparation and biocompatibility testing that were crucial upon compliment of this research.

Lastly, I would like to acknowledge and thanks to all my family members especially my parents, Mohamed bin Yaacob and Nazirah binti Mahasan and my sister siblings for their encouragement, deepest love, emotional support and believing me throughout the years of my study for this award.

Thank you all.

ABSTRAK

Kobalt krom molibdenum (Co-Cr-Mo) telah digunakan secara rutin dalam implan bebanan galas kerana kekuatan bahan dan daya pakai yang sangat baik, rintangan terhadap kehausan dan kakisan. Walaubagaimanapun, implan Co-Cr-Mo mempunyai kekakuan (220 GPa) yang tinggi berbanding sifat tulang (1-30 GPa). Perbezaan kekakuan ini menyebabkan bebanan tegasan dipindahkan melalui implant, dikenali sebagai fenomena *stress shielding* di mana penyebab utama untuk pembedahan gantian. Walaupun pembuatan berdaya tambah mempunyai kelebihan dalam menghasilkan bahagian berbentuk rumit, kualiti produk hasilan seperti kemasan permukaan, kejituan, ketumpatan, sifat mekanik dan taraf keserasian biologi adalah masih terhad. Justeru, kajian ini membentangkan rekabentuk metabiobahan dengan sifat geometri yang dikawal untuk menyesuaikan kekakuan dan menyediakan ruang untuk tindakbalas biologi yang dibuat daripada serbuk Co-Cr-Mo dengan teknik laser lebur terpilih (SLM), salah satu teknik pembuatan berdaya tambah. Unit sel metabiobahan dinamakan *square* dan *diamond* dengan panjang unit sel, L_{cell} dipelbagaikan dari ukuran 1.5 mm sehingga 2.5 mm, saiz topang, Φs dari 0.4 mm sehingga 0.6 mm yang dijana oleh perisian SolidWorks dan difabrikasi oleh proses SLM dengan menggunakan parameter tetap. Ketumpatan relatif dan ketepatan dimensi diukur manakala keadaan permukaan dan kebolehhasilan dinilai secara pemerhatian mikroskopik. Keberkesanan metabiobahan terhadap sifat mekanikal dan keserasian biologi ditentukan melalui ujian mampatan dengan bebanan 100 kN dan kajian cerapan MTT dimana sampel dikategorikan kepada dua kumpulan berdasarkan kaedah pensterilan sinaran gamma dan autoklaf. Sebagai hasilan, metabiobahan mempamerkan peratus keliangan dari 44.8 sehingga 88.1% dan saiz pori dari 0.9 sehingga 2.1 mm. Metabiobahan berketumpatan relatif yang tinggi di mana 84.7% hingga 97.7% peratus dan dipengaruhi oleh ketumpatan tenaga yang tinggi semasa proses pembuatan. Pemerhatian melalui permukaan optik mendedahkan zarah serbuk separa cair melekat pada teras topang manakala kebolehhasilan memenuhi ketepatan geometri dengan baik apabila dibandingkan dengan model asal. Fenomena *overhang* iaitu kecenderungan pembentukan lebihan berlaku pada kawasan yang tiada sokongan dengan toleransi kurang 1% dan pengecutan pada dimensi ciri ketinggian unit sel *square* diperhatikan. Sifat kekakuan metabiobahan adalah dalam lingkungan sifat tulang berliang (*cancellous*) di antara 0.45-8.75 GPa dan kekuatan mampatan antara 10.77-245.03 MPa. Dari kajian cerapan MTT, sampel SL25T04 dan DL25T04 (saiz pori 2.1 mm dan 1.7 mm) mencatat bacaan 0.6 dan 0.45 OD yang menunjukkan bilangan sel paling banyak melekat pada sampel. Dari kajian cerapan MTT telah menunjukkan bahawa sampel yang dihasilkan oleh SLM tidak berbahaya kepada sel. Hasilan dari kajian ini adalah penting untuk digunakan sebagai asas implan bebanan galas. Pertimbangan ke atas kajian lanjutan terhadap analisis keletihan, in vivo (dalam haiwan) keserasian biologi dan pelepasaan ion logam dan penilaian fizikal kerana proses parameter yang dipelbagaikan adalah dicadangkan.

ABSTRACT

Cobalt chrome molybdenum (Co-Cr-Mo) alloy has been routinely used in load bearing implants due to the biocompatibility, excellent strength and toughness, and high resistance to wear and corrosion. However, the implants possess high stiffness (220 GPa) compare to human bone (1-30 GPa). The difference in the stiffness caused stresses to be transferred predominantly through the implant, known as stress shielding phenomenon, where is the main reason for revision surgeries. Despite of advantages of additive manufacturing (AM) in producing complex shape parts, the quality of the produced components such as surface finish, accuracy, density, mechanical properties and biocompatibility status are scarce. Thus, this research study presents the designs of metabiomaterials with controlled geometrical for the possible way to tailor the stiffness and provide the space for biological response of implant part made by Co-Cr-Mo alloys powder manufactured through selective laser melting (SLM), one of the AM techniques. The metabiomaterials unit cell of square and diamond type with varied geometrical unit cell length, L_{cell} ranged from 1.5 mm to 2.5 mm and strut size, Φs ranged from 0.4 mm to 0.6 mm generated through SolidWorks software and then manufactured with default manufacturing process parameters. The relative density and dimensional accuracy tolerance were calculated while morphology and manufacturability were evaluated. The mechanical and biocompatibility properties are determined through compression test with load 100 kN and *in vitro* MTT assay where the samples are grouping into two groups based on sterilisation methods of gamma irradiation and autoclave techniques. As the results, the metabiomaterials exhibit porosity ranged from 44.8 to 88.1% and pore size range from 0.9 to 2.1 mm. The metabiomaterials resulted higher relative densities ranged from 84.7 to 97.7% influenced by higher energy density during manufacturing process. Morphology evaluation revealed partially melted powder bonded to the strut core while the manufacturability for metabiomaterials met a good geometrical agreement with original CAD models. The overhang phenomenon, as stresses tend to dross formation occurred at unsupported region with tolerance less 1% and the shrinkage on height feature dimension of the square unit cell was observed. The stiffness of metabiomaterials resulted in properties of cancellous (spongy) bone ranged from 0.45 to 8.75 GPa and the compression strength ranged from 10.77 to 245.03 MPa. From MTT absorbance assay, the samples SL25T04 and DL25T04 (pore size 2.1 mm and 1.7 mm) resulted the highest absorbancy of 0.6 and 0.45 OD which shown the highest cells viable in the samples. MTT assay demonstrated that components produced by SLM are not harmful to the cells and no proof to cells death. The outputs from this research are significant to be used as the groundwork for further development of metabiomaterials Co-Cr-Mo produced by SLM for load bearing implants. Consideration on further study on fatigue analysis, biocompatibility *in vivo* (in animal), amount of metal-ion released and physical evaluation on varied manufacturing process parameters are suggested for future works.

TABLE OF CONTENT

LIST OF TABLES

LIST OF FIGURES

LIST OF SYMBOLS

C	Constant
E	Elastic modulus
E_s	Elastic modulus of solid material
E^*	Elastic modulus of cellular structure
E_{eff}	Effective stiffness
L_{cell}	Unit cell length
n	Number of test replication
$P0$	Primary passage
$P1$	Passage 1
Ti	Titanium
V_P	Volume porous
V_B	Volume bulk
V_S	Volume obtained from SolidWork
w	Weight
Φ_P	Pore size
Φ_S	Strut size
φ	Porosity
ρ	Density
ρ^*	Density of cellular structure
ρ_s	Density of solid material

LIST OF ABBREVIATIONS

AM	Additive manufacturing
AMRIC	Additive Manufacturing Research and Innovation Centre
ASTM	American Society for Testing and Materials
CAD	Computer aided design
CO_2	Carbon dioxide
Co-Cr	Cobalt chrome
Co-Cr-Mo	Cobalt chrome molybdenum
CVD	Chemical vapour deposition
DC	Direct current
DMEM	Dulbecco's Modified Eagle Medium
DMLS	Direct metal laser sintering
DMSO	Dimethylsulfoxide
DNA	Deoxyribonucleic acid
EBM	Electron beam melting
EDC	Electrical discharge compaction
EDM	Electrical discharge machining
EDX	Energy dispersive X-ray
EOS	Electro Optical System
FBS	Foetal bovine serum
FDM	Fused deposition modelling
HRC	Rockwell C-scale hardness
HV	Vickers hardness
IIUM	International Islamic University Malaysia
KKTM	Kolej Komuniti Tinggi Mara
LDH	Lactate dehydrogenase
LENS	Laser engineered net shaping
M-O-M	Metal-on-metal
M-O-P	Metal-on-polymer
MTT	3-(4,5-dimethylthiazol-2-yl)-2,5-diphenyltetrazolium bromide
NaCl	Sodium chloride
Nd:YAG	Neodymium-doped yttrium aluminium garnet
OOWD	Orderly oriented wire mesh deposition
PAS	Plasma activated sintering
PBS	Phosphate buffered saline

SEM	Scanning electron microscopy
SLA	Stereo-lithography
SLM	Selective laser melting
SLS	Selective laser sintering
SPS	Spark plasma sintering
STL	Standard triangulation language
THA	Total hip arthroplasty
THR	Total hip replacement
Ti-6Al-4V	Titanium 6% aluminium 4% vanadium
TJR	Total joint replacement
TKR	Total knee replacement
USA	United State of America
WST	Water soluble tetrazolium

CHAPTER 1

INTRODUCTION

1.1 Research Background

Over the past century, bone-joint defects and musculoskeletal disorder diseases such as osteoporosis (weakening of the bones), osteoarthritis (inflammation in the bone joints) and trauma from accidents hindered the lower limbs to support the body weight and affect the human mobility (Calmar et al., 2002; Murnaghan et al., 2010; Salih et al., 2013). The use of medical implants and the field of arthroplasty particularly in bone joint have become popular among medical surgeons extended from the past decades, owing to increased human life expectancy, changing lifestyle and advanced implant technology. In orthopaedic, metallic implants are used in a broad range of applications including reconstructive implants, fracture fixation devices, spinal disk, and joint replacement. One of the main achievements in the field of arthroplasty is development of total joint replacement (TJR) such as for hip and knee joint replacements known as load bearing implants. Diseased bone-joint parts are replaced surgically by load bearing implants for restoring mobility, reducing pain, and improving the quality and longevity of patients (Gossec et al., 2011; Lappalainen et al., 2014; Street et al., 2017).

TJR have been found to be of critical importance in young patients' surgeries, where the demands and revision surgeries are expected to increase up by 17 times, from 59,077 in 2006 to 999,104 procedures at the end of 2030 for total knee replacements. Meanwhile, total hip replacements are anticipated to grow by 5.9 times from 35, 380 to 208, 760 procedures (Kurtz et al., 2009). Despite the large number of existing orthopaedic medical devices and applications, there are only a few biomaterials dominating the medical market (Hallab et al., 2013). Metallic biomaterials have played a predominant role as materials in reconstructive surgery primarily for load bearing implants due to their satisfactorily mechanical strength and toughness compared to

other biomaterials such as polymers and ceramics (Planell et al., 2009). Cobalt chrome molybdenum (Co-Cr-Mo) alloys, 316L stainless steel and titanium (Ti) alloys are the most used metallic biomaterials in load bearing implants. The metallic biomaterials exhibit high stiffness (Co-Cr-Mo 220 GPa, 316L stainless steel 210 GPa, Ti 110 GPa) (Q. Chen et al., 2015) compared to human bone properties (1-30 GPa) (R. Fuchs et al., 2009) that caused stress shielding phenomenon and poor osseointegration (biological integration between implant and bone tissue). The mismatch stiffness between implants and bones leads to implant failure, where the main reason for revision surgeries.

Thus, the restricted life span and biocompatibility of total joint prostheses are becoming an increasing concern for medical community for younger and active patients nowadays. The other factors of revision surgeries in load bearing implant besides of high stiffness of biomaterials (Mitsuo Niinomi, 2008) are unsuitable design for integration between implant and human bone (Hayes et al., 2014), toxicity of biomaterials leading to adverse reaction (Denkhaus et al., 2002), poorness of surface functionality, wear and corrosion in human body environment (Adebiyi et al., 2015; Antunes et al., 2012) Recently, cementless total hip replacement (THR) is widely used in younger and active patients, where the cup of THR is manufactured with tailored surface to induce the bone ingrowth for stability fixation within the implant and the human bone (Gutierres et al., 2008; Hanzlik et al., 2013; Kienapfel et al., 1999).

Orthopaedic implants demand the high performance and advance biomaterials with the final outcomes of patient's requirement to be fulfilled. Consequently, the application of additive manufacturing (AM) technology has become popular in producing complex-shaped components, which can mimic human bone properties that are known as metabiomaterials. Metabiomaterials might be a possible way to match the stiffness and availability of biological response for implants with longer life span and can reduce revision surgeries. AM process is based on laser and electron melting that produces part direct from computer-generated model from powder to solid parts (X. Ren et al., 2016). The reliability of AM seems beneficial in producing medical component with tailoring mechanical properties and chances of biological response between implant and human bone (Jardini et al., 2017; Munsch, 2017). Thus, the manufacturing process and the produced components made by AM should possess the *better-quality* outcomes such as physical, mechanical and biological properties status.

The manufacturing technology produces load bearing implants with tailoring mechanical properties that match human bone properties and provide space for biological integration by introducing periodic cellular structure into the implant components that can mimic the bone features.

In the new era of orthopaedic industry, venturing into the developments of load bearing implants has motivated considerable number of studies on the interaction of cellular structures between mechanical properties and biological fixation to yield long-term durability of the orthopaedic implant. The interconnected cellular structure also provides space and channels for new tissue to ingrowth from surface into the interior of the implants (Chang et al., 1996; Goriainov et al., 2014; Tang et al., 2015). Hence, the biological interaction and fixation between bone tissues and the implants can be strengthened for better outcomes after implantations. Recently, researchers have shown an increased interest in employing latest manufacturing technologies to produce potential cellular structure for porous implant devices. As a result of the reliability of manufacturing process, a new class of materials is developed known as metabiomaterials (Amin Yavari et al., 2015; Méjica et al., 2013).

Metamaterials are a group of engineered components which are generally made of periodically repeated metallic patterns (X. Xia et al., 2007) in all directions (x, y and z) or non-periodic structure. They exhibited properties that are not yet found in nature and in the constituent materials (Sihvola, 2007). The behaviours and properties of metamaterials are not derived from the compositional materials properties but from their rationally designed structures, where the precise shape, geometry, pore size, orientation and arrangement of unit cell can affect the homogenous manner of metamaterials (Shamonina et al., 2007). In the past decades, metamaterials are mostly found in diversity of electromagnetic microwave (Acher, 2009; Starodubtsev, 2010), radio communication (Kante et al., 2008), optical (S. He et al., 2009) and photonic applications (Lourtioz, 2008) with properties of negative permeability and permittivity, also negative refractive index optical frequency. Recently, metamaterials have been studied in bone tissue regenerative (Hedayati et al., 2017) and orthopaedic implant for sufficient mechanical strength (Kadkhodapour et al., 2016; Zadpoor, 2017) and fatigue behaviours known as metabiomaterials (Amin Yavari et al., 2015; Speirs et al., 2017; Van Hooreweder et al., 2017).

Most orthopaedic implants require strict process techniques and controls to achieve tolerances, individualised anatomical design to imitate bone, and to provide sufficient biomechanical fixation. The metabiomaterials components cannot be fully controlled since the majority of existing production technologies do not allow for limitation for precise control of the shape, size and cellular pore distribution (Bechmann, 2014; Podshivalov et al., 2013). The requirements with complex shape and fully tiny details make the metabiomaterials difficult to manufacture using conventional process such as space holder and gas foaming methods (Brenne et al., 2013). From this scenario, modern industries are able to implement highly attractive additive manufacturing (AM) technologies for producing the complex three-dimensional structures (Emmelmann et al., 2011; Murr, 2015; Su et al., 2012).

AM technology is an extension of rapid prototyping that uses additive method, fundamentally layer-by-layer fabrication technique. This advance technology allows the production of components directly from the information that is obtained from a three-dimensional (3D) computer-aided design (CAD) system, and then the model is converted to standard triangulation language (STL) file. Further, the file will be generated and sliced to 2D contour line for physical production from bottom to top parts and imported to AM setup (Murr et al., 2012; Stampfl et al., 2014). Nowadays, AM technology empowers the quick production and cost saving of ready-to-use implants and component parts that are designed to customise individual patient's anatomy in areas of medical fields with optimum size, shape, and materials properties. AM technology has crucial benefits in the medical field since the reliability to manufacture complex geometry to fulfil patient-specific requirements with less cost and manufacturing time for a single production process compared to other conventional manufacturing processes (Frazier, 2014; Huang et al., 2013).

1.2 Problem Statement

Metallic biomaterials with superior combination of mechanical strength and toughness with excellent corrosion resistance such as 316L stainless steel, cobalt chrome based alloys and titanium alloys are routinely used as orthopaedic implants (Q. Chen et al., 2015). The tremendous demands in the worldwide cases have brought metallic implants to restoring the lost function and sustaining the mobility of the patients. However, the main problem of metallic implants is their high relative stiffness

compared to human bone properties, which may causes the stress shielding phenomenon that leads to revision surgeries (M. Niinomi et al., 2012; Yamako et al., 2014). Hence, the stiffness of biomaterials for metallic implants should be tailored by introducing porosity in the implants components (Abidi et al., 2015; Limmahakhun et al., 2017). In addition, the implants with the porous structure could provide space or accommodation for tissue regeneration and are helpful in biological fixation between the implants and host bone after implantation (Matassi et al., 2013; Sumner, 2015).

Geometrical properties of porous structure for load bearing implants are difficult to control when manufactured by conventional process (Heinl et al., 2008; Ryan et al., 2006). The latest technology, the AM has brought the reliability to produce the complex shape and highly controlled geometrical parameters in order to meet the homogeneity between material properties and behaviours known as metamaterials based on computer-aided design (CAD) (Jared et al., 2017; Vaezi et al., 2013; K. Wang et al., 2016). However, the key concept of metamaterials, particularly the optimum geometrical parameters that should meet the features for reducing stiffness and enhance the tissue regeneration, are difficult to determine since no attempt of specification from previous researchers has been made. Thus, the potential metamaterials for load bearing implants need to undergo an in-depth investigation including mathematical modelling and experimental testing.

Another problem of using metallic biomaterials is their metal toxicity (Anisimova et al., 2015; Hedberg et al., 2014; Y. Wang et al., 2017). The problem is exaggerated when aggressive body fluid environment dealing with foreign component after been implanted in the human body. The produced component by additive manufacturing technique must undergo the cytotoxicity test in order to confirm the biocompatibility and to determine that there is no adverse effect on human body. Therefore, the characterisation of fabricated samples for evaluating the stiffness, manufacturability, and biocompatibility is needed to be carried out for the metallic biomaterials, which can be further developed for use as load bearing implants.

1.3 Research Objectives

The aims of this research are to investigate the design parameters of metabiomaterials Co-Cr-Mo, namely the unit cell types, strut length for load bearing

implant manufactured using additive manufacturing process selective laser melting (SLM). The Co-Cr-Mo metabiomaterials should tailor the stiffness of mechanical properties to match those of human bone and biocompatible with the biological activities between the implants and human bone tissue. The main objectives of this research are as follows:

i. To design metabiomaterials with highly controlled unit cell geometries for matching elasticity of human bone and demonstrating biocompatibility.

ii. To assess the accuracy of additive manufactured metabiomaterials based on physical evaluations.

iii. To determine the elastic modulus and biocompatibility of produced metabiomaterials using standard mechanical and *in vitro* tests.

1.4 Research Scopes

This study consists of elements that are limited by following scopes; (1) material and design of metabiomaterials for load bearing application, (2) manufacturing process of the designed metabiomaterials by SLM and (3) experimental evaluation and characterising of the produced metabiomaterials. The detailed scopes are as follows:

i. Metabiomaterials are designed with varied geometrical parameters of unit cell type, unit cell length, L_{cell} and strut size, Φ_S to possess porosity that can match elastic modulus and biocompatibility by SolidWork software.

ii. Physical evaluation including density, accuracy and morphology will be evaluated for assessment accuracy of selective laser melting process performed with default parameters during fabrication.

iii. Mechanical compression and *in vitro* biocompatibility study using animal cells will be performed to evaluate and determine the mechanical elastic modulus, compression strength, and biological response of produced metabiomaterials by selective laser melting.

1.5 Thesis Outline

The thesis composed of five (5) chapters. Chapter 1 outlines the research background, problem statement, aims and research objectives, as well as research scopes. Chapter 2 comprises the literature review of the ideal considerations of biomaterials, design and manufacturing process of load bearing implants, challenges of producing metabiomaterials, the advantages of metabiomaterials for load bearing implants and suitable testing on metallic implants. Chapter 3 elaborates the methodologies of the research from designing and predicting the effective elastic modulus, material preparation, manufacturing process and post processing, experimental on physical evaluations, mechanical compression testing, and *in vitro* biocompatibility on produced metabiomaterials. Chapter 4 discusses the results obtained from the investigation of the effective elastic modulus and the experimental testing on density, dimensional accuracy, performance and manufacturability, compression elastic modulus, and *in vitro* biocompatibility. Finally, Chapter 5 presents the conclusions and recommendations for future works derived from the current study.

CHAPTER 2

LITERATURE REVIEW

2.1 General Introduction

This chapter presents a review of literature including designing metabiomaterials, manufacturing process considerations and characterisation towards the consideration of rationally designed geometrical parameters on mechanical properties and biocompatibility of produced metabiomaterials. Special attention is directed toward the essential consideration of successful load bearing implants including selected biomaterials, design and manufacturing process. For biomaterials selection, the ideal for load bearing implants should have sufficient mechanical strength and fracture toughness such as metallic biomaterials with excellent wear resistance in cyclic loading mechanism. This chapter explores the suitable metallic biomaterials for load bearing implants on the consideration of current designs for bearing resurfacing of load bearing implants. The designs of load bearing implants are investigated and compared with the conventional solid parts design with recent consideration of cellular structure to better serve as lightweight components and the chances of biological response toward the implants. The manufacturing process directly from the design parts of load bearing implants is discussed. The complex shape that suit patient-specific characterisation has motivated the employment of additive manufacturing since this technique is capable to produce components rapidly and efficiently down to microscales level. In this chapter, the effectiveness design towards the properties of metabiomaterials is explored for suitable characterisation by experimental work with consideration for both mechanical and biocompatibility properties. All the findings and topics, including the design of metabiomaterials, the challenges in manufacturing metabiomaterials, and the available testing on metallic implants, are presented in this chapter.

2.2 Ideal Consideration for Load Bearing Implants

The increased in human life expectancy and recent implant devices have been routinely performed on younger and active patients, which motivated the improvements in load bearing implants. Generally, the requirements of modern implants expected to be considered are divided into three groups as schematically represented in Figure 2.1.

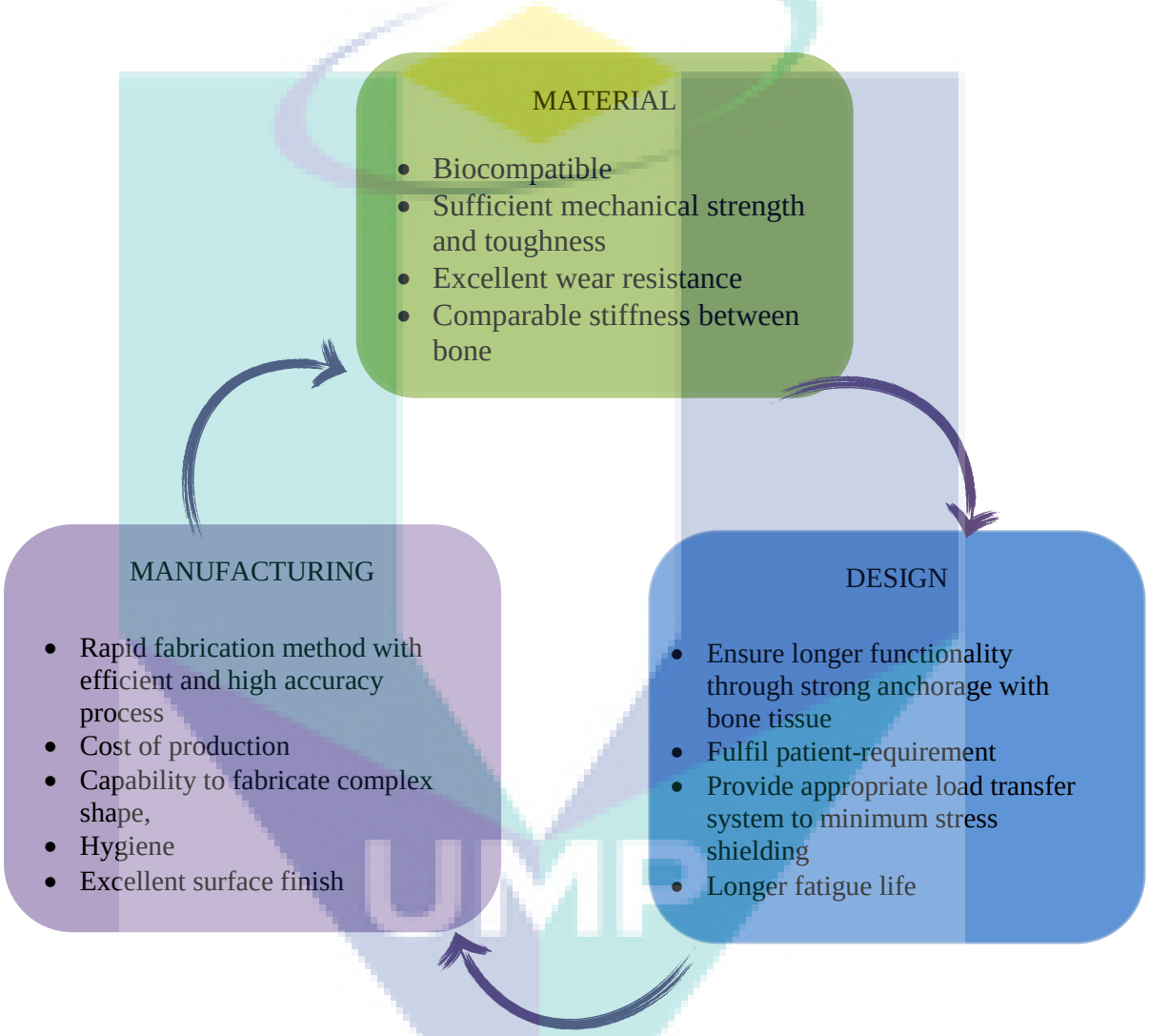

Figure 2.1 Essential considerations of successful load bearing implants

The ideal biomaterials for orthopaedic implant applications, especially for load bearing joint replacements, are expected to exhibit excellent biocompatibility with no adverse tissue reaction or short-term rejection (Elshahawy, 2011) and excellent corrosion (degradation) resistance (Geringer et al., 2014). In addition, excellent combination of mechanical properties of acceptable strength to sustain the cyclic

loading endured by the joint and bone (Tan et al., 2017), low elastic modulus to minimise bone resorption affected by stress-shielding effect (Tan et al., 2017), high fatigue resistance (de Krijger et al., 2017) are important to optimise the functionality and high wear resistance to minimise debris particle generation (Amaral et al., 2015).

The design for load bearing implant will be different depending on patients' applications. The goal in designing load bearing application is to enhance the good quality of implants. Agarwal et al. (2015) focused on components that were designed in order to approach closer geometrical shape to the natural human bone, higher mobility, and better outcomes after the implantation. In order to minimise the early failure resulting from aseptic loosening, M. Bahraminasab et al. (2013) found that material, design, and manufacturing process are the main factors that need to take into accounts in regards to load bearing implants requirement. It is crucial to design bearing surface of total joint replacement as close enough to articular cartilage, which is a smooth and glassy appearance thin layer of cartilage that covers the ends of long bones (N. Kumar et al., 2014). The significant to mimic the articular cartilage as the structures provides a low friction surfaces that is wear resistant and helps to distributes uniform loading response in load bearing joints (Lees et al., 2016).

Integration between biomaterials and design characteristics is crucial in the successful in producing of implants with longer lifespan. Since orthopaedic implants demand high performance of biomaterials with unique designs, the advanced manufacturing techniques need to be considered to produce a new level of their performance accuracy and functionality (Tigani et al., 2013). James (2005) noted in his studies that the performance of components and structures particularly under dynamic loading application are strongly influenced by the interaction between designs, materials, and manufacturing processes. Thus, fabrication technologies, which can ensure customised net-shape fabrication capability, sufficient mechanical strength and high level of biocompatibility are believes as significant importance for load bearing implants.

2.3 Biomaterials for Load Bearing Implants

The use of medical implants has expanded from past decades owing to the increased human life expectancy, changing lifestyles, and advanced progress in implant technology. The success of orthopaedic implants in restoring mobility, reducing pain, and improving the quality and longevity of life in patients is reflected in the worldwide development of biomaterials for orthopaedic applications. Biomaterials are defined as any materials that are designed for implantation and incorporate intimate contact with human or animal biological system in order to perform their intended function for a specific application without any harmful effects (Kulinets, 2015). Biomaterials can be classified either synthetic or natural. Figure 2.2 illustrates the definitions boundaries for biomaterials in medical application of implanted and non-implanted biomaterials. The biomaterials including metals, polymers, ceramics, and composites are in synthetic implanted biomedical materials.

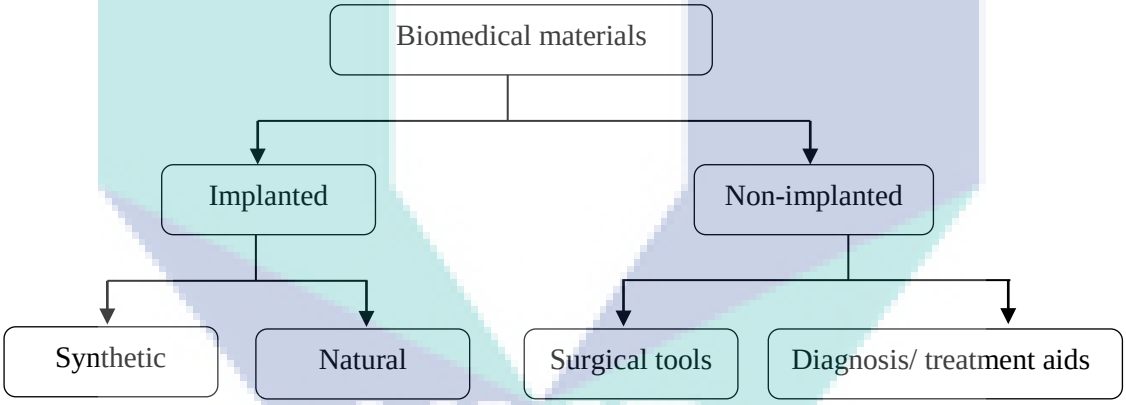

Figure 2.2 Definition of biomaterials in medical application

Source: Q. Chen et al. (2015)

Katti (2004) stated that the two important considerations of bone-joint substitution are mechanical properties and biocompatibility of the used biomaterials. In this case, the mechanical properties refer to sufficient strength with excellent fatigue resistance to support the load during human movement. Black (2005) reported that in hip joint, the average load is estimated to be up three times of the body weight, while the peak load during other vigorous activities, such as jumping, can be ten times of body weight. In addition, hip joint bones are subjected to cyclic loading including walking and running as 10^6 cycles per year. Thus, a favourable combination of strength,

fracture toughness, and fatigue strength warrants the applications of selected biomaterials in orthopaedic such as artificial bone joints, orthodontics and dentistry, cardiovascular and neurosurgical devices (Ivanova et al., 2014a). The biocompatibilities properties refer to the biomaterials with no adverse tissue reaction in body system reaction such as toxicity and carcinogenic (J. B. Park et al., 2002).

Ceramic are one of the biomaterials possess good biocompatibility and are utilised in joint replacement as bearing surfaces (Affatato et al., 2015) due to their hardness that improves wear resistance. Ceramic are suitable to use as coating to improve bone tissue bonding (McEntire et al., 2015) related to exhibit similar structure with bone mineral. Ceramics have been reported to form the oxide ceramics layer when reacted with oxygen act as a coating film. Therefore, wear debris generated by bearing surfaces that induced the osteolysis and lead to implant failure and adverse tissue reactions can be minimised (Kaivosoja et al., 2013). However, the ceramic biomaterials are inherently brittle and difficult to fabricate considering recent improvements of patient specifics in prosthesis design (Kluess et al., 2010). In addition, the ceramic biomaterials have been determined to exhibit low bending strength. The brittleness tends to limit the applications of ceramic biomaterials to the implants that are subjected to predominantly compressive load in nature and as coating on the implant parts (Jin et al., 2016).

On another note, polymer materials have a number of advantages. They are cost-efficient, easy to use, and have good biocompatibility (Milosevic, 2016; Shi et al., 2015). Like ceramic, polymer materials cannot stand the force in cyclic loading mechanism such as load bearing implants. In the load bearing surfaces, the debris generated from the polymer have been reported to attack the immune system of human body and lead to osteolysis or bone loss (Bozic et al., 2005; Diomidis, 2013). The custom of polymer materials in permanent load bearing implants is limited due to their inadequate mechanical properties and degradation properties (Gohil et al., 2017). However, due to the degradation properties, the polymer materials have been extensively used in tissue engineering for bone scaffold (K. M. Kennedy et al., 2017; Maksimkin et al., 2017). The types of commonly used biomaterials in orthopaedic application are summarized in Table 2.1.

Table 2.1 Types of biomaterials in orthopaedic application

Materials	Mechanical properties	Biological categories
Bone	Lightweight, strong, low modulus	Bioceramic
Metallic	Strong, tough, easily formed into complex shape	Bioinert, biocompatible
Ceramic	Not resilient, brittle, difficult to fabricate	Bioactive, inert
Polymer	Resilient, easily fabricated, deform and degrade with time	Biodegradable, biocompatible

Source: Philip (2008)

For load bearing application, the satisfactory strong and tough biomaterials are suitable for implants and must be able to provide sufficient mechanical performance related to stiffness (Nakano, 2010; Narushima, 2010). Metallic biomaterials with excellent corrosion resistance, sufficient strength and toughness, such as 316L stainless steel, cobalt chrome-based alloys and titanium-based alloys, are routinely used in load bearing applications (Hermawan et al., 2011; Nasab et al., 2010). A summary of mechanical properties of these commonly used metallic biomaterials in load bearing implants is presented in Table 2.2.

Table 2.2 Mechanical properties of commonly used metallic biomaterials and human bone

Biomaterials	Young's Modulus (GPa)	Ultimate strength (MPa)	Toughness (MPa)
Co-Cr based alloys	240	900-1540	100
316L stainless steel	200	450-1000	100
Ti based alloys	105-125	900	80
Human bone	1-30	130-150	2-12

Source: Q. Chen et al. (2015) and Katti (2004)

It is important to mention that all these three metallic biomaterials have shown higher elasticity when compared to human bone properties. The mismatch modulus causes the stress shielding effect particularly around the implant site, where further revision surgery is crucially required. The advantages and disadvantages of commonly used metallic biomaterials are then summarized in Table 2.3.

Table 2.3 Characteristics of commonly used metallic biomaterials in orthopaedic application

	316L Stainless steel	Cobalt based alloys	Titanium based alloys
Advantages	Low cost, availability of processing	Excellent wear resistance, corrosion resistance and fatigue strength	Biocompatibility, lightweight, excellent corrosion resistance
Disadvantages	High modulus, pitting corrosion under high stress loading, Ni and Cr allergy	High modulus, difficult to machine, Ni and Cr allergy	Poor wear resistance, low shear strength, Expensive
Primary utilisation	Temporary devices (bone plate, screws), THR stem (with Nitrogen added)	Dental implants, THR and TKR components	Permanent bone fracture devices (plate and screws), stunts

Source: Long et al. (1998)

The used of 316L stainless steel drove the evolution of modern orthopaedic devices in the past century. However, reports of failure of the 316L stainless steel devices revealed aseptic loosening emerged due to poor resistance to fatigue and corrosion (Chen et al., 2015). In addition, 316L stainless steels have long-term issues including poor wear resistance, as well as carcinogenicity and toxicity of released nickel and chromium under high stress condition (Asri et al., 2017; Manam et al., 2017). Nowadays, 316L stainless steel are rarely used in permanent orthopaedic devices and been replaced by superior corrosion and fatigue resistant alloys such as Co-Cr based alloys and Ti based alloys.

Cr-Co based alloys are superior in corrosion resistance demonstrating excellent performance in a chloride-rich environment related to their chemical properties. ASTM F75 Co-Cr-Mo alloys are commonly used in load bearing application due to their superior wear resistance (Guo et al., 2015). The superior wear resistance of Co-Cr-Mo compared to the other metallic biomaterials such as 316L stainless steel and Ti based alloys is attributed to the fine and uniform carbide structure resulting the excellent mechanical properties and tribological properties (Liao et al., 2013). In addition, superior fatigue resistant of Co-Cr based alloys becomes an ideal choice of materials for TJR. However, there are issues associated with Co-Cr based alloy including high stiffness and concerns about metal toxicity of element released such as nickel, chromium and cobalt (Ivanova et al., 2014b).

Though titanium and its alloys possess several favourable characteristics, such as low elasticity and excellent biocompatibility, the superior corrosion resistance and biocompatibility of titanium alloys arise from the presence of passive oxide layer known as titanium oxide (TiO_2) (Mouthuy et al., 2016; Ye et al., 2014). However, the titanium and its alloys are limited in articulating surface application due to poor tribological properties (Budinski, 1991; Long et al., 1998). The poor tribological property is due to their low resistance to plastic shearing and low protection induced by surface oxides (D. He et al., 2015; Hua et al., 2017). Thus, Co-Cr based alloys displays a better performance as selected biomaterials for articulating system in load bearing implant.

2.4 Design of Load Bearing Implants

Orthopaedic implants are routinely used for fixation of long bone fractures, correction and stabilisations of spinal bone fracture and deformities, arthritic joints replacement, dental restoration, and maxillofacial application (Goodman et al., 2013). The estimate purpose of the implant devices is to provide mechanical stabilisations, so that optimal and homogenous alignment and functionality of bone can be restored during physiologic loading such as walking, running, and eating between implants and bones or joints. As a result, the implant devices facilitate the relief of pain, maintain functionality and mobility as normal used for the injured or damage limb or other body parts (Kulinets, 2015). Table 2.4 shows the orthopaedic implants in various types of load bearing applications.

Table 2.4 Classification of orthopaedic implant for load bearing application

Category	Devices example	References
Fracture fixation	Clamps, braces, wire, pins and fixator rods) Cannulated bone screw, intramedullary nails rods, wires, screws and plates)	(Taljanovic et al., 2003)
Joint replacement	Hip arthroplasty, knee arthroplasty, spine arthroplasty, shoulder arthroplasty, elbow arthroplasty, wrist arthroplasty, ankle arthroplasty and finger arthroplasty	(Hallab et al., 2013; Murray, 2006)
Dynamic stabilisation	Spinal lumbar disk	(Molinari, 2007)
Dental restoration	Root screw, crown bridge	(Figliuzzi et al., 2012)
Contouring implant	Reconstruction plates, pelvic plates, mandibular plates, craniofacial mesh plates, and spinal rods.	(Disegi, 2000; Nakayama et al., 2004)

The most significant development in orthopaedic implants is in total hip replacement surgery, where both acetabular and femoral bearing surfaces are replaced with artificial materials such as metal, ceramic, and polymer, when the first standard concept of low friction arthroplasty was introduced by Sir John Charnley in 1958 using metal on high density polyethylene as bearing surface (Blunn, 2013; Charnley, 1961). Currently, total hip replacement consists of metal-head and metal-socket known as metal-on-metal (M-O-M) load bearing implant. This model type is expected as one of the next generation load bearing implants after conventional metal-on-polymer (M-O-P) type load bearing (F. E. Kennedy, 2013; Pezzotti et al., 2014). Figure 2.3 shows the variety of bearing surfaces for THA for metal-on-metal, ceramic-on-ceramic, and metal-on-polymer types.

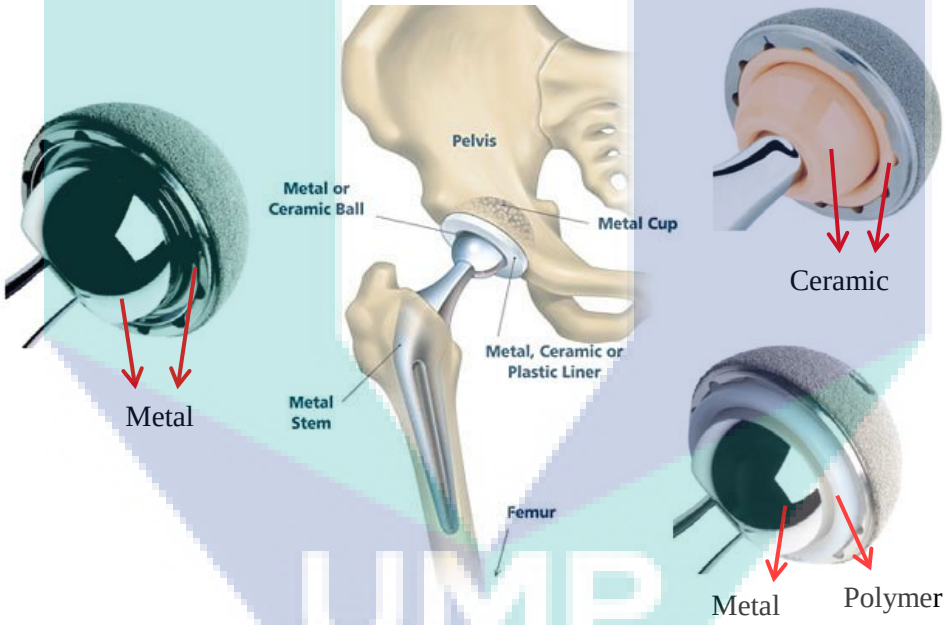

Figure 2.3 Variation of bearing type in total hip replacement which is metal-on-metal, ceramic-on-ceramic and metal-on-polymer

Despite a number of excellent results of M-O-P load bearing implant, the release element or debris due to wear and corrosion leading to periprosthetic osteolysis and aseptic loosening of local tissues become the great concern in THR outcomes (K. Ren et al., 2013). The main concern regarding failure of THA has been the biological response to particulate polyethylene debris generated at bearing surfaces. An improvement in total hip arthroplasty (THA) materials, design, and implant fixation has led to the development of better wear resistance bearing surfaces, which involves the

application of hard-on-hard bearing surfaces, such as M-O-M and ceramic-on-ceramic. These bearing surfaces were developed to provide advantages in improvement of implant tribology (lubrication, friction and wear), implant longevity, and reduced dislocation rate primarily in younger and active patients (Hosseinzadeh et al., 2012; Kamath et al., 2013; Sonntag et al., 2012).

Table 2.5 summarises the advantages and disadvantages of each type of bearing surfaces for THA. From the table, the meta-on-metal bearing surfaces are superior compared to other bearing surfaces due to better wear resistance. However, the bearing surfaces are having disadvantages for metal toxicity issue.

Table 2.5 Advantages and disadvantages of bearing surface types for THA

Bearing surface	Advantages	Disadvantages
Metal-on-polyethylene	Cost effective, predictable lifespan	Wear debris leading to aseptic loosening
Metal-on-metal	Low wear, dislocation resistance, larger femoral head, increase stability and larger range of movement	Metallosis, carcinogenic risk and metal sensitivity
Ceramic-on-ceramic	Low friction, low wear and no metal ion release	Easy to fracture under high impact loading, design limitation (thick femoral head result in high risk of dislocation), poor surface quality due to brittleness

Source: Cuckler (2006), Kim et al. (2008) and Lappalainen et al. (2014)

2.4.1 Solid Parts

More than half a century, metallic biomaterials have been used as orthopaedic implant biomaterials. Most metallic implants in clinical practice are fully dense and exhibit higher stiffness of the implants than human host bone. This situation can easily cause stress shielding due to significant difference in elastic modulus between the implant and host bone that leads to the premature failure and fractures. The best solution to reduce the stiffness of metallic materials is by generating the voids into bulk materials known as open cellular structures (Montazerian et al., 2017; Ryan et al., 2006). The cellular structures are designed to reduce and tailor the elastic modulus of the biomaterials. Meanwhile, the periodic cellular structures are designed to homogenously distribute voids and strut, and therefore, contribute to predictable

behaviours and biomaterials properties compared to stochastic metallic foams (Chunze et al., 2015; Parthasarathy et al., 2011).

Despite the tremendous increase in the demand of metallic load bearing replacements, the application have been limited due to the loosening where the revision surgeries are needed (Geetha et al., 2009; Sumner, 2015). The critical issue has been reported often, where 10%-20% of joints need to be replaced within 15-20 years and approximately 80% of the revision surgeries (Marjan Bahraminasab et al., 2013; Garcia Cimbrelo et al., 1995; Garellick et al., 1994; Landgraeber et al., 2014). The main challenges faced by many metallic implants are aseptic loosening and stress shielding phenomenon, caused by mismatch of the stiffness between implants and the human bone. The phenomenon is due to the change of mechanical loading environment of the femur and can cause a reduction on periprosthetic bone density, especially in the proximal femur bone (Huiskes et al., 1992; Ten Broeke et al., 2014; Yamako et al., 2014). Bone resorption at the periprosthetic bone may be caused by the use of solid metallic materials and improvement of solid implant into functional graded implant, which seems helpful to reduce these effects. Some of the factors that are found to influence the implant failure and lead to second surgeries are illustrated in Figure 2.4.

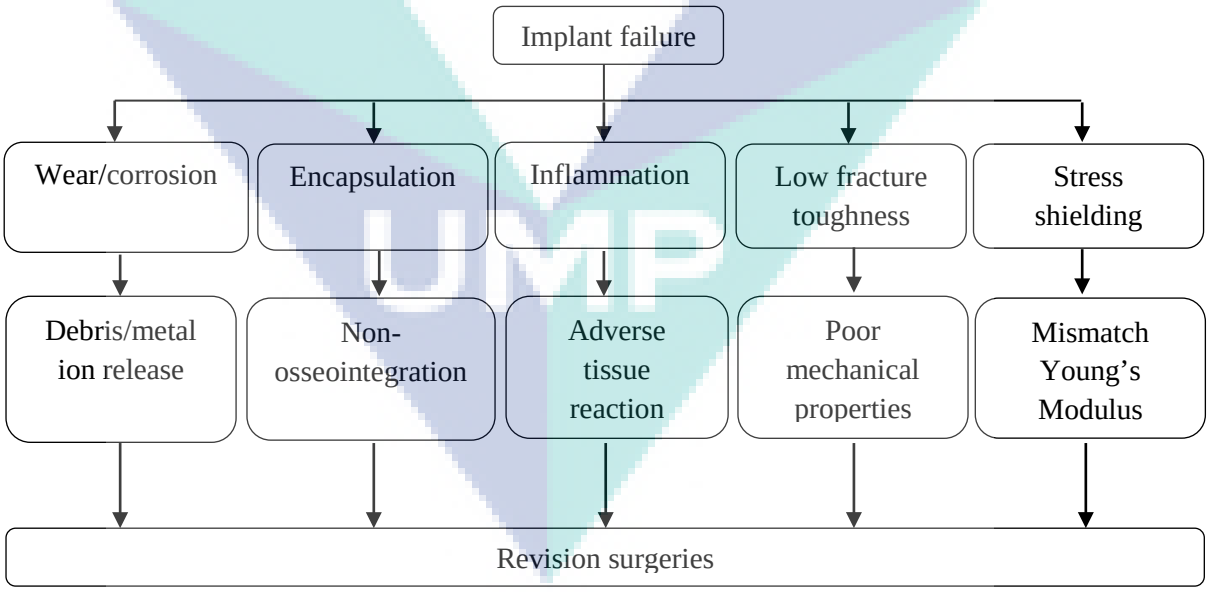

Figure 2.4 Factor of revision surgeries in implants

Source: Geetha et al. (2009)

2.4.2 Cellular Parts

Recent consideration for orthopaedic regenerative and load bearing implants is they can replicate the biomechanical properties of host human bones. Porous or cellular metallic structures have been found suitable in repairing and replacing the damaged bone and joint, since the stiffness and porosity can be tailored according to selected applications demands. The elasticity of human proximal femur bone is reported in range of 3-10 GPa, while the distal femur is in range within 10-30 GPa (Calmar et al., 2002; R. K. Fuchs et al., 2009). Figure 2.5 illustrates the possibility in tailoring stiffness of solid metallic implant components by introducing the cellular structures with the control porosity of the structures. Table 2.6 summarises the effectiveness of porosity percentage on tailoring the elastic modulus of Co-Cr-Mo metallic implants comparable to human bone properties. The elastic modulus of biomaterials decreased with increasing of volume porosity percentage.

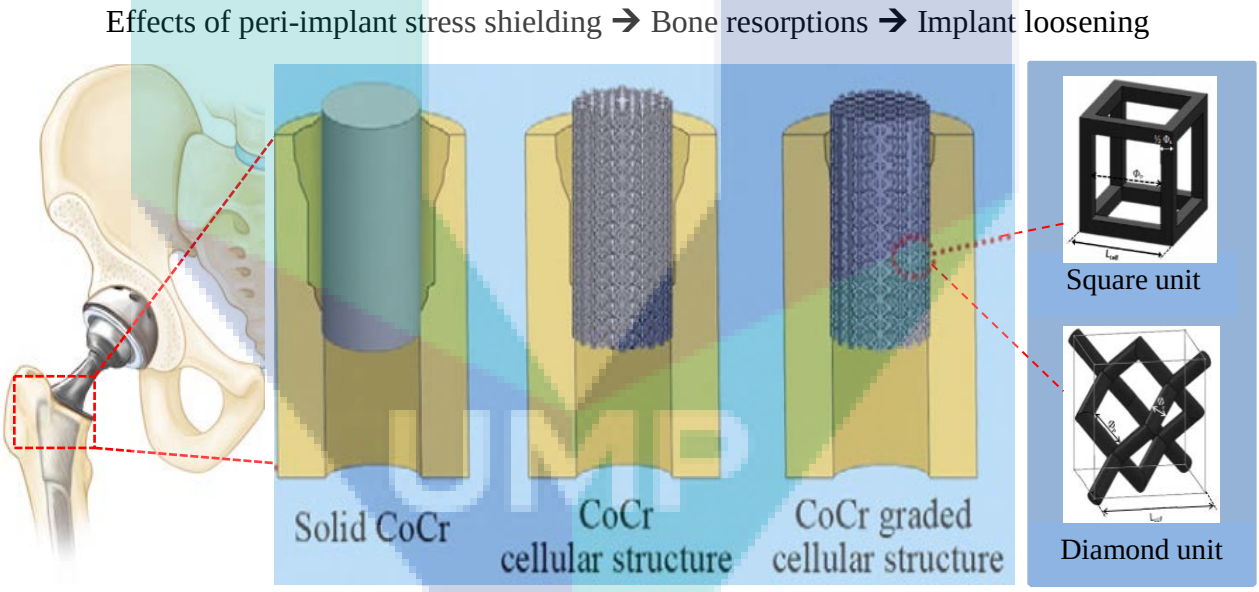

Figure 2.5 Hypothesis of application metabiomaterials used for reducing implant loosening due to bone resorption

Table 2.6 Elastic modulus of Co-Cr-Mo cellular structure from published correlations

(Limmahakhun et al., 2017)		(K. Hazlehurst et al., 2013)		(Anwar et al., 2016)	
Porosity (%	***E* (GPa)**	**Porosity (%)**	***E* (GPa)**	**Porosity (%)**	***E* (GPa)**
67	2.33	91	2.23	80	3.82
54	2.66	82	4.79	70	6.88
44	2.98	65	13.64	60	11.09
41	3.14	50	17.98		
14	5.26	45	25.25		

In addition, another advantage of cellular structures is providing spaces for the biological response of cell in-growth into the implant components especially at the interface area of implants and bone tissue. Hence, cellular structure allows the tissue regeneration and enhances better healing process with biological fixation. On the other hand, the study made by Yan et al. (2012) show that both relative density and measured density decrease with increment of unit cell size and volume porosity. While, (Chunze et al., 2015) found the high relative density where is above 99% achieved for diamond and gyroid type structure with porosities ranging from 80% to 95% where the porosity has little effect on the densities of components.

In general, cellular biomaterials have been used to describe this class of biomaterials. However, a modern term as metabiomaterials is suitable to clarify the connection of the biomedical application and distinguish them with the porous biomaterials manufactured by conventional processes. Metabiomaterials, which are known as combination of materials properties and structural behaviours, have been intensively investigated in medical applications, particularly in tailoring mechanical properties (Ahmadi et al., 2014; Campoli et al., 2013) and for tissue regeneration (Van Bael et al., 2012; Wauthle et al., 2015) of the implant parts. In the orthopaedic application, the integration between tailored mechanical properties and structure behaviours on new tissue regeneration on cellular materials play important roles in regulating the overall function of the implant system (Babaee et al., 2012).

2.4.3 Design of Metabiomaterials

Metabiomaterials are made from selected biomaterials for desired applications. The homogeneity of cellular structures resulted from highly controlled of geometrical

features started from a unit cell. The unit cells comprised of an interconnected network of solid struts which then are assembled linearly in order to provide lightweight porous structures. The metabiomaterials exhibit homogenous distribution of void space that leads to their homogeneous properties and behaviours. In regenerative orthopaedic approaches, metabiomaterials implants are often used in supporting the regeneration of bone tissue in segmental bone defects treatments. The gap of defected bone at bone-joint or bone structure is large after cut and removal than the natural healing process, where the healing process cannot bridge the gap without the presence of supporting or voids structures. Therefore, the metabiomaterials implants concepts in providing sufficient mechanical support and highly controlled pore geometries are important to be considered including to support, stimulate and guide the bone tissue regeneration.

The studies on highly controlled geometrical parameters of cellular structures have been carried in 2008. Heinl et al. (2008) performed the Ti-6Al-4V cellular structure through selective electron beam melting with geometrical design of two different structures based on CAD model of diamond lattice. The hatched structures generated by the scanning of powder layers in parallel lines with constant spacing of 1.0 mm. Both structures exhibit porosity of 80.5 % and a mean pore size of 1.23 mm for diamond and 61.3% and 0.45 mm for hatch structure. It was found that the mechanical properties of the structure are similar to human bone properties. Meanwhile, Warnke et al. (2008) fabricated cellular structure of Ti-6Al-4V using selective laser melting with square pore, ranging from 0.45 to 1.2 mm for cell ingrowth purpose. The varied pore sizes of the structures are to evaluate the biocompatibility of new manufacturing process and to grow the human cells in 3D cell cultures. The study determined that the pore overgrowth with osteoblast (bone) cells at bigger pore size but no pore occlusion was observed on the structure.

The concept of designed metabiomaterials is motivated by the desire to use the materials for a specific application. From mechanical viewpoints, a huge advantage offered by metabiomaterials is high strength accompanied by a relative low mass or lightweight. Geometrical parameters variations of metabiomaterials for orthopaedic applications are summarised in Table 2.5.

Table 2.7 Design of metabiomaterials for load bearing implants

Design	Geometrical	Findings	Reference
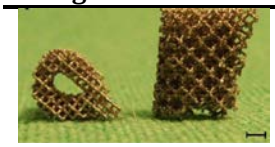 Dodecahedron	Strut = 120 & 230 µm Pore =240-730 µm Porosity = 68 & 88 %	Provide enough mechanical support & encouraged bone formation	(Van der Stok et al., 2013)
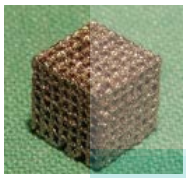 Cubic	Strut= 0.5 mm Pore = 0.45-1.2 mm	Compression strength decrease with increasing pore size & significant proportion in the range of 0.45 to 0.6 mm by osteoblast	(Douglas et al., 2009)
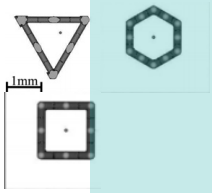 Triangular, hexagonal & rectangular	Pore =500 & 1000 µm	Lower pore size resulted higher cell attachment due to lower permeability & pore size is significantly influence cell growth	(Van Bael et al., 2012)
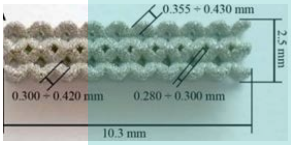	Pore size=280-420 µm	Surface coated doped with Mg implants are biocompatible with good bone-implant integration	(Mroz et al., 2015)
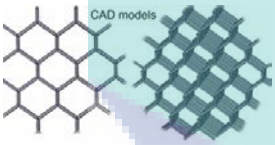 Mesh	Pore =640 & 1200 µm	Smaller pore size resulted more compatibility & better facilitate osteogenesis	(Lv et al., 2015)
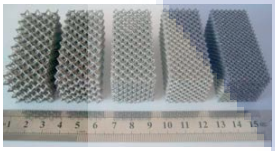 Mesh	Strut =0.72-1.08 mm Strut length=1.24-3.13 mm Porosity=62-86%	Possess comparable compressive strength (4-113 MPa) and elasticity (0.2-6.3 GPa) to human bone	(Cheng et al., 2012)
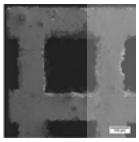 Cubic	Strut=400 µm Pore=1.2 mm	Tomography analysis revealed present of defects on samples and typical deformation followed by fracture observed in compression	(Petit et al., 2016)
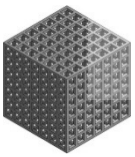 Cubic	Strut=0.2-2.5 mm Pore=1.44-1.88 mm Porosity=45-95%	The elasticity of samples with porosity higher than 65% are comparable to human bone	(K. Hazlehurst et al., 2013)

Table 2.7 Continued

Design	Geometrical	Findings	Reference
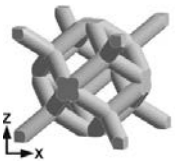 Rhombic dodecahedron	Unit cell size=3.33 mm Porosity = 75 %	Faster cooling rate in SLM promotes fine β dendrites that enhance compressive strength and lower elasticity	(Liu et al., 2016)
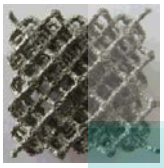 Rhombic dodecahedron	Unit cell size= 3 & 5 mm Porosity=84 & 87 %	The peal stress exhibits certain dependence on the loading rate for smaller cell size	(Xiao et al., 2017)
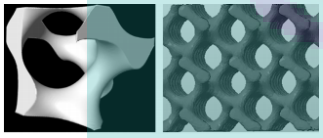 Gyroid	Cell size=5 mm Volume fraction=6, 8, 10, 12 & 15%	The yield strength and modulus increase with increased volume fraction	(Yan et al., 2014)
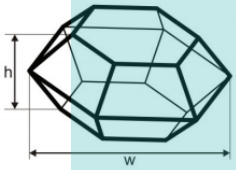 Hexagonal	Cell size=0.5-5 mm Porosity=70-90 %	SLM showed stable and robust build-up parts for 20°, 50° and 80° build angle	(Emmelmann et al., 2011)
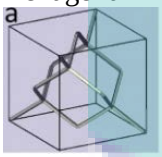 Diamond	Pore =300, 600 & 900 µm Porosity=65%	Suggested that samples with pore size of 600 µm best suited to orthopaedic due to highest bone-material fixation and bone ingrowth	(Taniguchi et al., 2016)
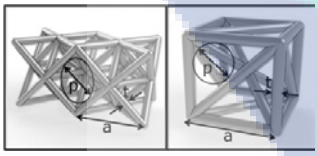 Octet truss & tetrahedron	Pore =770 & 500 µm Porosity=50-75 %	Both designs exhibits range of comparable stiffness with natural bone & bone ingrowth is higher in octet truss	(Arabnejad et al., 2016)
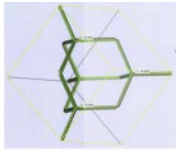 Diamond	Pore=500, 640, 800& 1000 µm Porosity=65-70%	Samples with pore size under 800 µm provided biological active and mechanically stable for implant fixation to bone	(Daisuke et al., 2016)
 Dodecahedron	Strut=150 µm Pore=500 µm Porosity=80%	Tantalum implants show excellent osteoconductivity, higher fatigue strength and high ductility	(Wauthle et al., 2015)

According to Table 2.5, majority of previous studies on metabiomaterials for load bearing implants with highly controlled geometries of pore shape, pore size, and porosity to tailor the mechanical stiffness comparable to human bone and to allow the cell growth in the structures for biological bonding. The unit cell type of dodecahedron made from Ti-6Al-4V was studied by Van der Stok et al. (2013). The structural variants including strut thickness of 120 and 230 µm, pore size is ranging from 240 to 730 µm, with porosity of 88 and 68%. In the study, the structures with strut size 230 µm provided mechanical support and encouraged bone tissue formation to repair the bone defect of rats after 12 weeks. On the other hand, Wauthle et al. (2015) produced dodecahedron unit cell structure made from tantalum with strut size of 150 µm and pore size of 500 µm that resulted in the overall porosity of 80%. Similarly, the study found that the structures exhibit mechanical properties parallel to cancellous human bone and appear to allow for bone ingrowth in animal (*in vivo*) studies evaluated after 12 weeks. Interestingly, the study reported the higher fatigue limit of investigated structures, which possess higher resistance to cyclic loading mechanism.

Recently, the innovation of dodecahedron unit cell design was performed by Liu et al. (2016) and Xiao et al. (2017), where the rhombic dodecahedron type was produced. Rhombic dodecahedron lattice is a type of structure of bending dominant as the minimum node connectivity is four (4) instead of twelve (12) by dodecahedron (Deshpande et al., 2001). Liu et al. (2016) produced structures with average strut size of 3.33 mm and porosity of 75% using two different additive manufacturing processes, while Xiao et al. (2017) produced components with unit cell size of 3 mm and 5 mm, porosity of 84 and 87%. The fabricated configurations for both studies are made by titanium alloys that resulted in the lower elastic modulus comparable to human bone. The major finding from these studies concluded that higher mechanical strength was obtained by structures with bigger unit cell sizes and higher porosity percentage.

Square type of metabiomaterials consist twelve (12) struts on each unit cell. This unit cell has been studied widely because it is basic types of unit cells for metabiomaterials and is easy to design. Douglas et al. (2009) has performed the cubic unit cells from titanium alloys with pore width ranging from 0.45 to 1.2 mm for maxillofacial mandible jaw bones. The study has found that after human osteoblasts cells were cultured on the samples with varied pore width, the cell overgrowth

increased during 6 weeks of culture at pore width of 0.45 and 0.5 mm, in the course of 3 weeks for pore size of 0.55, 0.6 and 0.7 mm, and no occlusion was observed on pores width of 0.9 to 1.2 mm. The major finding from the study concluded that porosity increases and maximum compressive load at failure decreases with increasing pore width, where the samples are biocompatible. K. Hazlehurst et al. (2013) has studied the square pore cellular structure for femur bone implants with strut size of 0.2 to 2.5 mm, and the pore size ranges from 1.44 to 1.88 mm. The porosity exhibits 45 to 95%. The study found that the elasticity of samples with porosity higher than 65% is comparable to human bone properties. On the other hand, Petit et al. (2016) studied the square type cellular structures with the strut of 400 µm and pore size of 1.2 mm. The study, from tomography analysis during compression test, found the presence of defects on the produced components and typical deformation followed by fracture stage.

Another unique type of cellular structure that has been extensively investigated is a diamond structure. The study was carried out by Taniguchi et al. (2016) and Daisuke et al. (2016). These previous studies explored the relationship of diamond unit cell in predicting mechanical properties of cellular structure and stability for implant fixation through bone and tissue regenerations. Taniguchi et al. (2016) produced diamond cellular structure with pore size of 300, 600 and 900 µm and controlled porosity of 65%. The study has suggested that the samples with pore size of 600 µm is best suited to orthopaedic implants due to highest material-bone response for bone cell ingrowth in enhancing the biological fixation at the material-bone interface. Meanwhile, Daisuke et al. (2016) studied the diamond type samples with pore size of 500, 640, 800 and 1000 µm and porosity ranging from 65 to 70%. Similarly, the study reported that samples with pore size ranged under 800 µm provided biological active and mechanical stable for implant fixation.

Besides that, structure with mesh type has been studied by Lv et al. (2015) with pore size 640 and 1200 µm. The study reported that smaller pore size resulted in higher compatibility and better facilitates new bone tissue formation. On the other hand, Cheng et al. (2012) investigated the titanium mesh with strut size of 0.72 to 1.08 µm, strut length 1.24 to 3.13 µm and porosity ranging from 62 to 86%. However, the study suggested that samples with higher porosity and bigger pore size possess comparable compressive strength and elasticity to human bone properties.

In another previous study, the designs of gyroid type structures have been investigated for load bearing implant applications by Yan et al. (2014) with unit cell of 5 mm in order to study the effect of increasing volume porosity of 6, 8, 12 and 15 % on elastic modulus. The study found that the yield strength and modulus increase with increasing volume fraction. Meanwhile, the hexagonal lattice structure type was studied by Emmelmann et al. (2011) with the cell size of 0.5 to 5 mm and porosity ranging from 70 to 90%. The study reported that the hexagonal type can be manufactured with the most stability during process by employed 20°, 50° and 80° build angle due to the planar face possessed by the structures.

In other research studies, the effect of two (2) different unit cell types for octet and tetrahedron trust has been studied by Arabnejad et al. (2016). These types have intersection node of the unit cell, where the structures possess pore size of 500 and 770 µm and porosity ranging from 50 to 75%. The study found that both designs exhibit a range of comparable stiffness with natural bone and interestingly, higher biological fixation is observed in octet truss. Moreover, Van Bael et al. (2012) has studied the effect of different pore shapes and pore sizes on biological response. The three (3) different unit cells have been proposed such as triangular, hexagonal, and rectangular with the pore size controlled as 500 and 1000 µm. The major finding of the study revealed that the cell growth of the pore size is influenced by the cell growth, where the 500 µm pore size resulted in higher cell attachment due to lower permeability. Nonetheless, the pore shape has influenced the occlusion of the cell in the structures. In general, the successful to produce metabiomaterials throughout an orthopaedic implant relies on manufacturing methods with beyond efficiency and best quality of products.

2.5 Manufacturing of Metabiomaterials

The key characteristics to design cellular metallic implants or metabiomaterials include careful selection of porosity, pore size, and pore interconnectivity, aiming to achieve satisfactory clinical outcomes such as mechanical elasticity and biological fixation with tissue regeneration. The metabiomaterials structures cannot be fully controlled, since the majority of existing production technologies do not allow for precise control of the shape, size and cellular pores distribution (Bechmann, 2014; Podshivalov et al., 2013). The requirements with complex shape and full tiny details make the metabiomaterials difficult to manufacture using conventional process, such as

space holder and gas foaming (Brenne et al., 2013). From this scenario, advance highly attractive AM technologies was adapted in allowing the production of complex three-dimensional structures and near-net-shaped parts (Emmelmann et al., 2011; Murr, 2015; Su et al., 2012). AM generates significantly reduce material cost and energy usage by using less material and eliminating steps in the production process (Brenne et al., 2013). The next section will discuss the current manufacturing process for cellular structure metallic implants through conventional and additive manufacturing processes.

2.5.1 Conventional Processes

Conventional process that is reliable for manufacturing porous structure metallic implants is divided by two (2) techniques: (1) non-homogenous pore distribution and (2) homogenous pore distribution. In the review by Ryan et al. (2006), non-homogenous pore distribution for porous metal can be produced by a number of techniques. The furnace sintered metal powders and fibres are the easiest fabrication method in making metallic foam fundamentally on partial densification during sintering of metal powders. The process technology is done by compacting, binding, and sintering metal powder at higher temperature caused the bonding between each powder particle (Roy et al., 1999; Saitou, 2006). However, difficulty to control the pore sizes and pore shapes that are controlled by the powder and shape during process has limited higher porosity, which directly limits the bone ingrowth (Rausch et al., 2002; Rezwan et al., 2006).

Besides that, space holder method is one of the popular manufacturing processes since the technique able to produce porous metallic components with greater porosity percentage. The used powder particles should be smaller than the average of the powder particles that act as space holder with sufficient compaction pressure to sustain the geometry throughout the foaming process (Hassani et al., 2012). The difficulty faced by this process is mainly related to the removal of large quantities of the space holder materials from the compacted mix that can affect the final porosity and might cause the contamination on produced parts. Thus, Bansiddhi et al. (2008) took into account the latter factor for porous biomedical implants application to prevent any contamination. Torres et al. (2012) investigated the sodium chloride (NaCl) percentage as space holder with the improvement procedure to eliminate salt before sintering process at temperature 50 to 60 °C.

Another approach that is basically related to space holder is known as replication technique that uses chemical as the pattern materials mould for void configurations (Jia Ping et al., 2002). The pattern of the final design of porous metallic implants is made and reproduced with the actual desired materials *via* intermediate infiltration step (Bram et al., 2000; Spoerke et al., 2005). On the other hand, the latest development of effective technique in producing high purity porous metal is known as combustion synthesis (Chu et al., 2004; Vollmer et al., 2012). The particle fusion is obtained in this process through an extreme rapid self-sustaining exothermic reaction driven by the large heat released in the synthesis (X. Zhang et al., 2000). This manufacturing process has advantage of high purity of resulting foams which is mostly due to the expulsion of volatile impurities under extreme high temperature during the process (Hunt et al., 2006).

There are many ongoing studies and works on manufacturing process of cellular structures for porous orthopaedic implants with homogeneous pore distribution such as orderly oriented wire mesh (OOWD) coating (Ducheyne et al., 1986a, 1986b) and ferromagnetic fibre assays. The porous parts are created by sparing a small quantity of fibres made from ferromagnetic materials with a slow setting aerosol and glue and then sprinkling some braze powder on parts (Markaki et al., 2004). Meanwhile, chemical vapour deposition (CVD) involved depositing a solid material by reaction in the gaseous phase (Bobyn et al., 1999; Delhaes, 2002). However, the conventional manufacturing processes have disadvantages of higher time consumption and manpower, lack of flexibility in design of parts on microscale levels related to using mould in producing functional graded metallic implants.

Other than that, functional graded pore distribution for porous orthopaedic implants can be manufactured by electrical field-assisted powder consolidation known as spark plasma sintering (SPS) (Miyao et al., 2000; Watari et al., 2002), plasma activated sintering (PAS) (Hu et al., 2014; Mishra et al., 1996), and electrical discharge compaction (EDC) (Jo et al., 2007; W. H. Lee et al., 2007). The consolidation process consists of two stages: (1) initial activation through voltage application and (2) subsequent heating and densification by using direct current (DC). Recently, a novel fabrication process in the form of *3D* printing that enables the production of porous implants with highly controlled size, shape and porosity distribution directly from a

CAD model such as additive manufacturing (Melican et al., 2001; Seitz et al., 2005; Stamp et al., 2009).

2.5.2 Additive Manufacturing and Selective Laser Melting

The high demands of better performance and customised products for selected applications lead to emergence of AM technologies which is believes capable to manufacture models that have greater levels of added value. One of the most significant emergences in advanced manufacturing is the reliable cost saving and efficiency to produce small-scale components with complexity of design (Despeisse et al., 2015; Weller et al., 2015). AM fundamentally produces parts with any possible designs fundamentally from powder materials layer by layer from the bottom to top of component directly from computer-aided design models. Ford et al. (2016) discussed the consequences in adopting production technology in order to provide the deep insight into the impacts of additive manufacturing on industrial sustainability.

Interestingly, three (3) dominant potential sustainability benefits of additive manufacturing were identified where (1) efficiency can be improved in both production and practice phases as manufacturing process and also the parts can be redesigned for production purpose, (2) the product life can be extended through technical approaches, socio-economic pattern and closer relationship between manufacturer and consumers as mentioned by Kohtala (2015), (3) reconfiguration of value chains through more localised production, innovative distribution model and opportunity to new collaborations.

Today, the use of the AM offers a significant potential for health systems as well as possibility in providing better quality of human life with optimum cost and time consumption, which may be subjected to various medical applications including orthopaedic, neurosurgery, maxillofacial and orthognathic surgery and traumatology, craniofacial and plastic surgery, dentistry and oncology (Luiz et al., 2014; Salmi et al., 2013; Stoor et al., 2014) There are many types of AM methods that are available based on the same principle of manufacturing layer-by-layer process. The main AM techniques used are selective laser melting (SLM), selective laser sintering (SLS), fused deposition modelling (FDM), stereo-lithography (SLA), laser engineered net shaping (LENS), direct metal laser sintering (DMLS), and electron beam melting (EBM), where

the raw material for fabrication is from a variety of powder form materials (Singh et al., 2017; Yadroitsev et al., 2010). To date, numerous medical devices and applications have been manufactured with available AM techniques, which include bone scaffold (Farag et al., 2014; A. Kumar et al., 2016), hip and knee joint (España et al., 2010; Lawrence et al., 2012), and dental implants (Figliuzzi et al., 2012; Jianyu et al., 2014). Figure 2.6 shows the schematic diagram of LENS, EBM and SLM systems.

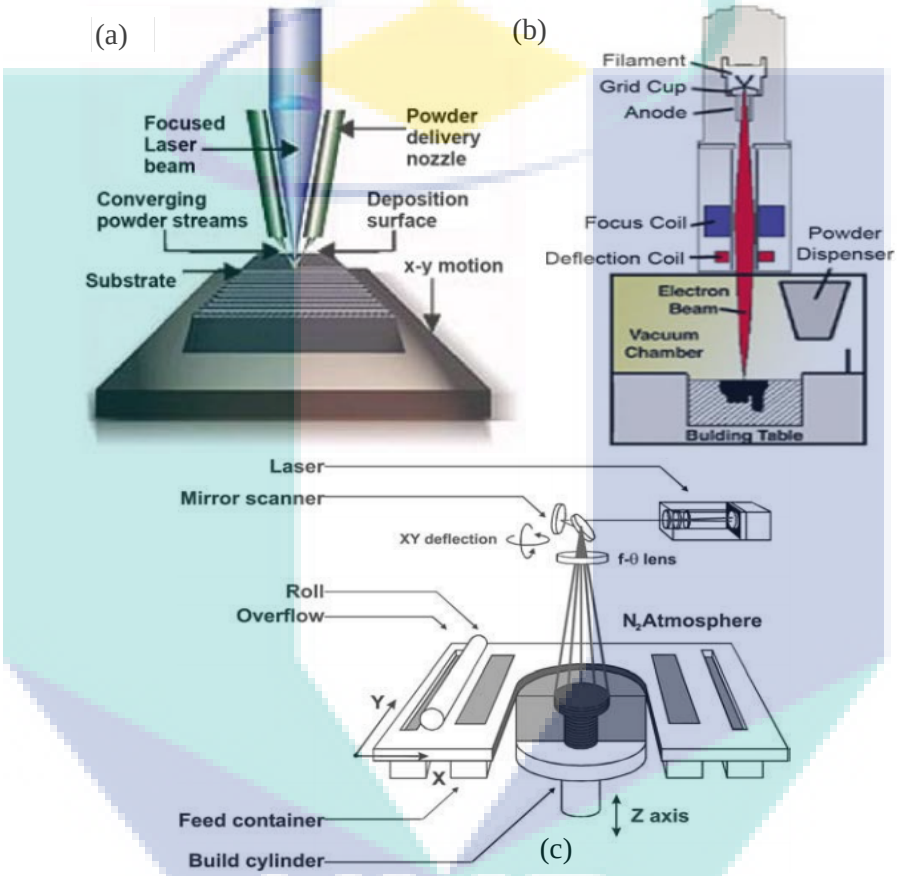

Figure 2.6 Schematic diagram of AM (a) LENS, (b) EBM and (c) SLM

Source: Hao et al. (2008), Bartolo et al. (2012) and Jean et al. (2005)

The first successful fabrication using selective laser melting technology for orthopaedic implants was performed in 2005 by Wehmöller et al. (2005). The cortical lower jaw geometry was fabricated in fully complexity using stainless steel with the supporting structure partly inserted as an example of the spongy structure. In SLM process, parameters that affect the process are generally related to powder, laser, and process technique. Metallic powder shape, size, type and properties can affect the overall process, powder bed density, flowability, and laser-material interaction during fabrication process. Schmidt et al. (2016) studied the effect of powder properties such

as particle size, shape, and flowability on the SLM process on the polymer powder. The study found the products quality is strongly determined by powder properties with good flowability, and high density is mandatory to obtain the solid components. S. Kumar (2014) mentioned that high powder bed density is preferred that lead to higher components density. The powder bed density and flowability depends upon powder particle shape (Masmoudi et al., 2015). Therefore, spherical shape and narrow powder size distribution are favourable characteristics in SLM manufacturing in order for powder to flow smoothly. The smooth surface in spherical shape with particle size distribution of titanium powder is shown Figure 2.7.

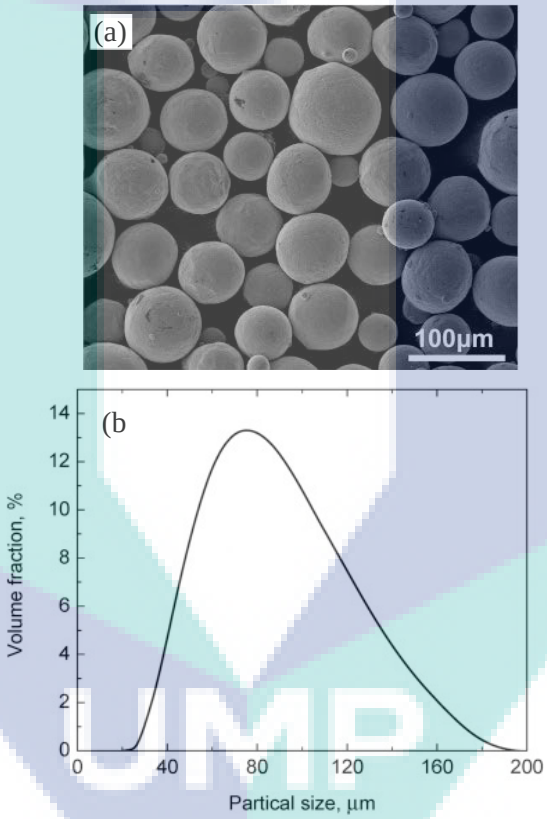

Figure 2.7 (a) The morphology and (b) particle size distribution of Ti powder particle
Source: Liu et al. (2016)

Laser power is the main parameter in the process, which aims to completely melt the powder for fabrication. Generally, SLM machines are equipped with laser powder ranging from 50 to 400 W, and the magnitude of laser power depends upon the type of selected materials (S. Kumar, 2014). Mostly, in SLM manufacturing process, laser types, such as CO_2 (polymer and ceramics), Nd: YAG or fiber laser (ceramic and metal), could be found with the wavelength ranging from 1.07 to 1.09 µm Laser spot

size could be defined as laser beam diameter, where the size is ranging from 30 to 600 µm for fabrication process (Thijs et al., 2010). Variation in laser energy density, precision, and production speed can be achieved with the varied laser spot size during process. X. Li et al. (2017) investigated the relationship of laser power between microstructure and mechanical properties of commercially pure titanium using SLM process. The study found that different laser powers lead to formation of different phase microstructures, textures, and mechanical properties. Consequently, the weak textured components with isotropic mechanical properties were achieved using laser power 250 W, while the strong textured parts with anisotropic mechanical properties were obtained using laser power of 50 W.

c In the SLM process, various parameters related to the process depends upon the scan spacing, scan speed, layer thickness. Scan spacing is the separation between two consecutive laser beams or also known as hatch spacing or hatch distance (S. Zhang et al., 2014). The scan spacing is measured from the centres of one beam line to the center of another beam line. The scan spacing is directly proportional to the production speed where the larger laser spot size is required in order to have large scan spacing prevent the porous products (Wits et al., 2016). Another approach in SLM manufacturing process is to avoid the porosity formation at the boundaries scan line. In this regard, overlap line beam is necessary by Gaussian beam theory where the laser power at the center of the scan is higher than at the boundary of scan due to temperature gradients (Childs et al., 2005). Figure 2.8 illustrates the scan spacing and layer thickness of manufactured part and also the scan spacing with line beam overlapping.

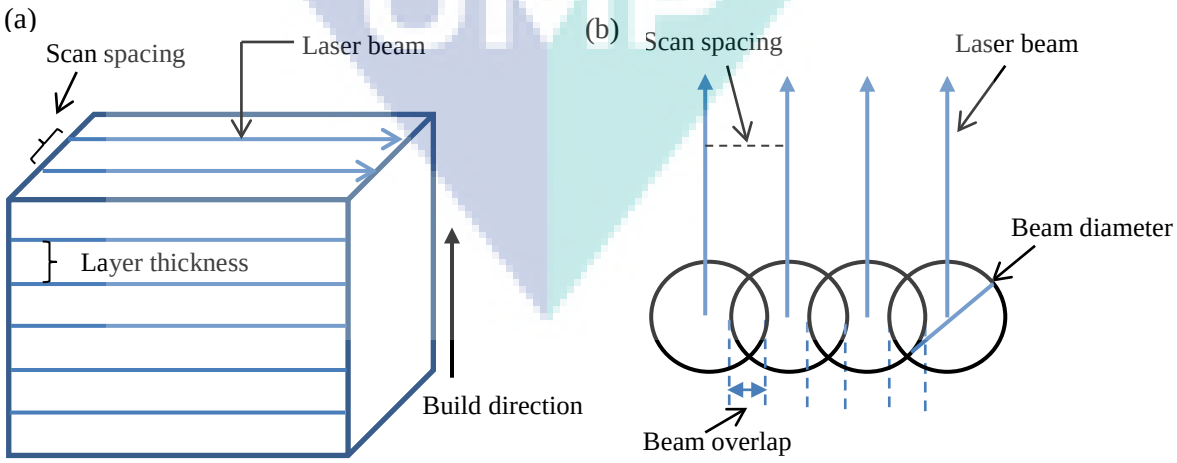

Figure 2.8 Schematic diagram of (a) scan spacing, layer thickness and laser beam (b) beam overlap in SLM manufacturing process

Another main process parameter is the scan speed which corresponds to the rate of the laser beam in scanning a line at the powder bed. The scan speed is directly proportional to the production speed, in which increased the scan speed can increase production speed as reported by (Louvis et al., 2011). However, at the very high scan speed and laser power, the time is not sufficient for higher heat to diffuse across the whole powder bed, which leads to insufficient melting and ablation of the powder particle during process. W. Li et al. (2016) performed a comprehensive study on laser scan speed on the microstructure, phase evolution, and nanohardness of the Ti alloys. The study reported that lower scan speed resulted in higher energy input density, which brought a longer time of reheating or remelting thus prolonging the recrystallisation. The value of scan speed generally found in SLM process is ranging from 0.1 and 15 mm/s (S. Kumar, 2014). It is important to note that the scan speed is determined by the melt pool length.

On the other hand, layer thickness is the thickness of a slice of 3D computer aided design (CAD) model of a desired product, which is then converted or translated into physical layer-by-layer processing. Layer thickness is directly related to the production speed while higher precision is achieved with decrease in layer thickness. Small layer thickness will result in the lower shrinkage after melting by moving the laser beam, which increases the dimensional accuracy and surface qualities (Jean et al., 2004). Sufiiarov et al. (2017) investigated the effect of layer thickness on nickel based superalloy fabricated by SLM. The study revealed that mechanical properties depend upon the strength and plasticity of the layer thickness during production of components, where at the higher layer thickness (50 µm), strength properties are lower while plasticity is higher in lower layer thickness (30 µm).

In the advantages of complexity built parts with efficiently and economically by SLM process, the choice of built orientation of the part and support structures can increase the efficiency of the produced components. For a complex shape components that could have many overhangs in various angles, the preferred and right orientation could prevent the overhang problems on produced samples (Cloots et al., 2013). Gan et al. (2016) studied the three types of support structures in designing the support structures for SLM process. The study revealed that orientation and distribution of the support structures influenced the levelness of the produced parts. Moreover, to make

parts in some build orientation support structure, support is required to prevent the build from falling, displacing and to assist in dissipating the heat that is entrapped in the components (Jhabvala et al., 2012). However, the support structures need to be removed after the fabrication. Thus, the minimal contact area with the parts is required to remove support structural easily and minimum surface finishing required after removal. Figure 2.9 shows the support structures at the component parts during fabrication process.

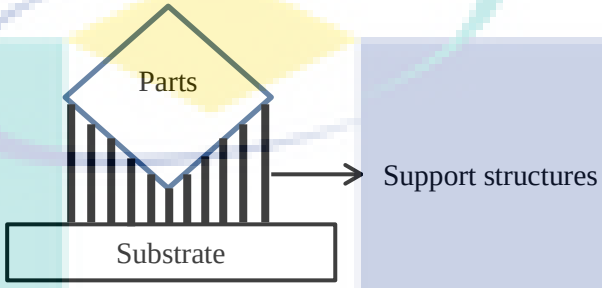

Figure 2.9 Build parts with support structures

2.5.3 Challenges of Additive Manufacturing Process

In this study, the focus is on the adaptation of additive manufacturing technologies, which is selective laser melting (SLM) process. As aforementioned, SLM can provide the opportunity to produce metabiomaterials with desirable designs and levels of volume porosity for selected applications. In the present study, the production of metabiomaterials is intended for orthopaedic application. Thus, the metabiomaterials must exhibit the potential function of osteoinductive with sufficient mechanical strength. However, there is a limit to which osteoinductive ability can be increased by increasing the micro porosity as the mechanically stable surface of the materials is needed in order to encourage bone growth and cell attachments. For specific bone tissues, such as femur bones, the bones are structurally organized in a way of the bone porosity varies from the cortical part perimeter to the inner section of cancellous part. Nevertheless, a single composition with uniform structure cannot satisfy all the requirements of bone implants, where the mechanical strength of the bone decreases gradually from the compact part into spongy parts consequently, which is regarded as a functionally graded structure that relates to the properties of metabiomaterials.

Recently, growing studies on fabrication of cellular structures using SLM demonstrated the capability from CAD models into different shapes of build-up

structures. However, the key challenges have been identified in this manufacturing area, where the partially melted powder adhered to the struts (Murr et al., 2010; Pattanayak et al., 2011) and there is difficulty in removing the adhered powder within the structures (Facchini et al., 2009; Hasib et al., 2015). Another limitations and challenges in manufacturing metabiomaterials is that single batch fabrication is usually restricted to one type of materials (Sing et al., 2016). Most of the recent AM technologies that are used to fabricate cellular materials are limited to produce a nominal strut thickness of 200 µm (de Wild et al., 2013; Harrysson et al., 2008). Thus, the metallic implants that require varying different materials in a single structure become constrained in the manufacturing using SLM.

España et al. (2010) designed and fabricated porous structure of Co-Cr-Mo alloy by laser engineered net shaping (LENS™) with the concern of not affecting the wear resistance of biomaterials through combining dense and porous structure in the samples. In other work, K. Hazlehurst et al. (2013) designed and manufactured Co-Cr-Mo with square pore structures using selective laser melting (SLM), with volume based porosity ranging between 25 and 95 %. However, biocompatibility results cannot be found in both studies. Both of the studies revealed the significance of fabricated porous by additive manufacturing that can potentially tailor Co-Cr-Mo effective modulus to match or be comparable to human bone properties.

The idea behind the successful AM production is the direct import of CAD models into STL file, where all the external boundaries and internal surface appear to be smooth and continuous using this file (Chakraborty et al., 2008; Nelaturi et al., 2015). The first drawback is starting from 3D space tessellation and ending with 2D building strategy, since the successful fabrication is relied on scanning layer-by-layer (Guessasma et al., 2015; Guessasma et al., 2016). The droplet-based printing is considered as the fused matter is no more connected in any direction and discontinuities may appear in all building up direction for the manufacturing process. Consequently, the produced parts possess dimensional inaccuracy, inacceptable surface quality, structural and mechanical anisotropies as being reported in previous research contribution (Ahn et al., 2002; C. S. Lee et al., 2007; Lee et al., 2014; Rosa et al., 2015; Salmi et al., 2013). Nonetheless, the formation of pores in solid produced part may occur inherently during SLM process (Louvis et al., 2011; Thijs et al., 2010).

This phenomenon happens during the interaction between laser beams with the metal powder, where the energy is absorbed by powder particles through bulk coupling and powder coupling mechanism (Fischer et al., 2003; Simchi, 2006). Concurrently, the formation of temperature gradient results in the shear stress and convective movement of melting pool, which is known as *Marangoni effect* (Rombouts et al., 2006; Song et al., 2014). During the rapid solidification, the gases or air bubbles formed can float to the melt layer due to *Marangoni* flow and escape from the melt pool or trapped in solidified structure and yet result in the pores (Alrbaey et al., 2014; Monroy et al., 2013). Alrbaey et al. (2014) suggested that the most considerable factor on the outcomes of produced parts during additive manufacturing process such as those factors of the laser power, scan speed, hatch spacing, focus distance, beam diameter, scanning strategy and environmental. Thus, all the limitations mentioned can be overcome in the near future in the SLM manufacturing of metabiomaterials by further research and development of optimum parameters during fabrication process. The performance of metabiomaterials must be investigated in order to understand and assured the mechanical strength and biocompatibility for load bearing implants.

2.6 Characterisation of Metabiomaterials

It is important to understand the mechanisms through which geometrical features interact to reduce stress shielding effect and influence the process of bone tissue regeneration in orthopaedic implants. There are several geometrical features that are shown in metabiomaterials performance including pore shape, pore size, porosity, and surface curvature. In this section, the testing and characterisation of produced metabiomaterials from other research correlation have been reviewed. Since medical implants are devices placed either inside or on the surface of the body for desired function of replacing, assisting or enhancing the biological functionality, the ideal requirements of the implants need to be characterised after the manufacturing process.

Characterisation on metallic implants through extensive study on mechanical properties for elastic modulus and materials strength, biological study including *in vitro* that is given procedure in a controlled environment outside a living organism, *in vivo* refer to animal study and *ex vivo* refer to experiment of organism tissues in external environment with mimic natural conditions, is summarised in Table 2.6.

Table 2.8 Characterisation on metallic implants

Parts	Materials	Mechanical	Biological	Reference
Femur	Ti-6Al-4V	Bending	In vivo & ex vivo	(Van der Stok et al., 2013)
Cancellous bone	Ti-6Al-4V	Compression	In vitro	(Douglas et al., 2009)
Bone	Ti-6Al-4V	Compression	In vitro	(Van Bael et al., 2012)
Bone	Ti-6Al-4V		In vivo	(Mroz et al., 2015)
Hip	Ti-6Al-4V		In vitro	(Hrabe et al., 2013)
Bone	Ti-6Al-4V		In vitro (cytocompatibility & osteogenesis)	(Lv et al., 2015)
Knee	Co-29Cr-6Mo Ti-6Al-4V	Tensile, hardness		(Murr et al., 2011)
Vertebra bone	Ti-6Al-4V	Tensile, fatigue	In vitro	(Hollander et al., 2006)
Femur	Co-Cr-Mo	Compression		(K. Hazlehurst et al., 2013)
Bone	Ti-6Al-4V	Compression	In vitro bioactivity	(Heinl et al., 2008)
Hip	Ti-6Al-4V	Compression		(Emmelmann et al., 2011)
Bone	Ti based alloys	Compression	In vivo	(Taniguchi et al., 2016)
Trabecular bone	Ti based alloys	Compression		(F. Li et al., 2015)
Femur	Ti-6Al-4V	Compression	In vivo	(Arabnejad et al., 2016; Daisuke et al., 2016)
Femur	Ti based alloys	Push-out testing, compression	In vivo	(Daisuke et al., 2016)
Femur	Tantalum	Compression, fatigue	In vivo, in vitro cytotoxicity, ex vivo	(Wauthle et al., 2015)
Dental	Ti-6Al-4V	Fatigue		(Jamshidinia et al., 2015)

From the Table 2.6, characterisations by experimental studies of cellular metallic implants mostly have been studied in femur long bone for cortical and cancellous parts, hip and knee bone joints, vertebra spinal bone, and also dental human body parts. Despite the excellent wear resistance, fracture toughness, and corrosion resistance of Co-Cr-Mo in load bearing implants, most previous studies investigated Ti-based alloys as bone substitution, where the biological studies has taken into account due to osseointegration properties exhibited by Ti-based alloys. Osseointegration is defined as direct bone to implant contact without any adverse reaction on soft tissue

(Carlsson et al., 1986) and successful integration with surrounding bone (Prasad et al., 2015).

For the cortical bone implants, majority of cellular metallic structures are made from Ti-based alloys such as Ti-6A-l4V, which is expected to have elastic modulus comparable to human bone properties, promote cell ingrowth, and support osseointegration. Mroz et al. (2015) investigated the assessment of *in vivo* response on Ti-6Al-4V cellular structure with pore size ranging from 280-420 µm, coated with magnesium and hydroxyapatite implanted in rabbit for six (6) months. From the studies, the produced parts are biocompatible and biological bonding between bone and implants, where penetration of new tissue through the structure into the center of the implants, was observed. This observation is important as no inflammatory cases were observed which demonstrated good biocompatibility of the implants produced by SLM.

On the other hand, Lv et al. (2015) performed the *in vitro* study in order to evaluate the biological response of the Ti-6Al-4V mesh unit cell structure with pore size 640 and 1200 µm fabricated by EBM on human bone marrow-derived mesenchymal stem cells. The study found that the pore size was responsible for disparate properties of porosity, specific surface area, and permeability, which can also impact cytocompatibility and osteogenic ability. Furthermore, the samples with small pore size were more compatible and served better in facilitating osteogenesis due to their larger specific area. The evaluation study of cellular structure will be more satisfied with systematic analyses on both mechanical properties and biology properties.

Consequently, Heinl et al. (2008) has studied the implant at the bone parts for mechanical compression test with a crosshead speed of 0.5 mm/min and *in vitro* chemical bioactivity, where the samples were soaked in simulated body fluid (SBF) for 6 days. Through this study, the compressive strength and elastic modulus were evaluated where the structures were similar to human bone. Meanwhile, the modified bioactive surface is expected to promote the biological fixation of the implant in the surrounding bone for long-term stability. The mechanical and *in vitro* study of implants at bone parts have been continued by Van Bael et al. (2012). In the study, as-produced samples were compressed with a 100 kN load cell and at a compression rate of 0.2 mm/min (n = 3).

Prior to *in vitro* study, the produced samples were sterilized using autoclave method. The cell proliferation was measured at day 1, 7 and 14 after cell culture under 37 °C and 5% CO_2 using cellular metabolic activity and DNA quantification. Meanwhile, Taniguchi et al. (2016) investigated bone implant with combination of mechanical properties and *in vivo* study. In the study, the assessment of mechanical properties, in accordance with ISO 13314:2011, was conducted on the samples with length and diameter of 12 mm at crosshead speed of 1 mm/min and calculated from the obtained stress strains slope. The samples were sterilised using ethylene oxide gas before being implanted in the bone of adult rabbit for eight (8) weeks for undergone bone in growth evaluations.

Characterisation of load bearing implants on the femur bone is crucial to examine. From the previous study, K. Hazlehurst et al. (2013) performed the mechanical compression subjected to human femur bone with load capacity of 100 kN and strain rate of 0.5 mm/min, where the components were loaded to failure or until the maximum load was reached. From the previous works, the load bearing implants for femur parts were mostly characterised by mechanical properties and *in vivo* study. Arabnejad et al. (2016) evaluated the elastic modulus of the implants with load 50 kN at strain rate of 0.01 mm/min whereas bone ingrowth is assessed *in vivo* canine models after eight (8) weeks. Daisuke et al. (2016) performed the similar experimental methods, where the samples were loaded force up to 450 N parallel to the long axis of the implants at cross head speed of 0.5 mm/min. Meanwhile, the animal study was assessed in adult rabbits after implantation up to twelve (12) weeks. Moreover, the bone bonding strength after implantation was performed by push-out testing with speed of 0.5 mm/min.

Wauthle et al. (2015) performed mechanical properties evaluation on femur bone implants with static and dynamic mechanical testing. The compression testing with load cell 30 kN at constant deformation rate of 1.8 mm/min and fatigue test with load cell 25 kN at loading frequency at 15 Hz was performed. The biological evaluation and bone regeneration was performed by *in vitro* cytotoxicity test according to ISO 10993-5 on fibroblast L929 cells, *in vivo* rat models, where the samples were implanted in rats for twelve (12) weeks and *ex vivo* testing was done by means of torsion test on the strength of the implant-bone bonding at rotation rate of 0.5 °/s. Meanwhile, Van der

Stok et al. (2013) performed animals study in rats, where the samples were implanted for twelve (12) weeks. After that, the biomechanical strength of treated femur bone was measured with three points bending test at a rate of 2 mm/min, until the peak load was reached.

In load bearing treated at cancellous bone, Douglas et al. (2009) performed mechanical characterisation on the samples with applied load of 1 kN at a speed of 1 mm/min. Meanwhile, the biocompatibility was assessed *via* fluorescence microscopy after cell viability staining techniques and common biocompatibility tests including lactate dehydrogenase (LDH), 3-(4,5-dimethylthiazol-2-yl)-2,5-diphenyltetrazolium bromide (MTT), 5-bromo-2-deoxyuridine (BrdU) and water soluble tetrazolium (WST) assay after 24 hours' culture, where the absorbance was measured at 450 nm. On the other hand, F. Li et al. (2015) found that the buckling on anisotropic mesh can be observed with mechanical compression on load frame at strain rate of 10^{-3} s^{-1}.

For hip and knee implants, Hrabe et al. (2013) performed the *in vitro* biological study on the periodic titanium hip implants, where the samples were seeded and cultured with osteoblast-like cells until four (4) weeks interval. The cell proliferation was determined with MTT assay and the absorbance read at 490 nm using a plate reader. Meanwhile, Emmelmann et al. (2011) stated that mechanical shielding of the bone tissue can be observed when mechanical load is applied on the implant. In addition, the bone degenerative occurs because of the lack of load induced promoting bone growth. On the other hand, Murr et al. (2011) has performed a few designs of porous total knee replacement that consist of Co-29Cr-6Mo femoral bone components and Ti-6Al-4V tibial bone components. The assessment of mechanical properties used Vickers microindentation hardness (HV) with a 100 gf load and Rockwell C-Scale hardness (HRC) with a 150 kgf load. The produced samples were investigated using tensile test conducted at room temperature a strain rate of 10^{-3} s^{-1}.

The characterisation on cellular structure implants for spinal back bone and dental investigation is not much explored in the previous works due to researchers are interested and focusing on bone joints such as hip and knee joints. Hollander et al. (2006) evaluated the implants sample on mechanical and *in vitro* experimental studies. Tensile testing was conducted according to standard DIN 10002-1 in order to determine the basic materials properties to match with American Society for Testing and Materials

(ASTM) standards for Ti-6A-l4V implants. Moreover, the fatigue testing was conducted according to DIN 50113 rotating bending fatigue testing standard with corresponding cycles up to 1×10^7 cycles. Meanwhile, the *in vitro* assessment was conducted using human primary osteoblast cells harvested from cancellous bone of femoral head. Prior to cell contact for cell culture up to day 14, all samples were sterilised by autoclave method. The metabolic activity of the cell growth was assessed using XTT assay, which is known as colorimetric assay based on the oxidation of the tetrazolium derivate XTT by vital cells and staining under fluorescence microscopy. Jamshidinia et al. (2015) investigated the fatigue properties of dental abutment implant with lattice structure according to standard ISO 14801. The test was carried out at loading frequency of 15 up to 5 million cycles.

Amin Yavari et al. (2015) found the significance of geometrical parameters of strut size and pores shape on material behaviours. The design controlled of porous structures or known as meta-material is important when the study at micro scale is considered. Previous studies by Ahmadi et al. (2014) on mechanical properties of open cellular lattice structures, the analytical solution and closed-form relationships for predicting the elastic modulus, Poisson's ration, critical buckling load and yield stress, are presented. It has been shown that the mechanical properties obtained using analytical and numerical solutions are in agreement with each other and with experimental observations.

In order to make the innovation of AM products approved to be marketed in medical fields, the orthopaedic devices need to undergo the experimental studies in particular for the mechanical properties, materials behaviours and also biocompatibility for toxicity measurement. As summarised in Table 2.6, previous researchers have performed the experimental on mechanical and otherwise the biocompatibility for *in vitro* or *in vivo* study. It is important to study both the mechanical and biocompatibility testing in order to observe and determine the interaction of sufficient mechanical properties with biological response in human or animal cases. From the experiment, mechanical elastic modulus should exhibit the match range for human bone properties and the biological response for cell proliferation and differentiation for tissue regenerative stability.

Figure 2.10 shows the applicability of additive manufacturing on producing metallic load bearing implants due to advantages of fabrication of complex products and functional gradient materials, efficient approaches that reduce production costs and speed time-to-market.

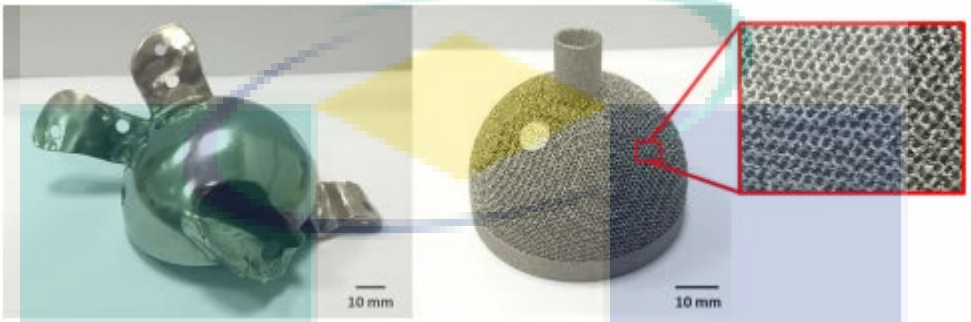

Figure 2.10 Hip joint components fabricated by AM for the solid and metabiomaterials structure

Source: Sing et al. (2016)

The effect of well-controlled geometries as mentioned above is also important for *in vitro* cell ingrowth or osseointegration experiment. Researchers have listed down the influencing factors for cell ingrowth and proliferation to happen, which include pore size, pore shape, porosity, and interconnectivity (Chen et al., 2010; Feng et al., 2011; Jones et al., 2009). Van Bael et al. (2012) found that pore size significantly influences cell bone growth into samples rather than pore shape. The studies reported higher living cell density on samples with greater pore size with non-circular pore shape.

2.7 Summary

Nowadays, AM has provided a good opportunity to fabricate customised lightweight components such as cellular structure with tailored mechanical properties from single metallic biomaterials as performed by (Murr et al., 2011) and España et al. (2010). Consequently, a new class of biomaterials that is aimed for biomedical implants has emerged, which is known as metabiomaterials. Metabiomaterials provide unprecedented opportunities for manufacturing load bearing implants with tailored mechanical properties to match properties of human bone (1-30 GPa) and to promote the osseointegration (the integration between implant and bone) for longer life span.

Earlier study made by Weber et al. (1972) investigated the cellular structure for biomedical implant has brought the development for investigating the advantages of metallic cellular structure to establish the longer life span biological fixation of orthopaedic implants and tissue scaffolds. Recently, the advantages of using lightweight metabiomaterials are limited to the unit cell geometry (K. Hazlehurst et al., 2013; Van Bael et al., 2012). Nonetheless, the relationship of the design of metabiomaterials to the performance under mechanical load and biological tests are lacking.

Although AM process has been employed and gained significance in the medical implants, the biocompatibilities of the produced components are scarce. The characterisation of designed and produced metabiomaterials for orthopaedic applications on mechanical and biocompatibility are important to perform. In addition, the effects of the metabiomaterials for both mechanical and biological compatibility have been studied by Wauthle et al. (2015), and there are limited studies done on the consideration of both mechanical and biological for Co-Cr-Mo metabiomaterials. In additional, previous studies reported that the porosity of 45%-90% are favourable for metallic implants with lower elastic modulus, while the pore size ranging from 200-1000 µm are suitable for cell ingrowth.

Thus, the studies on metabiomaterials with pore size bigger than this range have not yet been conducted. The success of cellular structure for lightweight, flexible and additional features of osseointegration has become popular in orthopaedic applications. From the literature, the mechanical properties and both *in vitro* and *in vivo* studies have been mostly performed in titanium-based metallic implants as the biomaterials exhibit biocompatibility for bone substitution. Although Co-Cr-Mo biomaterials are favourable for load bearing implants, there are limited studies for both mechanical properties and biocompatibility Co-Cr-Mo metallic implants produced by additive manufacturing.

In this research, the geometrical designs of metabiomaterials need to be determined. Followed by manufacturing of selected unit cells and finally the test should consist or carry out by two types of experimental which are mechanical properties and biocompatibility. In addition, physical evaluation should be carried out to determine in order to evaluate the accuracy and manufacturability of product quality.

CHAPTER 3

METHODOLOGY

3.1 General Introduction

This chapter elaborates the research strategies used to achieve the research objectives and aims of the designed and produced Co-Cr-Mo metabiomaterials manufactured through AM methods. The metabiomaterials is a possible way to reduce the mechanical stiffness to be comparable to human bone properties and provide space or accommodation of biological response into the interconnected porous structures. The experiment began with designing and physical simulation of metabiomaterials of two different unit cell types, namely square and diamond. Both the unit cell types were designed with rational unit cell length, L_{cell} and strut size Φ_S in order to produce the volume porosity in range of 40 to 90% as suggested in literature review chapter with pore size bigger than range of 200 to 1000 µm. Later, with the volume porosity, the effective elastic modulus, E_{eff} of the designed metabiomaterials were calculated in order to determine the elastic modulus that is comparable to human bone. After that, the preparation of samples for manufacturing process through AM is performed in producing metabiomaterials from Co-Cr-Mo powder as the selected metallic biomaterials. Then, metabiomaterials underwent post processing treatments for sample preparation for experimental characterisation. The produced metabiomaterials were characterised and evaluated physically for their morphology, manufacturability, accuracy, and density properties. The mechanical properties of produced metabiomaterials were determined experimentally in order to determine the elastic modulus and compression strength and compare with the stiffness of solid full dense Co-Cr-Mo parts. The biocompatibility of produced metabiomaterials was determined by *in vitro* (laboratory) study using animal cells at selected time point in order to observe the biological response of designed and produced metabiomaterials for implant devices.

The overall flow of the experiment particularly for designing, manufacturing and characterising sections of this study is illustrated in Figure 3.1.

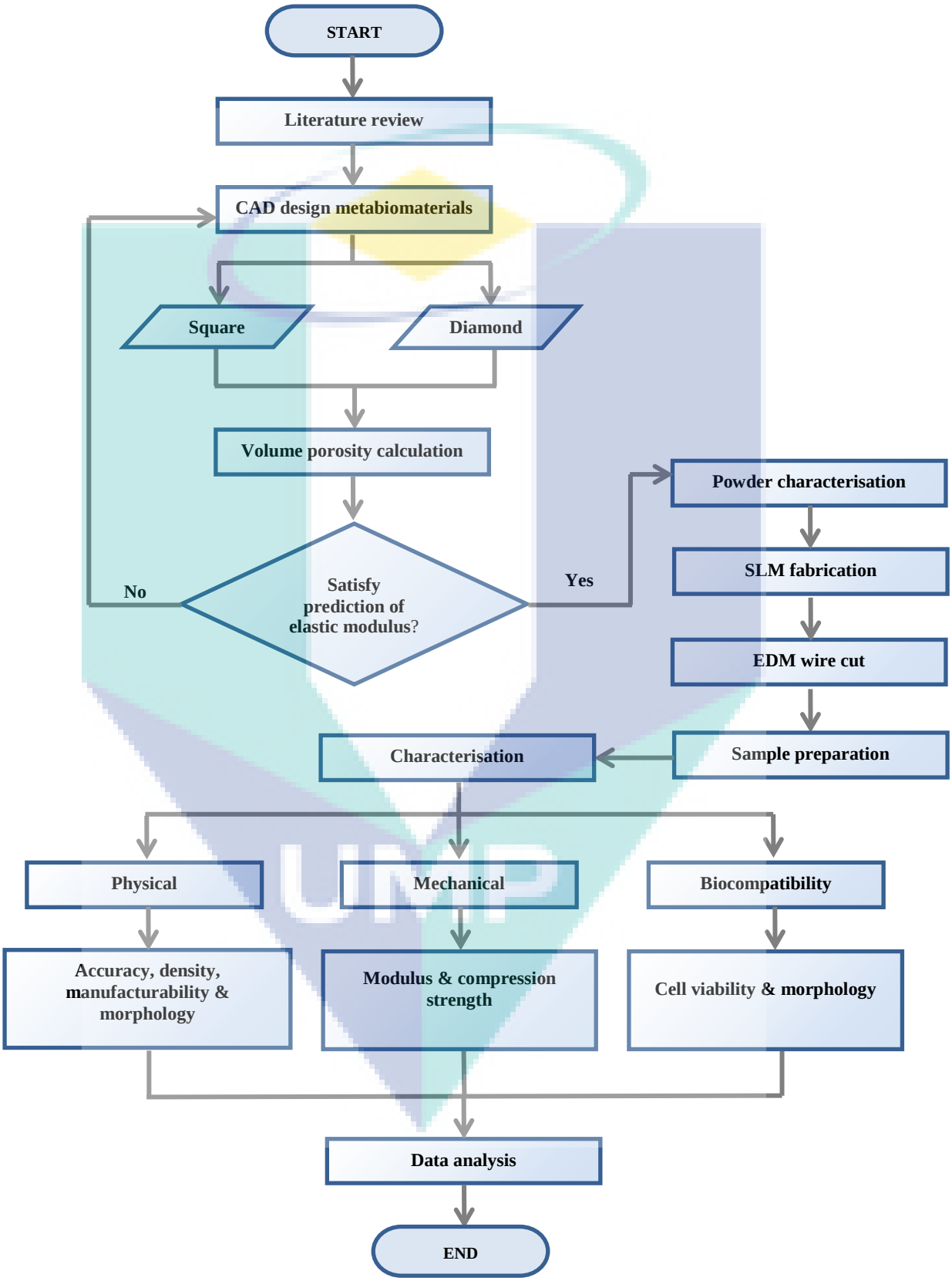

Figure 3.1 Flow chart of the research study

3.2 Design and Physical Simulation

This section discusses the details of metabiomaterials design based on the mathematical calculation of the designed metabiomaterials for the prediction of effective elastic modulus prior upon the manufacturing process. As discussed before, metabiomaterials were designed from unit cell and then were linearly patterned to form homogenous configurations.

3.2.1 Unit Cell of Metabiomaterials

The CAD models, square and diamond unit cell type of metabiomaterials, were selected for this research study and then was generated through SolidWork2013 software. The full dimensions of linearly replicated metabiomaterials into build parts can be referred to in Appendix C, respectively. The metabiomaterials were designed with rationally and highly controlled of varied geometrical parameters particularly for unit cell length, L_{cell} and strut size, Φ_s. Figure 3.2 shows the CAD models of unit cell metabiomaterials in this study.

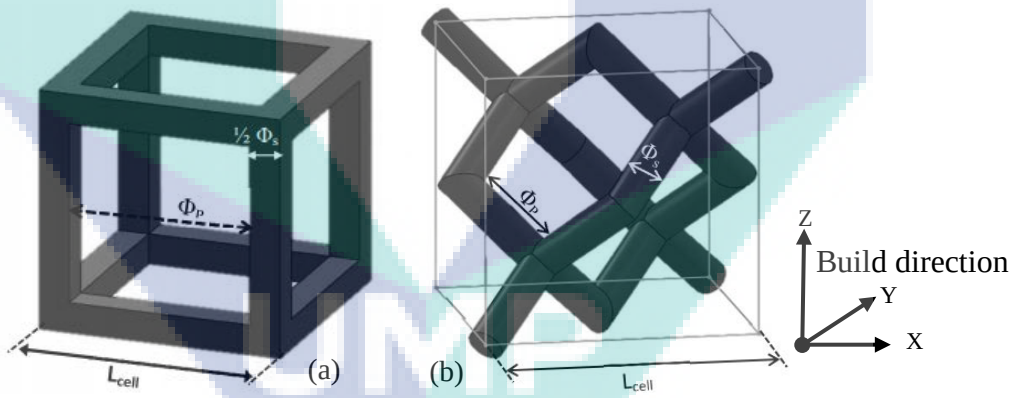

Figure 3.2 CAD models of unit cell type of metabiomaterials (a) square and (b) diamond unit cell type

The porosity of metabiomaterials was calculated according to the Equation 3.1 and Equation 3.2.

$$\varphi = V_P / V_B \qquad 3.1$$

$$V_P = V_B - V_S \quad (3.2)$$

Where: φ = Porosity;

V_P = Volume porous;

V_B = Volume bulk; and

V_S = Volume obtained from SolidWorks

The details of geometrical features including pore size and volume porosity of varied unit cell length, L_{cell} and strut size, Φ_S metabiomaterials are summarised in Table 3.1.

Table 3.1 Geometrical parameters of designed metabiomaterials

Unit cell	**Unit cell length, L_{cell} (mm)**	**Strut size, Φ_S (mm)**	**Pore size, Φ_P (mm)**	**Volume porosity (%)**
Square	1.5	0.4	1.1	79.8
		0.6	0.9	60.9
	2.0	0.5	1.5	81.2
	2.5	0.4	2.1	91.0
		0.6	1.9	81.7
Diamond	1.5	0.4	0.9	70.7
		0.6	0.7	44.8
	2.0	0.5	1.2	73.8
	2.5	0.4	1.7	88.1
		0.6	1.5	75.6

In this study, all the metabiomaterials were named according to prototype labelling as referred to in Figure 3.3.

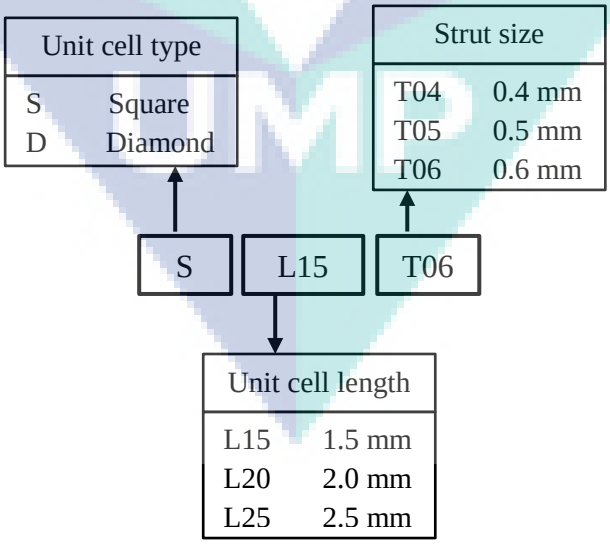

Figure 3.3 Prototype labelling for the metabiomaterials

Then, the files were converted to standard triangulation language (STL) file, and 2D sliced parts were generated prior to exporting to manufacturing machine setup. The full dense sample was also designed for control sample in order to compare the elastic modulus of solid samples and metabiomaterials and also to observe the response of cells on solid samples and metabiomaterials. The full dense samples of CAD model were shown in Figure 3.4 with dimension 12×12×15 mm.

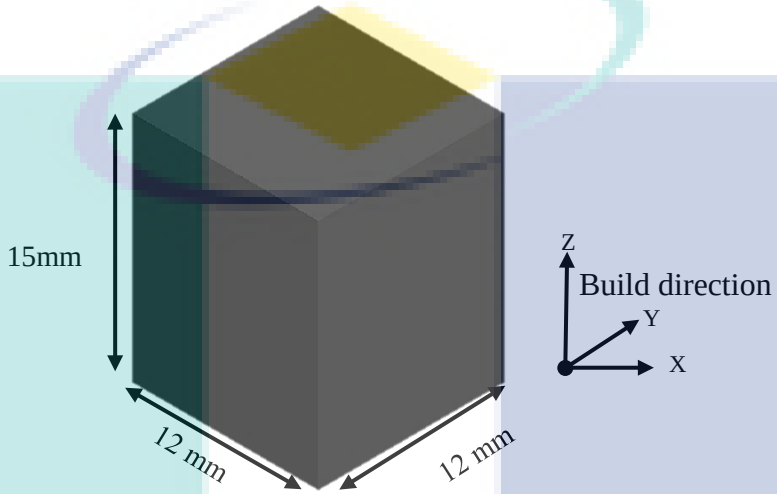

Figure 3.4 CAD models of full dense sample

3.2.2 Prediction of Effective Elastic Modulus using Gibson & Ashby Equation

In order to obtain a prediction of the effective elastic modulus of designed metabiomaterials, a model proposed by Gibson and Ashby (Gibson et al., 1999) was utilised and calculated using Equation 3.3 where the elastic modulus of solid material for Co-Cr-Mo is 220 GPa (Nakano, 2010).

$$E^*/E_s = C(\rho^*/\rho_s)^2 \qquad 3.3$$

Where: E^*= Elastic modulus of cellular structure;
E_s= Elastic modulus of solid material;
C= Constant;
ρ^*= Density of cellular structure; and
ρ_s= Density of solid material

From the Equation 3.3, it is proven that the elastic modulus is dependent upon the relevant density and the relevant density can be related to porosity by Equation 3.4 (Gibson et al., 1999).

$$(\rho^*/\rho_s)=1-\varphi \quad 3.4$$

Where: φ= Porosity

Therefore the Equation 3.4 can be rewritten as Equation 3.5 to calculate the effective elastic modulus (Gibson et al., 1999).

$$E_{eff}=E_s\left(1-\varphi\right)^2 \quad 3.5$$

Where: E_{eff}= Effective elastic modulus

Originally, the Gibson and Ashby model was developed to predict the elasticity of a three dimensional open cellular which is effective elastic modulus (E_{eff}) structure when the structure was loaded vertically upon unit cell geometry that is similar in this research study to determine the mechanical properties.

3.3 Manufacturing Process

This section states the overall manufacturing process of designed metabiomaterials using selective laser melting, one of the popular AM technologies in recent studies of metabiomaterials production. From the industry perspective, AM technologies have the potential to significantly impact the traditional manufacturing process due to dependencies of AM techniques on related technologies requirements such as mould and tooling. The selection of SLM, which is one of the AM technologies, is in consideration on fabrication of metabiomaterials with design flexibility on complex geometries shapes, increased need for industrial dimensional accuracy parts and time and cost efficiency in production run. The metallic biomaterials Co-Cr-Mo alloys due to suitability for load bearing implant for their excellent wear and fracture toughness as compared to other biomaterials (polymer and ceramic), also compared to other metallic biomaterials such as 316L stainless steel and titanium and its alloys. Co-Cr-Mo powder preparation

3.3.1 Co-Cr-Mo Powder Preparation

In this study, metabiomaterials were made from EOS GmbH Cobalt Chrome, which is Co-Cr-Mo based alloy in the powder form with the percentage principle alloying of Co (balance), Cr (27-30), Mo (5-7), Ni (0.5). The powder is suitable for

medical application and dental technologies due to their high biocompatibility, excellent corrosion resistance, and fatigue strength. The powder particle size, powder density and impurities, were investigated under scanning electron microscopy (SEM) and energy dispersive X-ray (EDX) in order to determine the particle powder size and chemical element composition of the powder focusing on amount of Ni elements. Then, the powder was loaded into preheated machine chamber at 150°C for automatic sieving. It was then followed with fabrication process.

3.3.2 Selective Laser Melting Fabrication Process

The designed samples were fabricated using selective laser melting process as one of the most famous AM technologies. The SLM manufacturing process was carried out using SLM® 125HL machine for production of the metabiomaterials used for morphology characterisation, static mechanical testing and biocompatibility. All the process occurred in enclosed chamber which continuously flushed with an inert argon atmosphere with purity of 5.0% in order to prevent oxidation and contamination of the produced components. The SLM machine used the 400 W Ytterbium fibre laser with an operation beam focus diameter to 80 µm and was preheated to 150 °C. The main process parameters for the selective laser melting process in this study, which include laser power, layer thickness, hatch spacing and scan speed, were the main factor for the output of energy density during the manufacturing process that affected the quality of the product outcomes as summarised in Table 3.3.

Table 3.2 Main parameters of selective laser melting manufacturing process

Parameter	**Value**
Laser power (W)	300
Scan speed (mm/s)	700
Hatch spacing (mm)	0.12
Layer thickness (µm)	30
Chamber atmosphere	Argon
Energy density (J/mm^3)	119.05

These factors determined the energy supplied by laser beam to a volumetric unit of material powder defined as energy density. Energy density has a large influence to density measurement of produced parts that lead to a higher density and also yield high residual thermal stress.

The energy density output during manufacturing process is calculated using Equation 3.6 (Taheri Andani et al., 2017).

$$Energy\ density = \frac{laser\ power}{laser\ speed \times hatch\ space \times layer\ thickness} \quad 3.6$$

3.3.3 Post Processing Treatments

All the fabricated samples were built by SLM process where a stainless steel-based plate is used as building platform and then left in the chamber until cooled down. After that, detachment of finish metabiomaterials from the base plate is performed using wire electrical discharge machining (EDM wire cut). The excessive support structures on the produced components were removed manually. The produced metabiomaterials were then subjected to a post processing of thermal stress-relieved through heat treatment that occurred in an argon atmosphere at temperature of 1050 °C for two hours which is then cooled down in the furnace (K. Hazlehurst et al., 2013). This is an effective way of relieving residual stress trapped inside the produced parts and allows partially melted powder on the struts to fuse and bond on the strut (Chunze et al., 2014).

The schematic graph of heat treatment for stress relief is shown in Figure 3.5, where the treatment started at the point of 30 °C with ramp time of 5 °C/min before soaking stage of 2 hours. All the treated samples were cooled down in furnaces.

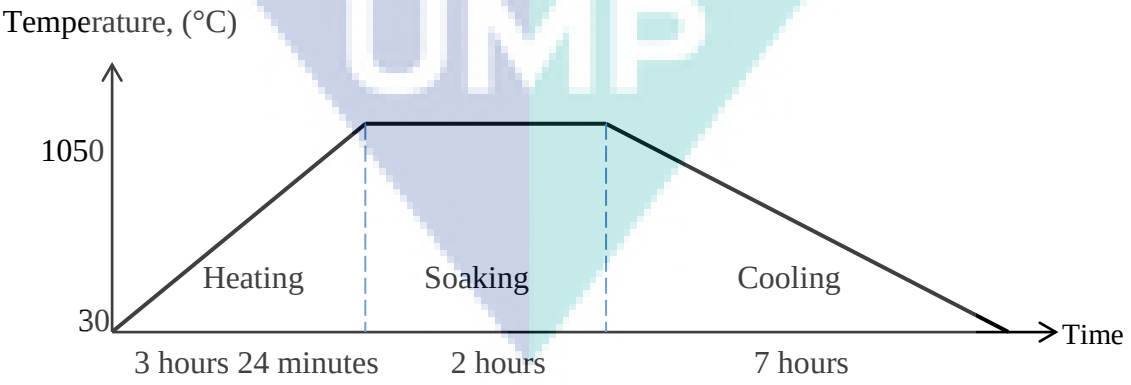

Figure 3.5 Schematic graph of stress-relieve on the samples

All the samples were placed in alumina boat and covered with alumina powder before proceed to the heat treatment procedures. The argon was used to flush out the

oxygen trapped in the furnace chamber and also to prevent the oxidation and contamination during the heat treatment. Figure 3.6 shows the sample preparation before the heat treatment where the samples were placed in alumina boat and then were covered with alumina powder in order to prevent the oxidation.

Figure 3.6 Components were placed in alumina boat before heat treatment

3.4 Physical Properties Evaluation of Metabiomaterials

This section states the details of experimental testing and evaluation on metabiomaterials characterisation including physical tests for surface morphology and manufacturability, where the optical microscope was used to observe the strut core feature and evaluate the strut size of the produced metabiomaterials. The dimensional accuracy was measured using vernier caliper and the tolerance was calculated while density and relative density were measured and calculated by using Archimedes' principle.

3.4.1 Surface Morphology and Manufacturability

An optical microscope (Dino-lite Digital Microscope) was used to investigate and analyses the strut size, Φ_S of produced samples in addressing the manufacturability and accuracy of SLM performance of the produced metabiomaterials. Ten dimensional values were measured at random point, and the average values were calculated for every measurement.

3.4.2 Dimensional Accuracy

The dimensional accuracy (print tolerance) determined the derivation of the finished model by comparing to the original CAD model. The dimensional accuracy of the produced metabiomaterials was measured using digital vernier caliper to determine

the shrinkage percentages, where ten random points were measured on the length, width, and height of the produced samples. The averages of dimensional measurement were then calculated. The standard deviation and errors of the dimensional accuracy were calculated to determine the accuracy of the manufacturing process on the produced metabiomaterials.

3.4.3 Density and Relative Density

The density of the fabricated metabiomaterials was measured according to Archimedes' principle. The relative density was calculated by the ratio of density of the produced metabiomaterials to the density of theoretical Co-Cr-Mo alloys. The calculation of density and relative density are according to Equation 3.7 and Equation 3.8, where the density of water, 1 g/cm^3 and theoretical density of Co-Cr-Mo alloys according to materials specification is 8.29 g/cm^3 (Dourandish et al., 2008).

$$Density, \rho = \frac{water\ density \times mass\ in\ air}{mass\ in\ air - mass\ in\ water} \quad 3.7$$

$$Relative\ density\ (\%) = \frac{measured\ density}{theoritical\ density} \quad 3.8$$

3.5 Mechanical Properties Evaluation of Metabiomaterials

Uniaxial compression testing was performed in order to determine the mechanical properties through Shimadzu, AGS-X series compression tester until the mechanical failure occurred by the samples. The compression test was performed at a constant speed of 0.1 mm/min with load of 100 kN (K. Hazlehurst et al., 2013) in order to obtain quasi elastic stage. All tests were run under normal atmospheric conditions with replication number for each design is n=3 as summarised in Table 3.4.

Table 3.3 Compression test parameter details

Machine	**Load, kN**	**Speed rate, mm/min**	**Replication number, *n***
Shimadzu AGS-X	100	0.1	3

The samples were loaded until failure occurred or until the 100 kN load capacity of the machined was reached. The stress stain curve for each individual component was

calculated and generated from the real-time force versus displacement data obtained from the test machine data. The following values were deviated from the compression test; (1) the elastic modulus as the slope of the compression stress-strain curve in the linear elastic region, (2) the compressive strength calculated by dividing the highest load by the support before the first fracture in force has occurred and (3) the compressive strain as the corresponding strain at the point of compressive strength. The testing set up was designed and performed in accordance to standard ISO (13314:2011), with the efforts shown in Figure 3.7 to ensure the uniaxial loading compression setup on produced component. The original length and area of all metabiomaterials can be referred to in Appendix C.

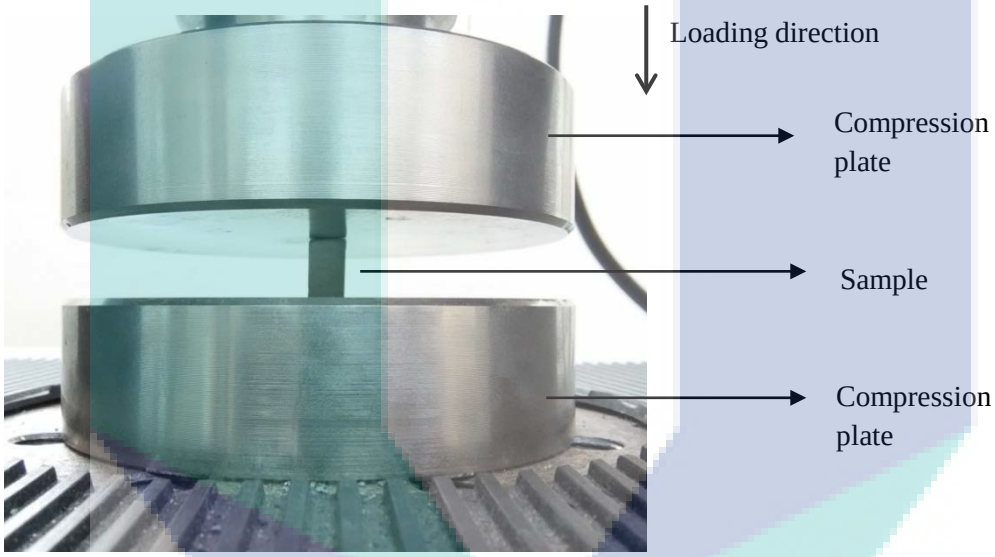

Figure 3.7 Experiment setup for uniaxial compression test

3.6 *In Vitro* Biocompatibility Properties

Biocompatibility testing was performed of an *in vitro* cytotoxicity test according to ISO 10993-5:2009 standard. The biocompatibility testing for this research study was preliminary study *in vitro* (in the laboratory) in order to determine the biocompatibility of produced metabiomaterials manufactured by SLM. The biocompatibility was determined by the viability cell using MTT assay and SEM observation on the selected time interval which is on day 14 and 21 of the cell culture. All the samples were assigned to two experimental groups, where the samples were sterilised using two different methods: (1) gamma irradiation ray and (2) autoclave technique. The overall flow for *in vitro* biocompatibility studies is illustrated in Figure 3.8.

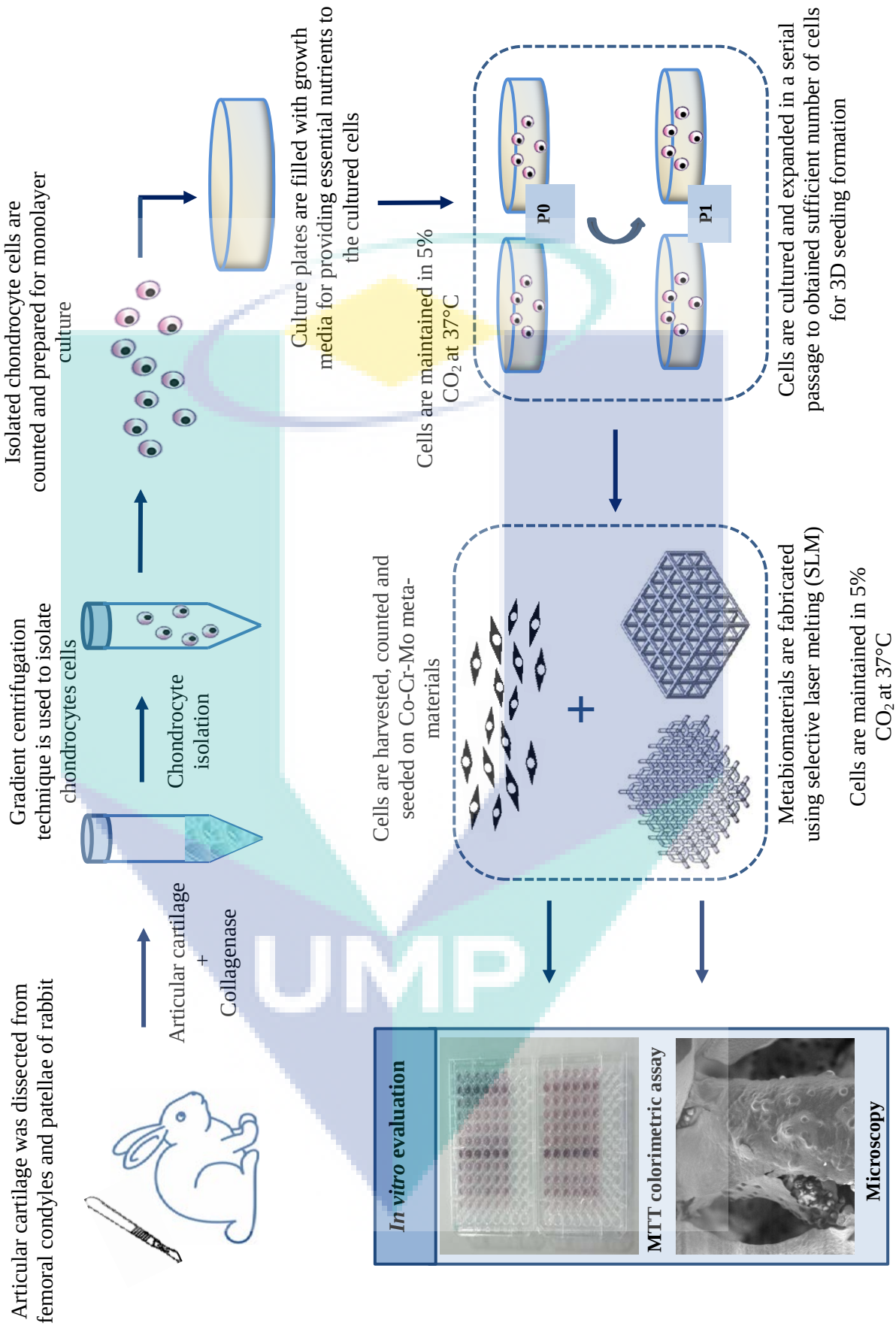

Figure 3.8 Experimental flows for *in vitro* biocompatibility test

3.6.1 Sterilisation Preparation

Sterilisation process in biological study refers to any process that eliminates all forms of microbial life including transmissible agents like fungi, bacteria and viruses from produced materials or any devices for medical applications (J. H. Park et al., 2012). The material or devices introduced *in vivo* and/or used for *in vitro* experiments must be sterilised to avoid subsequent infection that may lead to illness or death *in vivo* (in animal) and experimental failure *in vitro* studies (incubator) (Gu et al., 2012). Among various methods, ethylene oxide gas, gamma irradiation, and stem heat sterilisation (autoclave) are routinely used. Before materials for medical applications are approved for reuse, cleaning and sterilisation are key steps in the reconditioning of the devices to its initial state but may also contribute to the little modification from initial surfaces properties.

In this study, gamma irradiation was used where the gamma irradiation was selected due to strong ionized high energy to promote Deoxyribonucleic acid (DNA) damage of microbial without releasing toxic residues on materials (Allaveisi et al., 2014) with the dosage exposure of 25 kGy. Generally, 25 kGy dosage exposure is accepted as minimum required dosage to achieve the quality of bacterial reductions (Islam et al., 2015). The autoclave was used since it is the cheapest and basic sterilisation available in the laboratory as compared to with the gamma irradiated components results. The sterilisation method for metabiomaterials using gamma irradiation and autoclave is summarised in Table 3.5.

Table 3.4 Description of sterilisation techniques on metabiomaterials

Method	**Descriptions**
Gamma ray irradiation	Dose exposure = 25-40 kGy
Autoclave	Temperature range = 105-135 °C Liquid exposure= Ethanol Pressure = 0-4 MPa

3.6.2 Cell Preparation and Cell Culture

Articular cartilage was aseptically dissected from femoral condyles and patellae of an adult rabbit. The animal operation was performed under standard guidelines approved by the IIUM Research Ethics Committee (IREC) (reference number: IIUM/305/20/4/10). The articular cartilage was washed with phosphate buffered saline

(PBS pH 7.2) (Gibco, USA) containing 100 µg/ml penicillin and 100 µg/ml streptomycin. Then, the articular cartilage was minced into small fragments and digested with 0.6% collagenase A at 37 °C for 4 hours in orbital incubator at 250 rpm for chondrocyte isolation. The resulting cell suspension of chondrocyte cells was centrifuged at 60 rpm for 5 minute, 37 °C. The cell pellet was resuspended in PBS solution for total cell count with a haemocytometer. Cell viability was determined using the trypan blue dye exclusion test (Gibco, Invitrogen, USA). Harvested cells were then seeded in 6 well-plates (Thermo Scientific, Nunclon Delta Surface, Denmark) with initial seeding of 7,000 cells/cm2 in the primary passage (*P0*). Chondrocytes were cultured in equal mixture of Dulbecco's Modified Eagle Medium (DMEM) and F12 nutrient mixture (F12) supplemented with 10% foetal bovine serum (FBS) maintained in a standard condition of 37 °C and 5% humidified CO_2. All cultures were subcultured until passage 1 (*P1*) where the medium was changed every two days. The procedures steps in this section can be referred to in Appendix B4.

After confluence, the cells were harvested by trypsinization and counted for total cell and viability using haemocytometer. Approximately, 100,000 cells per sample were incorporated and resuspended in the culture medium for cell seeding. Cell suspensions in culture medium were seeded directly into each sample and were allowed to soak in orbital incubator at 130 rpm, 37 °C for 5 minutes. After soaking, all constructs were removed and placed into pre-wetted 24-wells plate for incubation in 5% CO_2 humidity at 37 °C with the medium changed every day. All constructs were cultured in 6-wells plate for each group for 14 for cell viability using MTT assay and day 21 for morphologies evaluation as in Figure 3.9.

Figure 3.9 Metabiomaterials were cultured media growth and culture until day 14 for cell viability test

3.6.3 MTT Cell Viability Assay

MTT cell viability was measured at day 14 of *in vitro* by using water soluble yellow tetrazolium MTT 3-(4, 5-dimethylthiazole-2-yl)-2, 5-diphenyltetrazolium-bromide that measures the decrease of tetrazolium component into a non-soluble formazan product by the mitochondria of living cells. The principle of MTT assay is the MTT solution enters the cells and passes into mitochondria, where it is reduced by mitochondrial dehydrogenases (enzyme) to an insoluble purple formazan product (Moodley et al., 2014).

After day 14 of culture, all constructs were transferred into new wells plate with 1 ml of new medium per well. 100 µl of MTT solution (0.5 mg/ml in PBS) was added into each well for 4 hour incubation at 37 °C with 5% CO_2 humidity. After incubation, all constructs were transferred into Eppendorf tubes (Eppendorf, Eppendorf Ag, Germany) that can be referred to in Appendix B4. Then, 1 ml per scaffold of dimethylsulfoxide (DMSO) was added to solubilize the formazan crystal at 1 hour, 37 °C in dark environment in order to minimise the reaction of light absorption of solubilized solution.

Then, 100 µl of solubilised mixture was taken by pipet and transferred into 96-well microtiter plates (NunclonTM Delta Surface, NUNC, Denmark). The solubilize solution was measured spectrophotometrically where the duplicate readings of absorption intensity were analysed by using ELISA plate reader (Versamax Microplate Reader, Molecular Devices, USA) at 570 nm yielding absorbance as a function of viable cell number that can be referred to in Appendix B4. The amount of formazan produced was directly proportional to the number of viable cells in the metabiomaterials.

3.6.4 Scanning Electron Microscopy Observation

The morphologies of the constructs were evaluated after day 21 using scanning electron microscopy (SEM). The samples were washed three times in PBS (Sigma) and fixed with 4% sterile paraformaldehyde (Sigma) for 1 hour. After fixation, the samples were rinsed again three times with PBS and subsequently dehydrated in a graded series of ethanol (30, 50, 70, 90 and 100%) for 10 minutes for each wash. All constructs were

placed in freezer and freeze-dried for 24 hours using freeze dryer to remove any remaining solvents before being observed under SEM.

3.7 Summary

In this research, the study of metabiomaterials was divided into three main parts which are designing, manufacturing, and experimental characterisations. The metabiomaterials were designed with two different unit cell types, namely square and diamond with varied geometrical parameters of L_{cell} ranging from 1.5 to 2.5 mm and Φs ranging from 0.4 to 0.6 mm generated using SolidWork software. Then, the files were converted into STL file for manufacturing process.

The metabiomaterials were manufactured using SLM created from medical graded Co-Cr-Mo powder. Prior to the manufacturing process, the powder had undergone microscopic evaluation where the average particles size was 22 µm and in spherical shape. The SLM manufacturing was performed in an inert atmosphere of argon gases to prevent contamination using default parameters supplied by manufacturer for Co-Cr-Mo components. The main manufacturing process parameters were power laser (300 W), scanning speed (700 mm/s), hatch spacing (0.12 mm) and layer thickness (30 µm) with energy density derived from these main process parameters of 119 J/mm^3. The produced metabiomaterials were detached using EDM wire cut from base plate, heat treatment at 1050 °C for 2 hours for stress relief and sterilisation for *in vitro* biocompatibility testing.

The metabiomaterials were characterised by experimental testing in order to determine their physical, mechanical, and biocompatibility properties. The morphology and manufacturability were observed and evaluated with optical microscope while the dimensional accuracy was evaluated with vernier caliper and tolerance. Meanwhile, by using Archimedes' principle, the density was measured and calculated for assessment of manufacturing accuracy and products qualities. Uniaxial compression testing with load 100 kN was performed to evaluate the elastic modulus and compression strength of metabiomaterials, and they were then compared with bone properties. *In vitro* biocompatibility was evaluated by MTT absorbance assay, where chondrocyte cells harvested from a rabbit were used. The absorbance was evaluated at yield wavelength of 570 nm as the function of number of viable cells in the metabiomaterials.

CHAPTER 4

RESULTS AND DISCUSSION

4.1 General Introduction

This chapter discusses the results obtained from experimental testing, which was performed in order to achieve the objectives of the research study of rationally design metabiomaterials. The metabiomaterials were designed with varied geometrical parameters including unit cell type of square and diamond, unit cell length, L_{cell} ranging from 1.5 to 2.5 mm, strut size, Φ_S in ranged of 0.4 to 0.6 mm and volume porosity of 44 to 88%. The metabiomaterials were fabricated by selective laser melting made from Co-Cr-Mo powder. The physical evaluation including surface morphology, manufacturability by optical evaluation, dimensional accuracy, density and relative density by Archimedes', were observed for the assessment of manufacturing process accuracy with default main parameters including laser power, layer thickness, hatch spacing and scan speed. The mechanical properties were evaluated by compression test with load 100 kN where elastic modulus, compression strength, and ultimate compression strength were obtained from stress strain curve. The elastic modulus of metabiomaterials was expected to match or be comparable to human bone properties, ranging from 1-30 GPa. The biocompatibility was evaluated from *in vitro* study by using MTT cell viability assay. Biological response between chondrocytes cell (cartilage cell) culture from rabbit with produced metabiomaterials that exhibited pore size ranging from 0.7 to 2.1 mm was observed. On the other hand, the cytotoxicity of produced metabiomaterials by selective laser melting was determined by absorbancy MTT assays toxicity and biocompatibility of samples on animal cells. The morphology evaluation after cell culture for highest cells attached on samples was carried out using scanning electron microscopy.

4.2 Designed Metabiomaterials

CAD models of square and diamond metabiomaterials were generated through SolidWork software with rational unit cell lengths and strut sizes. The metabiomaterials were designed for possible ways to reduce stiffness of metallic biomaterials for load bearing implants and provide the space for biological response of cell in-growth into the metabiomaterials for tissue regeneration and biological fixation.

4.2.1 Geometrical Parameter Details of Metabiomaterials

The unit cell metabiomaterials was designed of square and diamond with varied unit cell length, L_{cell} range 1.5 to 2.5 mm and strut size, strut size, Φ_S in range of 0.4 to 0.6 mm. Table 4.1 summarises the individual components of metabiomaterials. The full dimension for each designed component was provided in the table. The full dimension of CAD model for each metabiomaterials can be referred to in Appendix B2.

Table 4.1 Geometrical of designed metabiomaterials

Sample	Pore size (mm)	Porosity (%)	Dimension (mm)
SL15T04	79.8	79.8	12.4×12.4×15.4
SL15T06	60.9	60.9	12.6×12.6×15.6
SL20T05	81.2	81.2	12.5×12.5×16.5
SL25T04	91.0	91.0	12.4×12.4×15.4
SL25T06	81.7	81.7	12.4×12.4×15.6
DL15T04	70.7	70.7	12×12×15
D L15T06	44.8	44.8	12×12×15
D L20T05	73.8	73.8	12×12×16
DL25T04	88.1	88.1	12.5×12.5×15
D L25T06	75.6	75.6	12.5×12.5×15

4.2.2 Physical Simulation of Effective Elastic Modulus

The Gibson and Ashby model was originally developed to predict the stiffness of three-dimensional open cellular structure when load is applied vertically upon unit cell geometry, which is a similar method used in this study (Gibson et al., 1999). Previous studies, which have indicated the use of the Gibson and Ashby model, agreed well with the values obtained from mechanical testing of cellular structures (J. P. Li et al., 2006; Mattew et al., 1995). The effective elastic modulus was obtained from the mathematical calculation for each individual metabiomaterials design.

Table 4.2 shows the effective elastic modulus of metabiomaterials, where it is directly proportional to the volume porosity. The labelling for metabiomaterials in the table can be referred prototype labelling in previous chapter (Figure 3.3). From the table, the highest effective elastic modulus was obtained from metabiomaterials of diamond unit cell with unit cell length, 1.5 mm, strut size, 0.6 mm and volume porosity of 44.8%. The effective elastic modulus obtained is 61.1 GPa. However, the square unit cell metabiomaterials with the same unit cell length and strut size also obtained high effective elastic modulus which was 30.6 GPa. However, the obtained effective elastic modulus is out of human bone properties range (1-30 GPa). The metabiomaterials exhibited low volume porosity due to more dense struts compared to the metabiomaterials with unit cell length of 2.0 mm and 2.5 mm. Overall, the rest of design metabiomaterials yielded the effective elastic modulus that was in range of human bone properties (1-30 GPa).

Table 4.2 Effective elastic modulus using Gibson and Ashby model

Sample	**Porosity (%)**	**Effective stiffness, E_{eff} (GPa)**
SL15T04	79.8	8.2
SL15T06	60.9	30.6
SL20T05	81.2	7.1
SL25T04	91.0	1.6
SL25T06	81.7	6.7
DL15T04	70.7	17.1
D L15T06	44.8	61.1
D L20T05	73.8	13.7
DL25T04	88.1	2.8
D L25T06	75.6	11.9

Meanwhile, Figure 4.1 shows the relationship of porosity and effective elastic modulus for square and diamond unit cells respectively with an indication of effective elastic modulus by Hazlehurst et al. (2013). The Gibson and Ashby equation was used to predict the obtainable elastic modulus based on the volume porosity theory. A bigger different of effective elastic modulus of physical test and prediction by Gibson and Ashby equation for metabiomaterials with lower than 60% volume porosity was shown in the graph. Interestingly, the elastic modulus for higher volume porosity are met a good agreement as the values are closer to the prediction values. Thus, experimental elastic modulus of metabiomaterials is predicted to have lower than modulus that obtained through Gibson and Ashby equation.

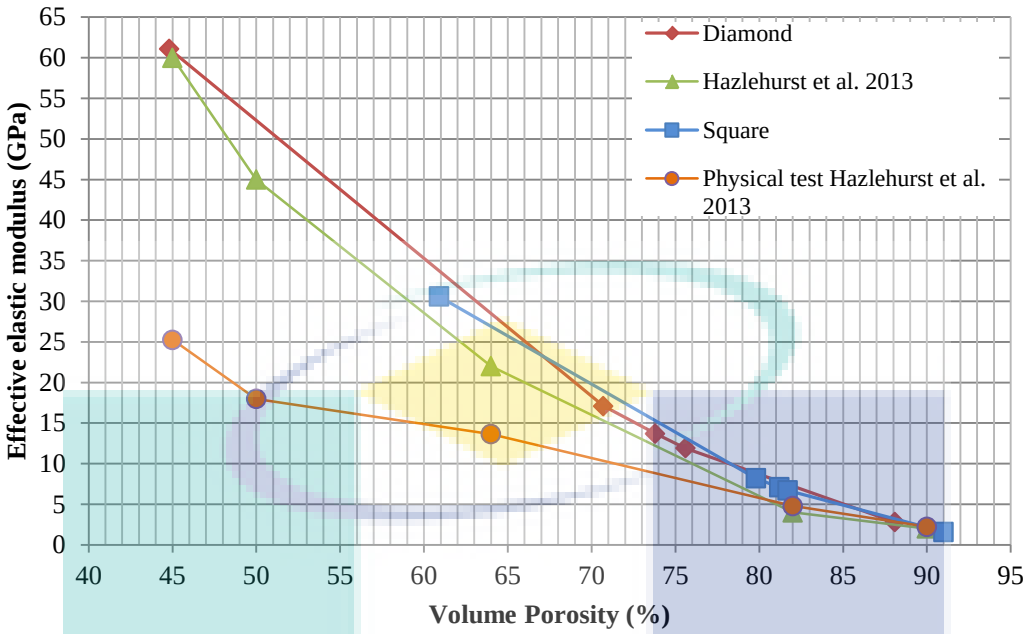

Figure 4.1 Relationship of porosity of metabiomaterials with effective elastic modulus square and diamond unit cell type

4.3 Manufactured Metabiomaterials

Prior to the manufacturing process using selective laser melting, the Co-Cr-Mo powder underwent morphological study by scanning electron microscope. Examination of powder revealed the major particles with a regular spherical and some irregular shape shown in Figure 4.2. The cross section in the figure shows the majority of the particle size 20-25 µm. As the average, the commercial Co-Cr-Mo alloys powder exhibit the particle size in the range of 22 µm (Hedberg et al., 2014). Figure 4.3 shows the EDX analysis results. Table 4.3 summarises the Co-Cr-Mo alloying chemical composition based on EDX analysis that comparable with standard materials element provided by manufacturer. The amount of Ni element was 0.1 *w*% where the Ni toxicity concern in biomaterials is less than 1 *w*% (M. Talha, 2013).

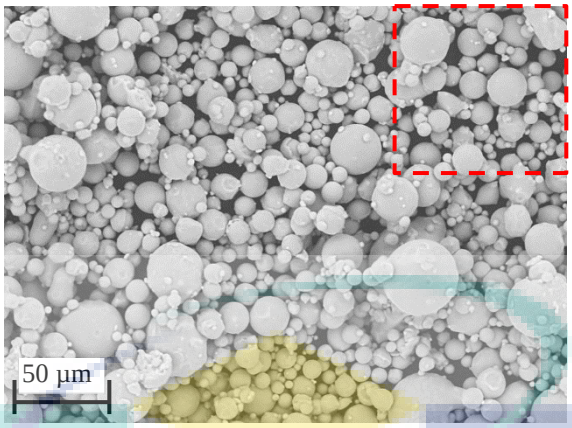

Figure 4.2 SEM images of Co-Cr-Mo powder

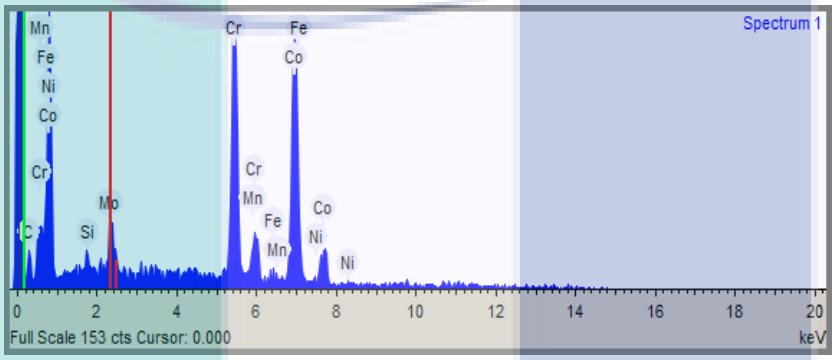

Figure 4.3 EDX analysis on Co-Cr-Mo powder

Table 4.3 Alloys composition of Co-Cr-Mo powder element (*w*%)

Element	**Co**	**Cr**	**Mo**	**Si**	**Mn**	**Fe**	**Ni**
Standard	60-65	26-30	5-7	1.0	1.0	0.75	0.1
EDX	61	30	5	0.6	1.0	1.0	0.1

After cooling temperature occurred, the produced metabiomaterials were taken out from the machine chamber. From the figures, square unit cell types were fabricated with the support angle of 45° in order to reduce the overhang on the samples. Meanwhile for diamond unit cell, the build direction was from bottom to top directions. Figure 4.4 shows the samples after fabrication process, where the samples were built on the stainless-steel plate. The produced metabiomaterials were then detached from the stainless-steel based plate using wire cut EDM and were prepared for physical evaluation for surface morphology and manufacturability used as built components as illustrated in Figure 4.5.

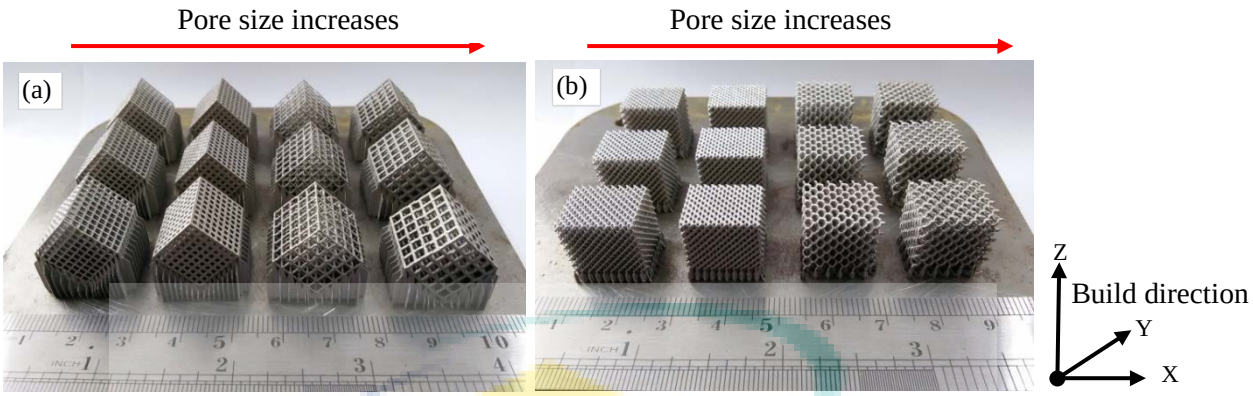

Figure 4.4 Produced metabiomaterials using selective laser melting on base plate a) square and b) diamond unit cell type

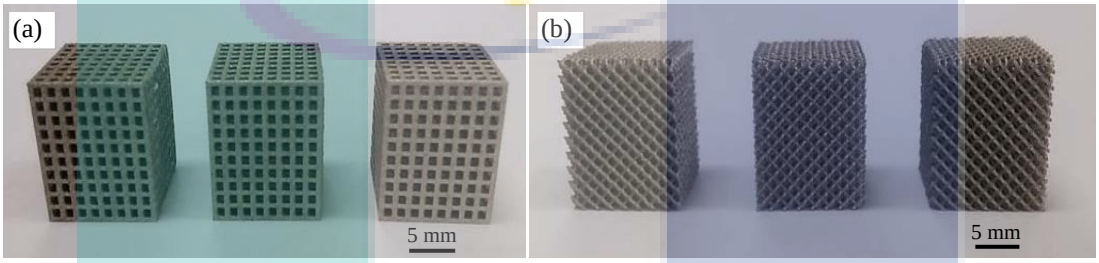

Figure 4.5 Produced metabiomaterials after detached from base plate a) square and b) diamond unit cell type

All excessive supports remained at the components was removed manually before undergoing stress relief by heat treatment at temperature 1050 °C for 2 hours. The heat-treated components underwent mechanical compression. Then, the results of the morphology, density, and dimensional accuracy will be discussed in the next section. The SLM manufacturing process has demonstrated that metabiomaterials designed for square and diamond unit structure with unit cell length, L_{cell} 1.5 to 2.5 mm and strut size, Φ_S 0.4 to 0.6 mm can be fabricated using standard operating parameters for Co-Cr-Mo. Table 4.4 shows the top and side view of metabiomaterials after all the supports were removed. All the samples are solid, interconnected and in good conditions where there are no defects as compared to CAD models.

Table 4.4 CAD view and actual view of the produced metabiomaterials

Sample	CAD top	Actual top	CAD front	Actual front
SL15T04	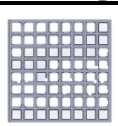		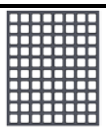	
SL15T06		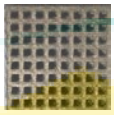	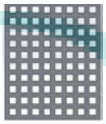	
SL20T05	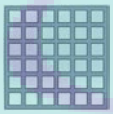	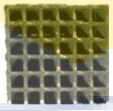	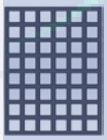	
SL25T04	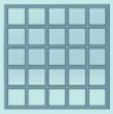	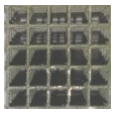	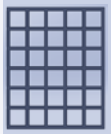	
SL25T06				
DL15T04	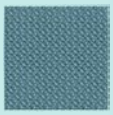			
DL15T06	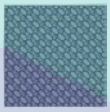	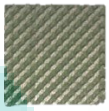		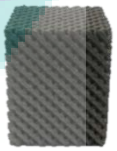
DL20T05	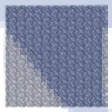	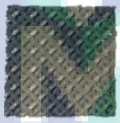	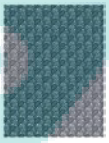	
DL25T04		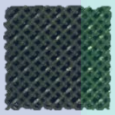		
DL25T06		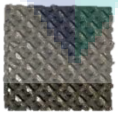		

5 mm

4.4 Physical Properties Evaluation

Physical properties evaluations of produced Co-Cr-Mo metabiomaterials were determined to confirm their surface morphology and manufacturability. The strut size of component was measured using optical evaluations, whilst the dimensional accuracy was determined by measuring the features of length, width and height of produced metabiomaterials. Lastly, density and relative density of produced metabiomaterials was determined using Archimedes' principle by the ratio of density of produced metabiomaterials with theoretical materials specification.

4.4.1 Surface Morphology and Manufacturability

The optical microscope images of as-built metabiomaterials are shown in Figure 4.6 where they clearly show that struts of meta-biomaterial were well fabricated by SLM process, where the struts are solid and interconnected even though the surfaces were rough. From the morphology evaluation, the struts of diamond metabiomaterials are smoother compared to square metabiomaterials. This is due to higher porosity percentage resulted bigger overhang on the square metabiomaterials.

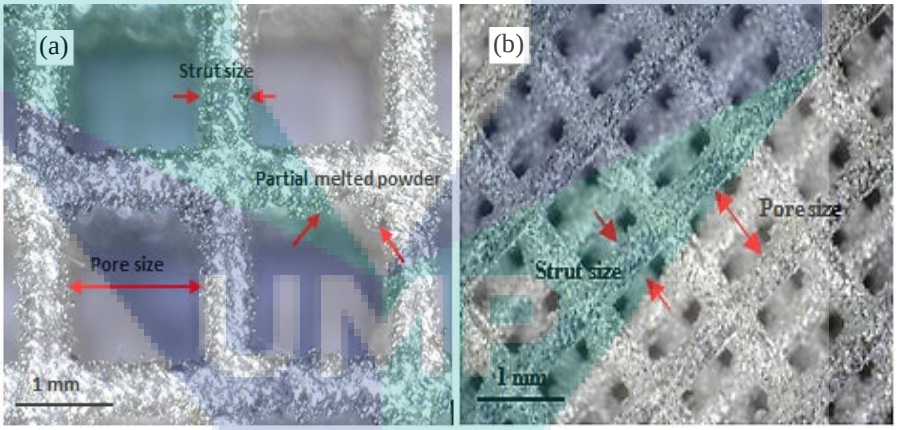

Figure 4.6 Optical microscope image of metabiomaterials of a) square and b) diamond

The rough surface was due to the existence of partially melted powder that bonded to the strut surfaces. The bonded powder particles on the strut surface were caused by two main factors; (1) the partially melted metal powder particles on the boundary of each layer in the SLM manufacturing process by contour laser track (Yan et al., 2012) and (2) angle strut was partially solidified on the loose powder due to big difference in temperature, leading to powder particles sticking to the strut surface (Chunze et al., 2014; Van Bael et al., 2011).

The struts size of produced metabiomaterials was measured using optical microscope at ten random points of each metabiomaterials (n=3) and the averages of strut sizes are summarised in Table 4.5. According to the table, the strut size are presented as 0.41, 0.61, 0.51, 0.41 and 0.61 mm against the designed strut size of original CAD models of 0.40, 0.60, 0.50, 0.40 and 0.60 mm for square unit type. The increase in the strut size compared to the original CAD models is the result of the partially melted powder particles which are attached to the strut core and melt pool size on the strut boundaries. From the table, the average actual strut sizes for square unit cell are higher than original CAD model. The overhang phenomenon as stresses tend to dross formation occurred at unsupported region on square unit cells and partially melted powder particles increased the average values of actual strut size.

Table 4.5 Manufacturability measured at strut sizes of produced metabiomaterials

Unit cell type	**Unit cell length, L_{cell} (mm)**	**Model strut, Φ_S (mm)**	**Actual strut, Φ_S (mm)**
Square	1.5	0.4	0.41 ± 0.002
		0.6	0.61 ± 0.004
	2.0	0.5	0.51 ± 0.003
	2.5	0.4	0.41 ± 0.001
		0.6	0.61 ± 0.002
Diamond	1.5	0.4	0.39 ± 0.011
		0.6	0.60 ± 0.008
	2.0	0.5	0.49 ± 0.006
	2.5	0.4	0.40 ± 0.004
		0.6	0.60 ± 0.003

On the other hand, the struts measured for diamond unit cell type are in good agreement with designed strut size. Interestingly, the good agreement of manufacturability is related to self-support feature exhibited in diamond unit cells type was due to inclination angle between the two adjacent layers of strut. The inclination angle of strut has the capability to support the fabrication of next layer after the first scanned layer during the manufacturing process (Yan et al., 2015). However, the smaller strut size of 0.4 and 0.5 mm resulted in inaccuracy and shrinkage due to loss connectivity between adjacent cell layers. In addition, the strut size of diamond types with 0.4 and 0.5 mm are too thin to be fabricated by SLM process. Moreover, it is important to notice that the strut angles for diamond type are lower than 45° from the horizontal plane or overhanging angle (>45°). Hence, deformation will occurred during

fabrication as the struts are mostly built on loose powder that can lead to the defect of the produced components (Mullen et al., 2009; Santorinaios et al., 2006)

4.4.2 Dimensional Accuracy

Dimensional accuracy of the produced metabiomaterials was measured to determine the shrinkage and the accuracy agreement with original CAD model. For each linear measurement of the feature length, width and height, the dimensional error was calculated as the absolute difference (mm) between the values obtained from the produced metabiomaterials and the CAD models of each component (Silva et al., 2008). The measurement and calculation of standard deviation and error of accuracy for each individual metabiomaterials, including the samples for full dense, are represented in Table 4.6. From the table, error of designed and measured dimensional was obtained is in range of 0.03 to 0.77%. The errors of less than 1% indicated the high accuracy of SLM with default parameters (Calignano, 2014).

Table 4.6 Dimensional measurements of produced metabiomaterials

Sample	Designed dimensional (mm)	Measured dimensional (mm)	Standard deviation (mm)	Error (%)
SL15T04	12.4×12.4×15.4	12.6×12.6×15.3	0.02	0.65
SL15T06	12.6×12.6×15.6	12.7×12.8×15.5	0.02	0.77
SL20T05	12.5×12.5×16.5	12.7×12.7×16.5	0.05	0.06
SL25T04	12.9×12.9×15.4	13.2×13.2×15.5	0.01	0.32
SL25T06	13.1×13.1×15.6	13.3×13.3×15.6	0.01	0.03
DL15T04	12×12×15	12.1×12.1×15.1	0.01	0.33
DL15T06	12×12×15	12.1×12.1×15.0	0.02	0.20
D L20T05	12×12×16	12.2×12.1×16.0	0.03	0.43
D L25T04	12.5×12.5×15	12.7×12.6×15.0	0.03	0.20
D L25T04	12.5×12.5×15	12.6×12.6×15.0	0.05	0.20
Full dense	12×12×15	11.9×12.0×15.0	0.06	0.13

For additional results of dimensional accuracy, a comparison on the height of each metabiomaterials is developed to determine the significant in shrinkage in build-up direction. Figure 4.7 shows the comparison of design height and measured height of produced metabiomaterials. From the graph, the square unit cell type with the unit cell length 1.5 mm and strut size of 0.4 and 0.6 mm show the shrinkage on the height dimension compared to CAD model measurement with 0.02 mm. Meanwhile, the diamond metabiomaterials have no significance in shrinkage behaviour. During the

SLM process, the short interaction of powder bed and heat source caused by the scanning speed of laser beam leads to rapid heating and the melting stage followed drastically (Dongdong et al., 2009; Zhou et al., 2015). This phenomenon caused the shrinkage in the components.

Figure 4.7 Dimensional of height of square and diamond metabiomaterials including full dense

On the other hand, the square unit cell with unit cell length 2.5 mm and strut size of 0.4 mm obtained the expand dimension due to broaden of the pore with 0.01 mm. It is due to the length of unsupported region in the square was expanded and then lead to increment of critical overhang dimension on the strut section. It is due to the as the top layers of the pores were scanned on loosed powder metallic powder, the melt pool sinks deep into underneath the powder and lead to formation of dross on the overhang region. This phenomenon also affects the diamond unit cell type of unit cell length 1.5 mm and strut size 0.4 mm with 0.01 mm related to their strut angle. The strut size enlarged on width at the strut angle that close to horizontal plane due to formation of melt pool sank deeper underneath of the powder during manufacturing process (Taib et al., 2016). There is no significant difference on height dimension accuracy for the rest of produced diamond unit cell metabiomaterials.

4.4.3 Density and Relative Density

The measured densities of fabricated Co-Cr-Mo metabiomaterials are calculated by using Archimedes' principle. Relative density was calculated by the ratio of measured density with specific density of Co-Cr-Mo alloys of 8.29 g/cm^3. The measured density and relative density for produced metabiomaterials and full dense sample are summarised in Table 4.7.

Table 4.7 Density and relative density of the produced Co-Cr-Mo metabiomaterials

Sample	Porosity (%)	Measured density (g/cm^3)	Relative density (%)
SL15T04	79.8	8.09 ± 0.07	97.67 ± 0.07
SL15T06	60.9	7.67 ± 0.45	92.49 ± 0.45
SL20T05	81.2	7.92 ± 0.15	95.52 ± 0.15
SL25T04	91.0	7.75 ± 0.14	93.48 ± 0.14
SL25T06	81.7	7.99 ± 0.17	96.37 ± 0.17
DL15T04	70.7	7.02 ± 0.62	84.68 ± 0.62
D L15T06	44.8	7.69 ± 0.32	92.70 ± 0.32
DL20T05	73.8	7.40 ± 0.39	89.29 ± 0.39
D L25T04	88.1	8.07 ± 0.07	97.29 ± 0.07
DL25T06	75.6	7.67 ± 0.29	92.57 ± 0.29
Full dense	-	8.23 ± 0.01	99.29 ± 0.01

According to the table, the relative densities of all metabiomaterials are varied in range from 84.7 to 97.7%. Meanwhile, relative density for full dense sample is of 99.3%. The relative density of full dense sample indicate that the produced Co-Cr-Mo parts demonstrated the possession of low porosity which might be developed as consequences of balling formation and entrapment of gas in melting powder (Mumtaz et al., 2008). A high energy input during manufacturing process has influenced and lead to a higher density of the produced parts. A reduction of porosity in the manufactured parts is due to increased energy density that results in a higher attained temperature of melted powder and therefore promotes an improved interlayer connection between layers in sample parts (M. Xia et al., 2016).

Thus, the correlation between volume porosity and the density and relative density has investigated. Figure 4.8 shows the graph of density and relative density for square and diamond metabiomaterials comparable to full dense density.

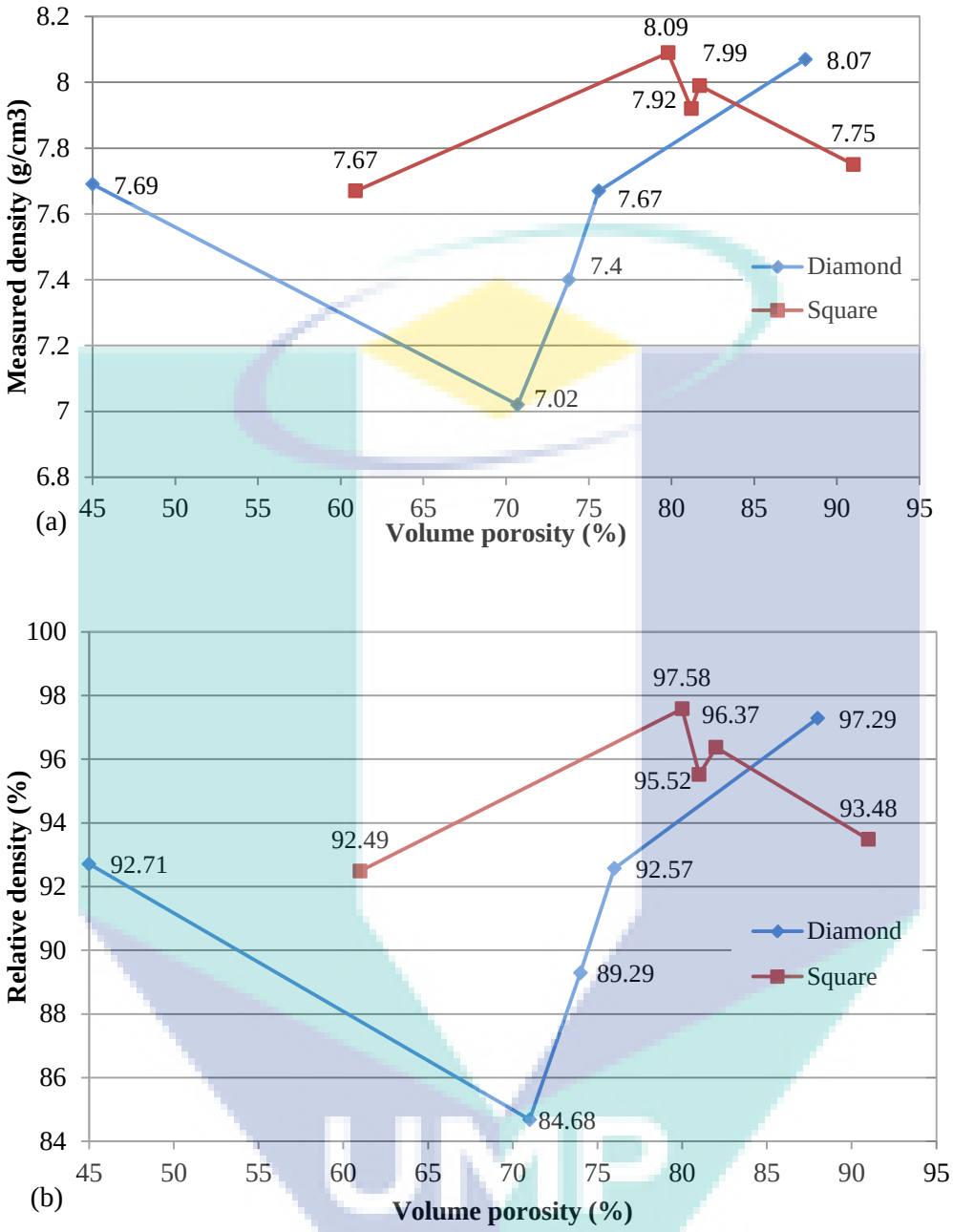

Figure 4.8 Relationship of a) measured density and b) relative density between volume porosity of metabiomaterials

From the graph, the density and relative density of square and diamond metabiomaterials shown to decreased with increasing volume porosity due to less solid strut in the metabiomaterials component. However, for metabiomaterials with bigger strut size of 0.6 mm even that share same unit cell length which is square with 1.5 mm strut size and diamond with 2.5 mm strut size possesses lower density and relative density. These might due to more partially melted powder and more pores on the bigger

solid struts. The cross section area of strut might become smaller in the internal of metabiomaterials component. The scan vector lengths may become shorter when the scanning area becomes smaller for bigger strut size. Hence, the adjacent tracks are scanned more swiftly one after the other layer and leaving less cool down time in between them that lead to higher temperatures of the scanned boundaries (Chunze et al., 2014; Yan et al., 2012).

Consequently, better wetting conditions presented to form denser strut in the smaller strut size for both square and diamond unit cell types. Jean et al. (2005) noted that the processing parameters and scan strategy during SLM manufacturing process play an important role in produced high density components. Therefore, it is worthy to carefully investigate the effects of the SLM process parameters and scan strategy on the products density in the future works. It is seem that better density of the metabiomaterials could be achieved at the smaller strut size and to confirm the cross section on the internal structure of metabiomaterials, evaluation using micro-CT images could be suggested as studied by Chunze et al. (2014) and Pyka et al. (2014).

4.5 Mechanical Properties Characterisation

One of the main goals of this study is to obtain the metabiomaterials with tailored mechanical stiffness with an improved strength to weight ratios comparable to the human bone properties. Thus, from compression test, the elastic modulus exhibited properties with trabecular bone. The results of the compression test that includes elastic modulus, 0.2% yield strength and compression strength are summarised in Table 4.8.

Table 4.8 Mechanical properties of metabiomaterials

Sample	**Elastic modulus, *E* (GPa)**	**0.2 % Yield Strength (MPa)**	**Compression strength (MPa)**
SL15T04	4.47 ± 0.67	47.68 ± 0.77	59.97 ± 2.37
SL15T06	8.75 ± 0.12	154.93 ± 1.23	245.03 ± 4.25
SL20T05	2.91 ± 0.66	54.30 ± 1.28	46.67 ± 0.83
SL25T04	0.92 ± 0.09	12.08 ± 1.28	11.81 ± 1.12
SL25T04	2.10 ± 0.05	46.88 ± 2.08	41.10 ± 1.77
DL15T04	2.83 ± 0.21	73.85 ± 2.60	62.93 ± 3.97
D L15T06	7.47 ± 0.08	247.68 ± 1.50	240.08 ± 0.99
DL20T05	2.29 ± 0.09	54.48 ± 2.17	44.59 ± 0.99
D L25T04	0.45 ± 0.02	11.40 ± 0.94	10.77 ± 5.49
DL25T06	1.93 ± 0.10	44.54 ± 1.53	40.04 ± 1.63
Full dense	224.63 ± 0.27	NA	NA

According to the Table 4.8, the elastic modulus for all designed Co-Cr-Mo metabiomaterials is decreased in elasticity values. It is shown that the elastic modulus of the metabiomaterials is within the range of 0.44 and 8.75 GPa. The values of elastic modulus are comparable with the elastic of human cancellous bone (10 to 15,700 MPa) (An et al., 1999). However, the ultimate compression strength and compression strength of full dense sample cannot be obtained due to limitation of the machine load. Hence, for future works, it is recommended to use the compression tester with higher loading. As expected, the elasticity of Co-Cr-Mo can be tailored when the cellular structure was employed on the bulk components particularly the highly controlled of geometrical parameters as in metabiomaterials structure (Malek et al., 2015).

The evolution of deformation and failure for the metabiomaterials was dominated by the shear stress at the 90° for square type metabiomaterials and at 45° for the diamond type metabiomaterials. On the other hand, the failure of square was largely due to the bending, whereas the failure for diamond metabiomaterials was largely due to the bulking at low density or thin strut (Limmahakhun et al., 2017).

The conditions of metabiomaterials before the loading were applied during uniaxial compression test, and the fracture behaviours after maximum load achieved are summarised in Table 4.9. From table, square metabiomaterials exhibit the fracture at the bottom part in uniaxial compression testing except the metabiomaterials SL15T06, where the part bending was due to the bigger solid strut of 0.6 mm. It was observed that buckling and fracture towards diagonal axis for diamond metabiomaterials. The cell struts began to bend under compressive loading, and after slight bending, some of the struts experienced brittle fracture. In this case, the deformation or fracture shows that for square type metabiomaterials, horizontal shear band at the bottom parts has been observed after bending, whereas, an observation of a diagonal (45°) shear band of the diamond type metabiomaterials has been observed after buckling in the struts. Previously, this behaviour has been documented similarly by (Hasan et al., 2011; Maskery et al., 2016; Qiu et al., 2015).

Table 4.9 Initial and fracture stage of metabiomaterials of compression test

Sample	Initial	Fracture
SL15T04		
SL15T06		
SL20T05		
SL25T04		
SL25T04		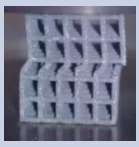
DL15T04		
D L15T06	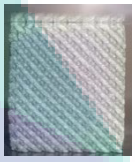	
DL20T05		
D L25T04		
DL25T06		

5 mm

The orientation of the unit cells of metabiomaterials attributed to unit cell length, the position of the strut towards the force loading, and the position of strut angle affected the mechanical properties and materials behaviour. These factors resulted in the 45° shear deformation on twisted type structure such as diamond metabiomaterials (Weißmann et al., 2016). The anisotropic geometries of the structure are important to be taken into account due to the influence of the strut to acting force on the mechanical properties. The cell size and porosity play a role in the mechanical behaviour and have a good agreement with other researchers (Andrews et al., 2001; Onck et al., 2001).

The stress-strain curves of the compression tests on the square and diamond metabiomaterials are shown in Figure 4.9. The stress strain curves were split into separated graphs of compression strength above 100 MPa and below 100 MPa. From the stress-strain curve, the metabiomaterials experienced an initial settling period represented plateau stress which is show as non-linear and concave upwards line. The behaviour might due to uneven flat surface and broken strut edges when they are detached or cut from post processing. After that, the stress-strain curves show an elastic region due to plastic deformation of metabiomaterials with the high degree of linearity. The diamond metabiomaterials with volume porosity of 44.8, 70.7, 73.8, and 75.6 % show the bigger elastic region compared to square metabiomaterials. This indicated higher strut strength of diamond metabiomaterials under compressive strength.

The modulus and initial yield strength of dominated to bending and buckling behaviour of metabiomaterials. The elastic modulus are much greater for metabiomaterials that in range of volume porosity lower than 81% which is samples with unit cell length 1.5 and 2.0 mm. This is related to higher relative density of the metabiomaterials. Following that, deformation occurred shown the elastic-plastic behaviour of metabiomaterials which is indicated the ductility and brittleness of metabiomaterials. The diamond metabiomaterials are tougher and ductile compared to square metabiomaterials due to capability to absorb energy during loading impact and higher resistance to plastic buckling. This behaviour indicated to the curve of the line with expanded strain. Square metabiomaterials are strong except for SL25T04 but more brittle due to less strut features to support the unit cells from fracture under high loading. Final stage is the fracture or failure occurred at the higher loading force.

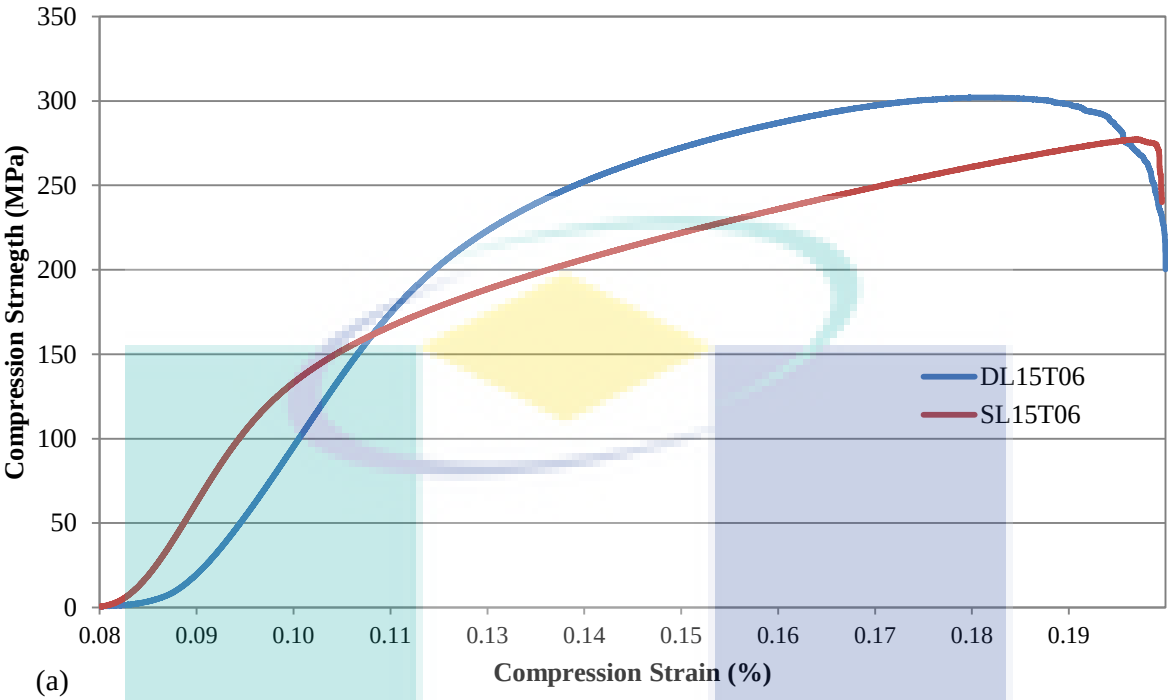

(a)

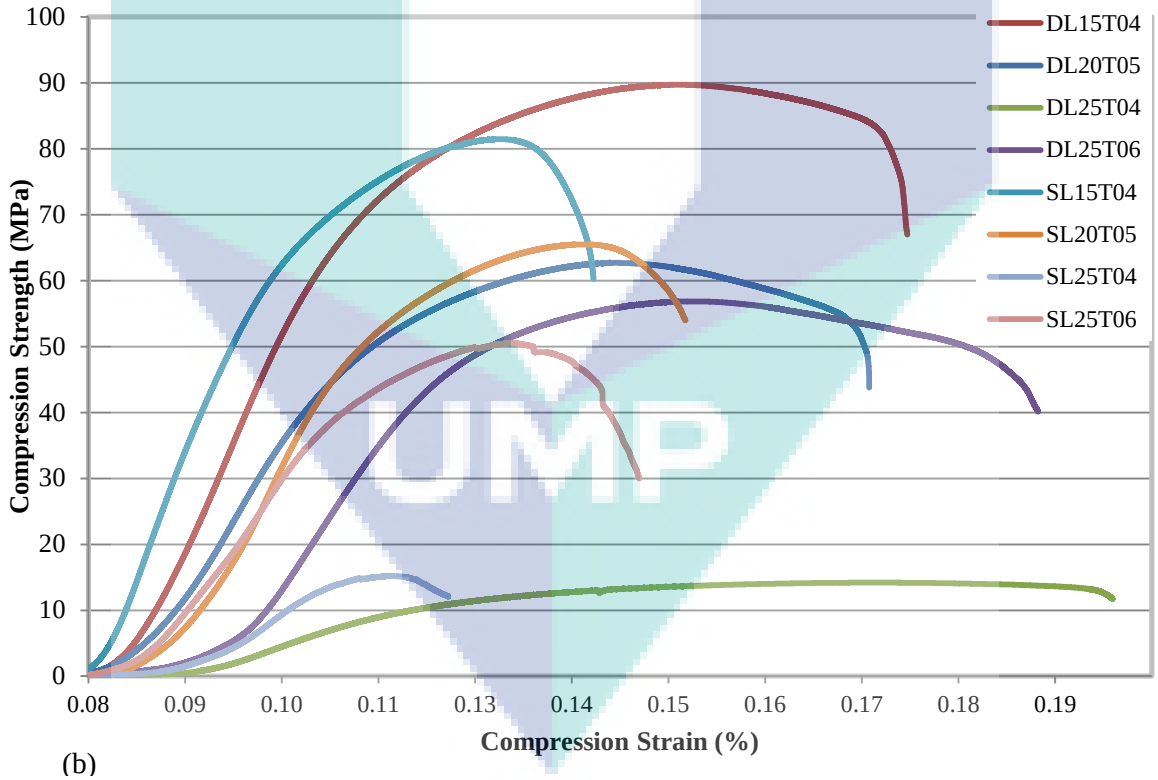

(b)

Figure 4.9 Stress strain curve of metabiomaterials (a) compression strength obtained to above 100 MPa (b) compression strength below 100 MPa

The stress-strain curves obtained from this study did not have and densification region due to typical elastic-plastic deformation has been observed (Liu et al., 2016; Maskery et al., 2016; Xiao et al., 2017). The densification after plastic region observed in metallic cellular structures by Gibson and Ashby (Gibson, 2005) under uniaxial loading was not observed in this study. This might be attributed to the brittle behaviours of the strut before the densification begins, which is in agreement with the findings by Gümrük et al. (2013), Limmahakhun et al. (2017) and McKown et al. (2008), The results of elastic modulus from this study are correlated with previous published work on Co-Cr-Mo cellular structures with varied ranges of porosity.

Figure 4.10 shows the relationship of the elastic modulus with porosity of metabiomaterials. A statistical measure of how close the coefficient of determination of volume porosity on elastic modulus indicated with (R^2) is shown in the graph. The significant of linear correlation between elastic modulus and porosity was found where the (R^2= 0.95) for square type metabiomaterials and (R^2= 0.99) for diamond type metabiomaterials. Thus, the higher R^2 has shown more accurate coefficient to mutual data. The high correlation of diamond metabiomaterials attributed to the orientation angle that lowers than 35° which results the better specific strength as increased strength with the decreasing angle degree in strut features (Yánez et al., 2016).

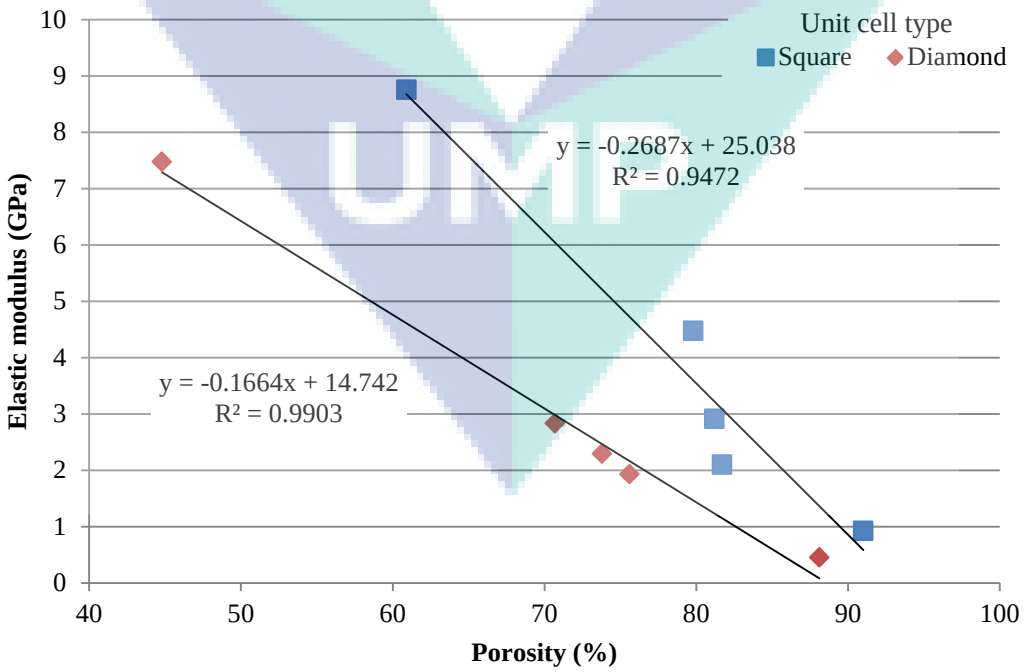

Figure 4.10 Relationship between porosity and elastic modulus of metabiomaterials

4.6 *In Vitro* Biocompatibility of Metabiomaterials

Biocompatibility of Co-Cr-Mo metabiomaterials produced by SLM has been studied *in vitro* by using chondrocytes cell harvested from a rabbit. From the biomaterial perspective, Co-Cr-Mo alloys have been routinely used in orthopaedic implants. However, in the SLM-manufactured metabiomaterials made from Co-Cr-Mo, *in vitro* biocompatibility studies to analyse the biological response towards the component are worth to be investigated. The preliminary study in this research has the replication number n=1. The harvested cells were then expanded through passage serial in order to have sufficient number for cell seeding.

The chondrocytes cells in this study underwent serial passage until passage 1 (*P1*), meaning that the subculture was performed where the cells from primary passage (*P0*) were transferred into another new plates or house for cell to grow and divide. After the confluence into sufficient number of cells, the cells were directly seeding into metabiomaterials for biological response study in the standard media growth until day 14 cell culture before MTT assay was performed. In order to maintain the life of the cells, the media culture was changed every single day with the fresh with supplemented nutrition to the chondrocytes cells in the simulated human body environment 37 °C and 5% CO_2. The healthy cultured cells can be observed under microscope, where the cells exhibited dendrites attached to other cells that allowed them to communicate to each other.

Figure 4.11 shows the confluence of cultured cells for primary passage (P0) and passage 1 (P1) in order to prepare the sufficient numbers of cells for 3D seeding construction process. From the figure, the cells have spheroid morphology under pathological conditions with diameter of 10-20 µm. The dendritic formation observed when the cells are attached to another which is allowing them to communicate and transferring nutrient (Barrere et al., 2008).

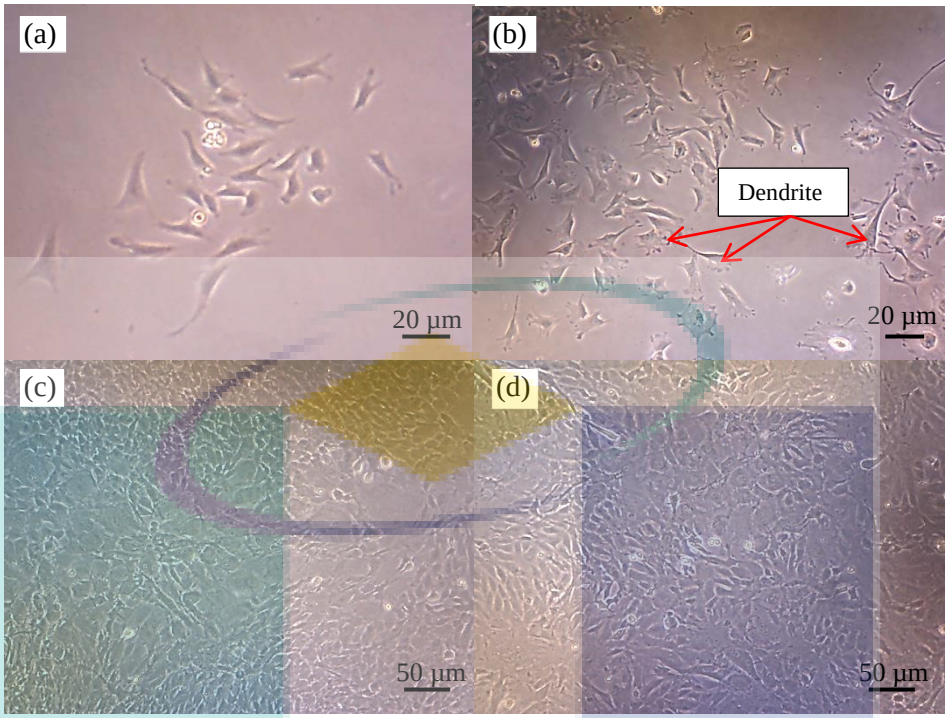

Figure 4.11 Cells culture of P0 (a) day 4, (b) day 9, (c) day 11 and P1 (d) day 4

4.6.1 MTT Absorbancy Reading

Regarding the *in vitro* biocompatibility test, the preliminary study should be declared in this research study due to limited number of samples for biocompatibility study. Consequently, the replication number of each design for two groups (1) gamma ray sterilised and (2) autoclave sterilised is n=1. The MTT absorbance cell viability was performed and spectrophotometric reading is at the wavelength of 570 nm for each group of metabiomaterials. The results for preliminary study suggested that chondrocytes cells from an adult rabbit could survive within Co-Cr-Mo metabiomaterials manufactured using SLM, since no proof of cell deaths within 14 days of cell culture. The absorbance results were compared with the samples for group gamma irradiated and autoclave components. The MTT absorbance viability cells on metabiomaterials and the cells remained in the wells plate were determined respectively as shown in the Figure 4.12 and Figure 4.13 after day 14 of cell culture for all groups of metabiomaterials.

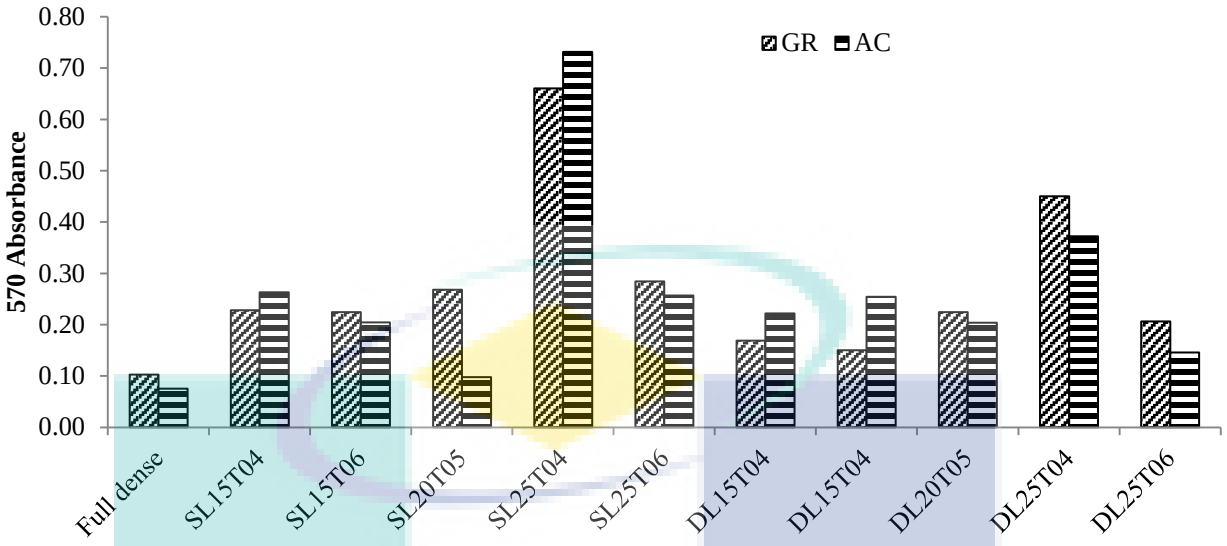

Figure 4.12 MTT absorbance on metabiomaterials after day 14 for gamma ray (GR) and autoclave (AC) sterilisation group

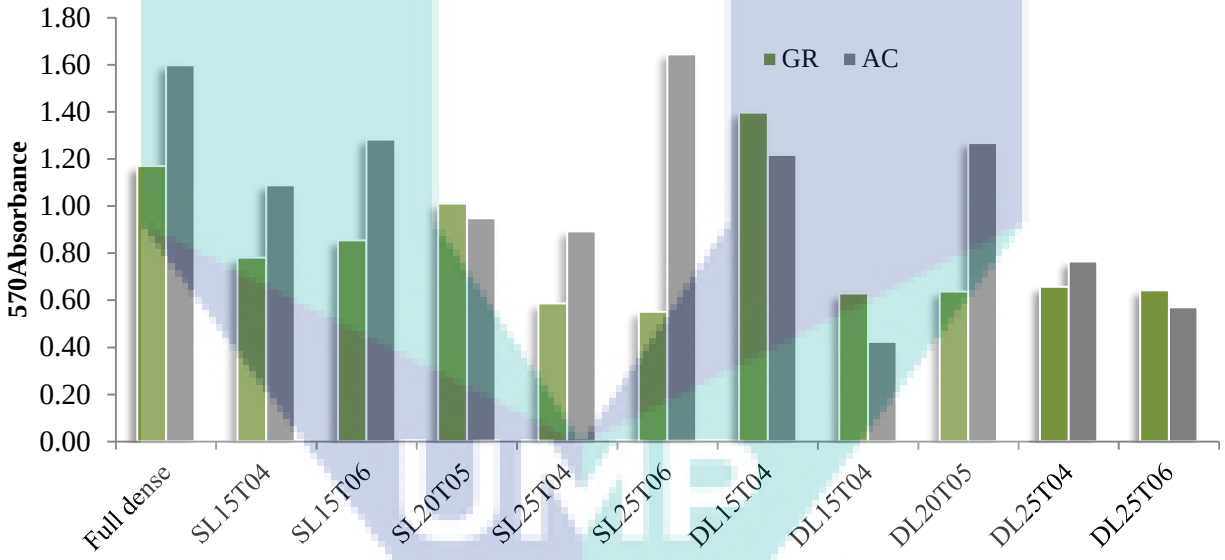

Figure 4.13 MTT absorbance on plate for each metabiomaterials after day 14 for gamma ray (GR) and autoclave (AC) sterilisation

As shown in the graph, metabiomaterials for square and diamond with unit cell length 1.5 mm and strut 0.4 mm obtained the highest reading of absorbance at day 14 that was evaluated from absorbance of cells attached on that metabiomaterials. At day 14, the cellular activities presumed at the optimum stage involved cell-to-cell communication and cell-to-matrix interaction with regard to new cells formation. Thus, this proves the viability of the cells in the *3D* constructs of fabricated Co-Cr-Mo

metabiomaterials using SLM. From this current result, the *in vitro* cell viability show the highest result for bigger pore size where the dependence of the pore shape. However, in this study, the stability and homogenous cell viability has been found in the pore size (1.1 to 1.7 mm). The local growth rate of tissue formation is strongly influenced by the geometrical features of channels in cellular structures where the pore curvature driven the effects and mechanical forced toward tissue regeneration (Rumpler et al., 2008). In this way, the angle of struts and larger surface area could rather promote and guide the tissue growth than influencing the cell behaviour in specific manner.

For the full dense sample and metabiomaterials that possess smaller pore size, the absorbance intensity was lower when cells cannot easily bridge the metabiomaterials pore. However, the absorbance intensity of the cells in the wells of full dense samples is higher for both groups. Thus, it is proved that the metabiomaterials manufactured through SLM were not harmful to the cells. In addition, the cells were able to grow healthy and proliferate among the produced metabiomaterials. The results of biocompatibility analysis in this study were in line with the previous study on Co-Cr-Mo produced by AM (España et al., 2010; Krishna et al., 2008) and commercial manufacturing process (Andrei et al., 2016; Riza et al., 2014) for orthopaedic implants applications.

4.6.2 SEM Morphology

The metabiomaterials of SL25T04 and DL25T04 was selected to undergone the morphology using scanning electron microscope (SEM). The selection was due to the formation of early cartilage tissue caused by the better interaction of cells within these two metabiomaterials. At the microscopic level observation, the metabiomaterials offer an adequate substrate that favourable to cell proliferation in the larger pore size component (2.1 mm and 1.5 m). Figure 4.14 shows the cell matrix formation on the metabiomaterials observed under scanning electron microscope (SEM) after day 21.

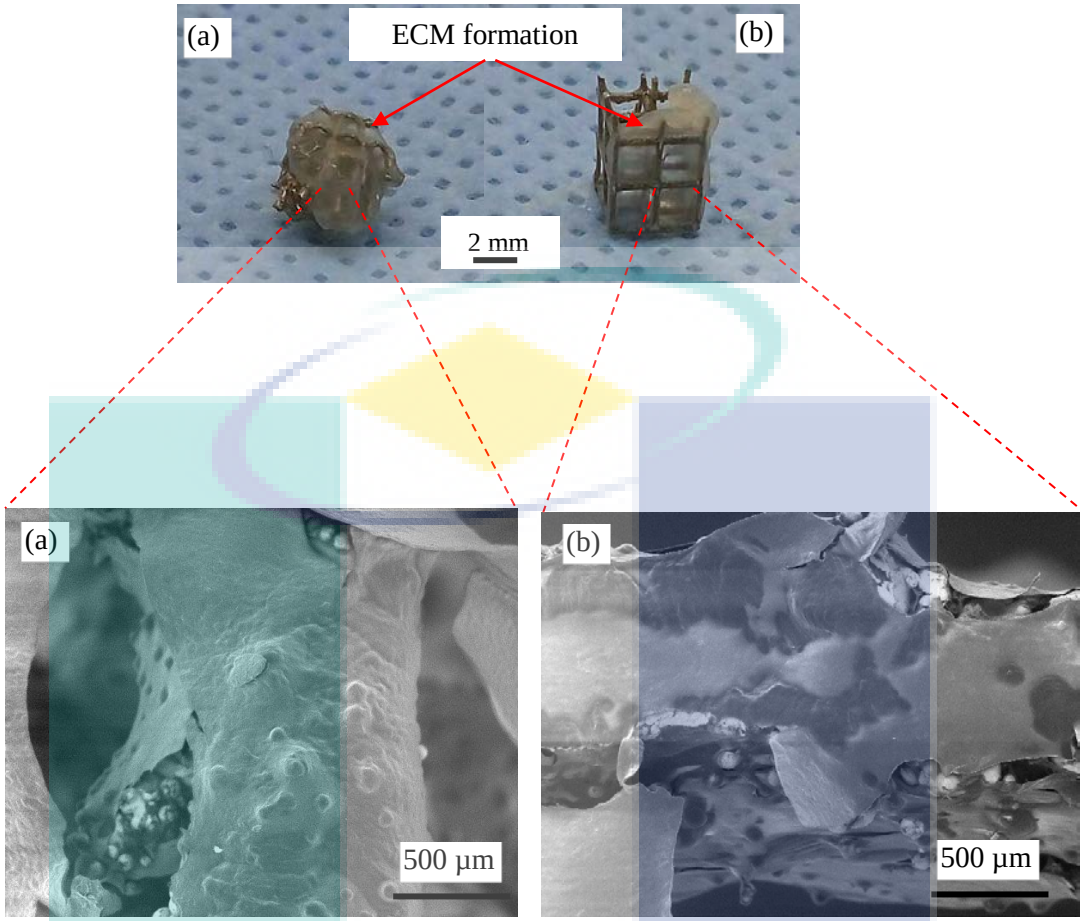

Figure 4.14 Above: Extra cellular matrix (ECM) formation on the a) DL25T04 and b) SL25T04. Below: SEM images of a) DL25T04 and b) SL25T04

According to the picture, the clear substance adhered and encapsulated both metabiomaterials design for all the metabiomaterials groups. The proliferation cells in the well plate adhered to each other and the metabiomaterials in dense aggregate which then allowed the cells to synthesize the cartilage extra cellular matrix (ECM) during the tissue formation process. It is proven that both metabiomaterials designed have optimum beneficial to cell growth and differentiate to initial tissue formation for integration between metabiomaterials. It is shown that the manufacturing process of SLM in this study does not contaminate the produced metabiomaterials. The interconnected metabiomaterials encouraged the cell growth and proliferation in the metabiomaterials except for full dense configurations where the mostly cells are gathered at the wells plate surface.

However, from the results obtained from the current preliminary study, the *in vitro* cell viability showed the highest result for bigger pore size with the dependence of the pore shape. From the previous study, the range of pore size for highest biological response for *in vitro* was 200 µm to 1000 µm, thus the important finding in this study was that the bigger pore size is significant for highest biological response between cells and metabiomaterials whose pore size for square is 2.1 mm and for diamond was 1.7 mm. In addition, the gamma irradiation and autoclave techniques showed the suitability for sterilisation of metabiomaterials constructer before the cell culture.

CHAPTER 5

CONCLUSIONS AND RECOMMENDATIONS

5.1 General Introduction

This chapter presents the conclusions for this research study and recommendations for future works. The conclusions and recommendations are drawn from the investigation of Co-Cr-Mo metabiomaterials manufactured by selective laser melting for orthopaedic load bearing implants with comparable mechanical stiffness with human bone properties and provided space for cell in growth into implant parts.

5.2 Conclusions

This study presents the designs of unit cell of metabiomaterials with highly controlled geometrical parameters particularly unit cell type, unit cell length, L_{cell} and strut size, Φ_S for the possible ways to reduce the high stiffness and to enhance the bio-functionality of metallic implants made by Co-Cr-Mo alloys. Co-Cr-Mo metabiomaterials namely square and diamond unit cell type with L_{cell} ranging from 1.5 mm to 2.5 mm and Φ_S ranged from 0.4 mm to 0.6 mm are aiming to match and tailor the stiffness of biomaterials with the human bone (1-30 GPa) and requirements for osseointegration and formation of new tissue at the interface of native bone and the implant with provided interconnected structures.

Selective laser melting (SLM) has successfully produced Co-Cr-Mo implants with default process parameters. The manufactured Co-Cr-Mo metabiomaterials were evaluated physically for surface morphology and manufacturability by optical evaluation, dimensional accuracy, and density by Archimedes' principle, underwent compression mechanical testing with load 100 kN and *in vitro* (in laboratory) biocompatibility testing by using MTT assay. The produced metabiomaterials yielded

good geometrical agreement with error <1%, good surface finish and higher density with relative density >85% that influenced higher energy density during manufacturing process, which is 119.05 J/mm^3. The manufactured Co-Cr-Mo implants with volume porosity between 44% and 88% possess the elastic modulus in the range of 0.4 MPa to 8.75 GPa, the compression strength of 10.77 MPa to 245.03 MPa, which are comparable to human bone properties.

Co-Cr-Mo metabiomaterials sterilised with gamma ray irradiation and autoclave method show the viability of the cells, where no effect is observed for the living cells. The highest absorbance reading is attributed to design square and diamond with unit cell 1.5 mm and strut size 0.4 mm (SL25T04 and DL25T04). Both metabiomaterials show optimum cellular activities significantly after day 14 of cell culture. There is no evidence that Co-Cr-Mo produced parts using selective laser melting are harmful or toxicity to the cells.

From this study, the metabiomaterials for both square and diamond types that exhibit porosity 60% to 80% and pore sizes range 1.2 to 1.7 mm are best suited for orthopaedic implants for their good mechanical strength and elastic modulus that is comparable to human bone properties and offer better biological response for *in vitro* studies.

5.3 Recommendations

Metabiomaterials made from medical graded Co-Cr-Mo are suitable for SLM fabrication with excellent performance and manufacturability. Additive manufacturing technologies seem reliable to manufacture and produce ready-to-use components, particularly in fulfilling patient-specific requirement and rapid production on orthopaedic applications. Furthermore, the investigation on the following should be considered for future works:

i. It is worthy to carefully investigate the effects of the SLM process parameters particularly for laser power, laser speed, hatch spacing and scan strategy since these parameters become the main factor in influencing the final outcomes of produced parts such as surface finish, density, dimensional accuracy, and tolerance.

ii. In this study, the biocompatibility testing of metabiomaterials produced by additive manufacturing is limited to *in vitro* study and the study on the biological response *in vivo* (in animal) by staining cell observation, metal ion released in simulated body fluid and also corrosion rate suggested for in-depth study especially for medical implants application.

iii. Fatigue analysis should be considered in metabiomaterials or cellular structure, since the failure and fracture might be affected in cyclic loading or dynamic stress in order to determine the fatigue life.

iv. The ultimate compression strength and compression strength of full dense sample cannot be obtained due to limitation of the machine load. Hence, for future works, it is recommended to use the compression tester with higher load such as 300 kN.

REFERENCES

13314:2011, I. ISO 13314: 2011 (E)(2011) Mechanical testing of metals—ductility testing—compression test for porous and cellular metals. *Ref Number ISO, 13314*(13314), 1-7.

Abd Malek, N. M. S., Mohamed, S. R., Che Ghani, S. A., & Wan Harun, W. S. (2015). *Critical evaluation on structural stiffness of porous cellular structure of cobalt chromium alloy.* Paper presented at the IOP Conference Series: Materials Science and Engineering.

Abidi, I. H., Khalid, F. A., Farooq, M. U., Hussain, M. A., & Maqbool, A. (2015). Tailoring the pore morphology of porous nitinol with suitable mechanical properties for biomedical applications. *Materials Letters, 154*, 17-20.

Acher, O. (2009). Copper vs. iron: Microwave magnetism in the metamaterial age. *Journal of Magnetism and Magnetic Materials, 321*(14), 2093-2101.

Adebiyi, D. I., & Popoola, A. P. I. (2015). Mitigation of abrasive wear damage of Ti–6Al–4V by laser surface alloying. *Materials & Design, 74*, 67-75.

Affatato, S., Ruggiero, A., & Merola, M. (2015). Advanced biomaterials in hip joint arthroplasty. A review on polymer and ceramics composites as alternative bearings. *Composites Part B: Engineering, 83*, 276-283.

Agarwal, R., & García, A. J. (2015). Biomaterial strategies for engineering implants for enhanced osseointegration and bone repair. *Advanced Drug Delivery Reviews, 94*, 53-62.

Ahmadi, S. M., Campoli, G., Amin Yavari, S., Sajadi, B., Wauthle, R., Schrooten, J., & Zadpoor, A. A. (2014). Mechanical behavior of regular open-cell porous biomaterials made of diamond lattice unit cells. *Journal of the mechanical behavior of biomedical materials, 34*, 106-115.

Ahn, S. H., Montero, M., Odell, D., Roundy, S., & Wright, P. K. (2002). Anisotropic material properties of fused deposition modeling ABS. *Rapid Prototyping Journal, 8*(4), 248-257.

Allaveisi, F., Hashemi, B., & Mortazavi, S. M. J. (2014). Effect of gamma sterilization on microhardness of the cortical bone tissue of bovine femur in presence of N-Acetyl-L-Cysteine free radical scavenger. *Physica Medica, 30*(3), 314-319.

Alrbaey, K., Wimpenny, D., Tosi, R., Manning, W., & Moroz, A. (2014). On optimization of surface roughness of selective laser melted stainless steel parts: a statistical study. *Journal of Materials Engineering and Performance, 23*(6), 2139-2148.

Amaral, M., Maru, M. M., Rodrigues, S. P., Gouvêa, C. P., Trommer, R. M., Oliveira, F. J., & Silva, R. F. (2015). Extremely low wear rates in hip joint bearings coated with nanocrystalline diamond. *Tribology International, 89*, 72-77.

Amin Yavari, S., Ahmadi, S. M., Wauthle, R., Pouran, B., Schrooten, J., Weinans, H., & Zadpoor, A. A. (2015). Relationship between unit cell type and porosity and the fatigue behavior of selective laser melted meta-biomaterials. *Journal of the mechanical behavior of biomedical materials, 43*, 91-100.

An, Y. H., & Draughn, R. A. (1999). *Mechanical testing of bone and the bone-implant interface*: CRC press.

Andrei, M., Galateanu, B., Hudita, A., Costache, M., Osiceanu, P., Moreno, J. C., & Demetrescu, I. (2016). Electrochemical comparison and biological performance of a new CoCrNbMoZr alloy with commercial CoCrMo alloy. *Materials Science and Engineering: C, 59*, 346-355.

Andrews, E. W., Gioux, G., Onck, P., & Gibson, L. J. (2001). Size effects in ductile cellular solids. Part II: experimental results. *International Journal of Mechanical Sciences, 43*(3), 701-713.

Anisimova, N. Y., Kiselevsky, M. V., Sukhorukova, I. V., Shvindina, N. V., & Shtansky, D. V. (2015). Fabrication method, structure, mechanical, and biological properties of decellularized extracellular matrix for replacement of wide bone tissue defects. *Journal of the mechanical behavior of biomedical materials, 49*, 255-268.

Antunes, R. A., & de Oliveira, M. C. L. (2012). Corrosion fatigue of biomedical metallic alloys: Mechanisms and mitigation. *Acta Biomaterialia, 8*(3), 937-962.

Anwar, C. G. S., Syamsi, A. M. N. M., Sharuzi, W. H. W., Zahrul, A., Faisae, A. R. F., Hazlen, R. M., & Asnawi, O. M. (2016). Finite element analysis of porous medical grade cobalt chromium alloy structures produced by selective laser melting. *Advanced Materials Research, 1133*.

Arabnejad, S., Burnett Johnston, R., Pura, J. A., Singh, B., Tanzer, M., & Pasini, D. (2016). High-strength porous biomaterials for bone replacement: A strategy to assess the interplay between cell morphology, mechanical properties, bone ingrowth and manufacturing constraints. *Acta Biomaterialia, 30*, 345-356.

Asri, R. I. M., Harun, W. S. W., Samykano, M., Lah, N. A. C., Ghani, S. A. C., Tarlochan, F., & Raza, M. R. (2017). Corrosion and surface modification on biocompatible metals: A review. *Materials Science and Engineering: C, 77*, 1261-1274.

Babaee, S., Jahromi, B. H., Ajdari, A., Nayeb Hashemi, H., & Vaziri, A. (2012). Mechanical properties of open-cell rhombic dodecahedron cellular structures. *Acta Materialia, 60*(6–7), 2873-2885.

Bahraminasab, M., Sahari, B. B., Edwards, K. L., Farahmand, F., & Arumugam, M. (2013). Aseptic loosening of femoral components – Materials engineering and design considerations. *Materials & Design, 44*, 155-163.

Bahraminasab, M., Sahari, B. B., Edwards, K. L., Farahmand, F., Hong, T. S., & Naghibi, H. (2013). Material tailoring of the femoral component in a total knee replacement to reduce the problem of aseptic loosening. *Materials & Design (1980-2015), 52*, 441-451.

Bansiddhi, A., & Dunand, D. (2008). Shape-memory NiTi foams produced by replication of NaCl space-holders. *Acta Biomaterialia, 4*(6), 1996-2007.

Barrere, F., Mahmood, T., De Groot, K., & Van Blitterswijk, C. (2008). Advanced biomaterials for skeletal tissue regeneration: Instructive and smart functions. *Materials Science and Engineering: R: Reports, 59*(1), 38-71.

Bartolo, P., Kruth, J. P., Silva, J., Levy, G., Malshe, A., Rajurkar, K., & Mitsuishi, M. (2012). Biomedical production of implants by additive electro-chemical and physical processes. *CIRP Annals-Manufacturing Technology, 61*(2), 635-655.

Bechmann, F. (2014). Changing the future of additive manufacturing. *Metal Powder Report, 69*(3), 37-40.

Black, J. (2005). *Biological performance of materials: fundamentals of biocompatibility*: CRC Press.

Blunn, G. (2013). (iii) Bearing surfaces. *Orthopaedics and Trauma, 27*(2), 85-92.

Bobyn, J., Stackpool, G., Hacking, S., Tanzer, M., & Krygier, J. (1999). Characteristics of bone ingrowth and interface mechanics of a new porous tantalum biomaterial. *J Bone Joint Surg Br, 81*(5), 907-914.

Bozic, K. J., & Ries, M. D. (2005). Wear and Osteolysis in Total Hip Arthroplasty. *Seminars in Arthroplasty, 16*(2), 142-152.

Bram, M., Stiller, C., Buchkremer, H. P., Stöver, D., & Baur, H. (2000). High-Porosity Titanium, Stainless Steel, and Superalloy Parts. *Advanced Engineering Materials, 2*(4), 196-199.

Brenne, F., Niendorf, T., & Maier, H. J. (2013). Additively manufactured cellular structures: Impact of microstructure and local strains on the monotonic and cyclic behavior under uniaxial and bending load. *Journal of Materials Processing Technology, 213*(9), 1558-1564.

Budinski, K. G. (1991). Tribological properties of titanium alloys. *Wear, 151*(2), 203-217.

Calignano, F. (2014). Design optimization of supports for overhanging structures in aluminum and titanium alloys by selective laser melting. *Materials & Design, 64*(0), 203-213.

Calmar, E. A., & Vinci, R. J. (2002). The anatomy and physiology of bone fracture and healing. *Clinical Pediatric Emergency Medicine, 3*(2), 85-93.

Campoli, G., Borleffs, M. S., Amin Yavari, S., Wauthle, R., Weinans, H., & Zadpoor, A. A. (2013). Mechanical properties of open-cell metallic biomaterials manufactured using additive manufacturing. *Materials & Design, 49*, 957-965.

Carlsson, L., Röstlund, T., Albrektsson, B., Albrektsson, T., & Brånemark, P. I. (1986). Osseointegration of titanium implants. *Acta Orthopaedica Scandinavica, 57*(4), 285-289.

Chakraborty, D., Reddy, B. A., & Choudhury, A. R. (2008). Extruder path generation for curved layer fused deposition modeling. *Computer-Aided Design, 40*(2), 235-243.

Chang, Y. S., Oka, M., Kobayashi, M., Gu, H. O., Li, Z. L., Nakamura, T., & Ikada, Y. (1996). Significance of interstitial bone ingrowth under load-bearing conditions: a comparison between solid and porous implant materials. *Biomaterials, 17*(11), 1141-1148.

Charnley, J. (1961). Arthroplasty of The Hip: A New Operation. *The Lancet, 277*(7187), 1129-1132.

Chen, & Thouas, G. A. (2015). Metallic implant biomaterials. *Materials Science and Engineering: R: Reports, 87*(0), 1-57.

Chen, J., Paetzell, E., Zhou, J., Lyons, L., & Soboyejo, W. (2010). Osteoblast-like cell ingrowth, adhesion and proliferation on porous Ti-6Al-4V with particulate and fiber scaffolds. *Materials Science and Engineering: C, 30*(5), 647-656.

Chen, Q., & Thouas, G. A. (2015). Metallic implant biomaterials. *Materials Science and Engineering: R: Reports, 87*, 1-57.

Cheng, X. Y., Li, S. J., Murr, L. E., Zhang, Z. B., Hao, Y. L., & Yang, R. (2012). Compression deformation behavior of Ti–6Al–4V alloy with cellular structures fabricated by electron beam melting. *Journal of the mechanical behavior of biomedical materials, 16*, 153-162.

Childs, T., Hauser, C., & Badrossamay, M. (2005). Selective laser sintering (melting) of stainless and tool steel powders: experiments and modelling. *Proceedings of the Institution of Mechanical Engineers, Part B: Journal of Engineering Manufacture, 219*(4), 339-357.

Chu, C., Chung, C., Lin, P., & Wang, S. (2004). Fabrication of porous NiTi shape memory alloy for hard tissue implants by combustion synthesis. *Materials Science and Engineering: A, 366*(1), 114-119.

Chunze, Y., Hao, L., Hussein, A., Bubb, S. L., Young, P., & Raymont, D. (2014). Evaluation of light-weight AlSi10Mg periodic cellular lattice structures fabricated via direct metal laser sintering. *Journal of Materials Processing Technology, 214*(4), 856-864.

Chunze, Y., Liang, H., Ahmed, H., & Philippe, Y. (2015). Ti–6Al–4V triply periodic minimal surface structures for bone implants fabricated via selective laser melting. *Journal of the mechanical behavior of biomedical materials, 51*, 61-73.

Cloots, M., Spierings, A., & Wegener, K. (2013). *Assessing new support minimizing strategies for the additive manufacturing technology SLM*. Paper presented at the 24th International SFF Symposium-An Additive Manufacturing Conference, Austin, USA, University of Texas at Austin.

Cuckler, J. M. (2006). Metal–Metal versus Ceramic–Ceramic: How to Choose? *Seminars in Arthroplasty, 17*(3–4), 184-189.

Daisuke, H., Nakashima, Y., Sato, T., Hirata, M., Kanazawa, M., Kohno, Y., & Yoshimoto, K. (2016). Bone bonding strength of diamond-structured porous titanium-alloy implants manufactured using the electron beam-melting technique. *Materials Science and Engineering: C, 59*, 1047-1052.

de Krijger, J., Rans, C., Van Hooreweder, B., Lietaert, K., Pouran, B., & Zadpoor, A. A. (2017). Effects of applied stress ratio on the fatigue behavior of additively manufactured porous biomaterials under compressive loading. *Journal of the mechanical behavior of biomedical materials, 70*, 7-16.

de Wild, M., Schumacher, R., Mayer, K., Schkommodau, E., Thoma, D., Bredell, M.,. Weber, F. E. (2013). Bone regeneration by the osteoconductivity of porous titanium implants manufactured by selective laser melting: a histological and micro computed tomography study in the rabbit. *Tissue Engineering Part A, 19*(23-24), 2645-2654.

Delhaes, P. (2002). Chemical vapor deposition and infiltration processes of carbon materials. *carbon, 40*(5), 641-657.

Denkhaus, E., & Salnikow, K. (2002). Nickel essentiality, toxicity, and carcinogenicity. *Critical reviews in oncology/hematology, 42*(1), 35-56.

Deshpande, V. S., Ashby, M. F., & Fleck, N. A. (2001). Foam topology: bending versus stretching dominated architectures. *Acta Materialia, 49*(6), 1035-1040.

Despeisse, M., & Ford, S. (2015). *The role of additive manufacturing in improving resource efficiency and sustainability.* Paper presented at the IFIP International Conference on Advances in Production Management Systems.

Diomidis, N. (2013). 9 - Wear phenomena of metal joints. In S. Affatato (Ed.), *Wear of Orthopaedic Implants and Artificial Joints* (pp. 246-277): Woodhead Publishing.

Disegi, J. A. (2000). Titanium alloys for fracture fixation implants. *Injury, 31, Supplement 4*(0), D14-D17.

Dongdong, G., & Shen, Y. (2009). Balling phenomena in direct laser sintering of stainless steel powder: Metallurgical mechanisms and control methods. *Materials & Design, 30*(8), 2903-2910.

Douglas, T., Warnke, P., Temel, B., Wollny, P., Becker, S., Springer, I., Sivananthan, S. (2009). *Rapid Prototyping: Porous Titanium Alloy Scaffolds Produced by Selective Laser Melting (SLM) for Bone Tissue Engineering.* Paper presented at the Tissue Engineering Part A.

Dourandish, M., Godlinski, D., Simchi, A., & Firouzdor, V. (2008). Sintering of biocompatible P/M Co–Cr–Mo alloy (F-75) for fabrication of porosity-graded composite structures. *Materials Science and Engineering: A, 472*(1), 338-346.

Ducheyne, P., & Martens, M. (1986a). Orderly oriented wire meshes as porous coatings on orthopaedic implants I: Morphology. *Clinical Materials, 1*(1), 59-67.

Ducheyne, P., & Martens, M. (1986b). Orderly oriented wire meshes as porous coatings on orthopaedic implants II: The pore size, interfacial bonding and microstructure after pressure sintering of titanium OOWM. *Clinical Materials, 1*(2), 91-98.

Elshahawy, W. (2011). Biocompatibility. In Costas Sikalidis (Ed.), *Advances in Ceramics - Electric and Magnetic Ceramics, Bioceramics, Ceramics and Environment* (pp. Ch. 15). Rijeka: InTech.

Emmelmann, C., Scheinemann, P., Munsch, M., & Seyda, V. (2011). Laser Additive Manufacturing of Modified Implant Surfaces with Osseointegrative Characteristics. *Physics Procedia, 12*, 375-384.

España, F. A., Balla, V. K., Bose, S., & Bandyopadhyay, A. (2010). Design and fabrication of CoCrMo alloy based novel structures for load bearing implants using laser engineered net shaping. *Materials Science and Engineering: C, 30*(1), 50-57.

Facchini, L., Magalini, E., Robotti, P., & Molinari, A. (2009). Microstructure and mechanical properties of Ti-6Al-4V produced by electron beam melting of pre-alloyed powders. *Rapid Prototyping Journal, 15*(3), 171-178.

Farag, M. M., & Yun, H.-s. (2014). Effect of gelatin addition on fabrication of magnesium phosphate-based scaffolds prepared by additive manufacturing system. *Materials Letters, 132*, 111-115.

Feng, B., Jinkang, Z., Zhen, W., Jianxi, L., Jiang, C., Jian, L., Xin, D. (2011). The effect of pore size on tissue ingrowth and neovascularization in porous bioceramics of controlled architecture in vivo. *Biomedical Materials, 6*(1), 015007.

Figliuzzi, M., Mangano, F., & Mangano, C. (2012). A novel root analogue dental implant using CT scan and CAD/CAM: selective laser melting technology. *International journal of oral and maxillofacial surgery, 41*(7), 858-862.

Fischer, P., Romano, V., Weber, H.-P., Karapatis, N., Boillat, E., & Glardon, R. (2003). Sintering of commercially pure titanium powder with a Nd: YAG laser source. *Acta Materialia, 51*(6), 1651-1662.

Ford, S., & Despeisse, M. (2016). Additive manufacturing and sustainability: an exploratory study of the advantages and challenges. *Journal of Cleaner Production, 137*, 1573-1587.

Frazier, W. E. (2014). Metal additive manufacturing: a review. *Journal of Materials Engineering and Performance, 23*(6), 1917-1928.

Fuchs, R., Warden, S., & Turner, C. (2009). Bone anatomy, physiology and adaptation to mechanical loading. *Planell JA, Best SM, Lacroix D et al. Bone Repair Biomaterials. Cambridge: Woodhead Publishing Limited and CRC Press, 200*, 25.

Fuchs, R. K., Warden, S. J., & Turner, C. H. (2009). 2 - Bone anatomy, physiology and adaptation to mechanical loading. In J. A. Planell, S. M. Best, D. Lacroix & A. Merolli (Eds.), *Bone Repair Biomaterials* (pp. 25-68): Woodhead Publishing.

Gan, M., & Wong, C. (2016). Practical support structures for selective laser melting. *Journal of Materials Processing Technology, 238*, 474-484.

Garcia Cimbrelo, E., Munuera, L., & Diez-Vazquez, V. (1995). Long-term results of aseptic cemented Charnley revisions. *The Journal of Arthroplasty, 10*(2), 121-131.

Garellick, G., Herberts, P., Strömberg, C., & Malchau, H. (1994). Long-term results of Charnley arthroplasty: A 12–16-year follow-up study. *The Journal of Arthroplasty, 9*(4), 333-340.

Geetha, M., Singh, A. K., Asokamani, R., & Gogia, A. K. (2009). Ti based biomaterials, the ultimate choice for orthopaedic implants – A review. *Progress in Materials Science, 54*(3), 397-425.

Geringer, J., & Macdonald, D. D. (2014). Friction/fretting-corrosion mechanisms: Current trends and outlooks for implants. *Materials Letters, 134*, 152-157.

Gibson, L. J. (2005). Biomechanics of cellular solids. *Journal of Biomechanics, 38*(3), 377-399.

Gibson, L. J., & Ashby, M. F. (1999). *Cellular solids: structure and properties*: Cambridge university press.

Gohil, S. V., Suhail, S., Rose, J., Vella, T., & Nair, L. S. (2017). Chapter 8 - Polymers and Composites for Orthopedic Applications A2 - Bose, Susmita. In A. Bandyopadhyay (Ed.), *Materials for Bone Disorders* (pp. 349-403): Academic Press.

Goodman, S. B., Yao, Z., Keeney, M., & Yang, F. (2013). The future of biologic coatings for orthopaedic implants. *Biomaterials, 34*(13), 3174-3183.

Goriainov, V., Cook, R., M. Latham, J., G. Dunlop, D., & Oreffo, R. O. C. (2014). Bone and metal: An orthopaedic perspective on osseointegration of metals. *Acta Biomaterialia, 10*(10), 4043-4057.

Gossec, L., Paternotte, S., Maillefert, J. F., Combescure, C., Conaghan, P. G., Davis, A. M., & Gunther, K. P. (2011). The role of pain and functional impairment in the decision to recommend total joint replacement in hip and knee osteoarthritis: an international cross-sectional study of 1909 patients. Report of the OARSI-OMERACT Task Force on total joint replacement. *Osteoarthritis and Cartilage, 19*(2), 147-154.

Gu, L., Zablocki, K., Lavelle, L., Bodnar, S., Halperin, F., Harper, I., & Moghe, P. V. (2012). Impact of ionizing radiation on physicochemical and biological properties of an amphiphilic macromolecule. *Polymer degradation and stability, 97*(9), 1686-1689.

Guessasma, S., Belhabib, S., & Nouri, H. (2015). Significance of pore percolation to drive anisotropic effects of 3D printed polymers revealed with X-ray μ-tomography and finite element computation. *Polymer, 81*, 29-36.

Guessasma, S., Belhabib, S., Nouri, H., & Hassana, O. B. (2016). Anisotropic damage inferred to 3D printed polymers using fused deposition modelling and subject to severe compression. *European Polymer Journal, 85*, 324-340.

Gümrük, R., Mines, R., & Karadeniz, S. (2013). Static mechanical behaviours of stainless steel micro-lattice structures under different loading conditions. *Materials Science and Engineering: A, 586*, 392-406.

Guo, Z., Pang, X., Yan, Y., Gao, K., Volinsky, A. A., & Zhang, T.-Y. (2015). CoCrMo alloy for orthopedic implant application enhanced corrosion and tribocorrosion properties by nitrogen ion implantation. *Applied Surface Science, 347*, 23-34.

Gutierres, M., Lopes, M. A., Sooraj Hussain, N., Lemos, A. F., Ferreira, J. M. F., Afonso, A., Santos, J. D. (2008). Bone ingrowth in macroporous Bonelike® for orthopaedic applications. *Acta Biomaterialia, 4*(2), 370-377.

Hallab, N. J., & Jacobs, J. J. (2013). Chapter II.5.6 - Orthopedic Applications. In B. D. R. S. H. J. S. E. Lemons (Ed.), *Biomaterials Science (Third Edition)* (pp. 841-882): Academic Press.

Hanzlik, J. A., & Day, J. S. (2013). Bone Ingrowth in Well-Fixed Retrieved Porous Tantalum Implants. *The Journal of Arthroplasty, 28*(6), 922-927.

Hao, L., & Harris, R. (2008). Customised implants for bone replacement and growth *Bio-Materials and Prototyping Applications in Medicine* (pp. 79-107): Springer.

Harrysson, O. L., Cansizoglu, O., Marcellin Little, D. J., Cormier, D. R., & West, H. A. (2008). Direct metal fabrication of titanium implants with tailored materials and mechanical properties using electron beam melting technology. *Materials Science and Engineering: C, 28*(3), 366-373.

Hasan, R., Mines, R. A., Shen, E., Tsopanos, S., & Cantwell, W. (2011). *Comparison on compressive behaviour of aluminium honeycomb and titanium alloy micro lattice blocks.* Paper presented at the Key Engineering Materials.

Hasib, H., Harrysson, O. L., & West, H. A. (2015). Powder removal from Ti-6Al-4V cellular structures fabricated via electron beam melting. *Jom, 67*(3), 639-646.

Hassani, A., Habibolahzadeh, A., & Bafti, H. (2012). Production of graded aluminum foams via powder space holder technique. *Materials & Design, 40*, 510-515.

Hayes, J. S., & Richards, R. G. (2014). Osteology: Osseointegration of Permanent and Temporary Orthopedic Implants *Reference Module in Biomedical Sciences*: Elsevier.

Hazlehurst, Jiang, C., & Stanford, M. (2013). Evaluation of the stiffness characteristics of square pore CoCrMo cellular structures manufactured using laser melting technology for potential orthopaedic applications. *Materials & Design, 51*(0), 949-955.

Hazlehurst, K., Wang, C. J., & Stanford, M. (2013). Evaluation of the stiffness characteristics of square pore CoCrMo cellular structures manufactured using laser melting technology for potential orthopaedic applications. *Materials & Design, 51*, 949-955.

He, D., Zheng, S., Pu, J., Zhang, G., & Hu, L. (2015). Improving tribological properties of titanium alloys by combining laser surface texturing and diamond-like carbon film. *Tribology International, 82, Part A*, 20-27.

He, S., Cui, Y., Ye, Y., Zhang, P., & Jin, Y. (2009). Optical nano-antennas and metamaterials. *Materials Today, 12*(12), 16-24.

Hedayati, R., Leeflang, A., & Zadpoor, A. (2017). Additively manufactured metallic pentamode meta-materials. *Applied Physics Letters, 110*(9), 091905.

Hedberg, Y. S., Qian, B., Shen, Z., Virtanen, S., & Odnevall Wallinder, I. (2014). In vitro biocompatibility of CoCrMo dental alloys fabricated by selective laser melting. *Dental Materials, 30*(5), 525-534.

Heinl, P., Müller, L., Körner, C., Singer, R. F., & Müller, F. A. (2008). Cellular Ti–6Al–4V structures with interconnected macro porosity for bone implants fabricated by selective electron beam melting. *Acta Biomaterialia, 4*(5), 1536-1544.

Hermawan, H., Ramdan, D., & Djuansjah, J. R. (2011). *Metals for biomedical applications*: INTECH Open Access Publisher.

Hollander, D. A., Von Walter, M., Wirtz, T., Sellei, R., Schmidt Rohlfing, B., Paar, O., & Erli, H.-J. (2006). Structural, mechanical and in vitro characterization of individually structured Ti–6Al–4V produced by direct laser forming. *Biomaterials, 27*(7), 955-963.

Hosseinzadeh, H. R. S., Shahi, A. S., & Eajazi, A. (2012). *The Bearing Surfaces in Total Hip Arthroplasty-Options, Material Characteristics and Selection*: INTECH Open Access Publisher.

Hrabe, N. W., Heinl, P., Bordia, R. K., Körner, C., & Fernandes, R. J. (2013). Maintenance of a bone collagen phenotype by osteoblast-like cells in 3D periodic porous titanium (Ti-6Al-4 V) structures fabricated by selective electron beam melting. *Connective tissue research, 54*(6), 351-360.

Hu, Y., Zhang, J., Zhang, X., Rong, H., Wu, Y., Yu, Y., & Hao, Q. (2014). Preparation and characterisation of porous titanium using plasma activated sintering technique. *Materials Research Innovations, 18*(sup2), S2-95-S92-100.

Hua, N., Chen, W., Zhang, L., Li, G., Liao, Z., & Lin, Y. (2017). Mechanical properties and bio-tribological behaviors of novel beta-Zr-type Zr-Al-Fe-Nb alloys for biomedical applications. *Materials Science and Engineering: C, 76*, 1154-1165.

Huang, S. H., Liu, P., Mokasdar, A., & Hou, L. (2013). Additive manufacturing and its societal impact: a literature review. *The International Journal of Advanced Manufacturing Technology*, 1-13.

Huiskes, R., Weinans, H., & Van Rietbergen, B. (1992). The relationship between stress shielding and bone resorption around total hip stems and the effects of flexible materials. *Clinical orthopaedics and related research, 274*, 124-134.

Hunt, E. M., Pantoya, M. L., & Jouet, R. J. (2006). Combustion synthesis of metallic foams from nanocomposite reactants. *Intermetallics, 14*(6), 620-629.

Islam, M. M., Khan, M. A., & Rahman, M. M. (2015). Preparation of gelatin based porous biocomposite for bone tissue engineering and evaluation of gamma irradiation effect on its properties. *Materials Science and Engineering: C, 49*, 648-655.

Ivanova, E. P., Bazaka, K., & Crawford, R. J. (2014a). 5 - Metallic biomaterials: types and advanced applications *New Functional Biomaterials for Medicine and Healthcare* (pp. 121-147): Woodhead Publishing.

Ivanova, E. P., Bazaka, K., & Crawford, R. J. (2014b). 6 - Cytotoxicity and biocompatibility of metallic biomaterials *New Functional Biomaterials for Medicine and Healthcare* (pp. 148-172): Woodhead Publishing.

James, M. N. (2005). Design, manufacture and materials; their interaction and role in engineering failures. *Engineering Failure Analysis, 12*(5), 662-678.

Jamshidinia, M., Wang, L., Tong, W., Ajlouni, R., & Kovacevic, R. (2015). Fatigue properties of a dental implant produced by electron beam melting®(EBM). *Journal of Materials Processing Technology, 226*, 255-263.

Jardini, A. L., Larosa, M. A., Kaasi, A., & Kharmandayan, P. (2017). Additive Manufacturing in Medicine *Reference Module in Materials Science and Materials Engineering*: Elsevier.

Jared, B. H., Aguilo, M. A., Beghini, L. L., Boyce, B. L., Clark, B. W., Cook, A., & Kaehr, B. J. (2017). Additive manufacturing: Toward holistic design. *Scripta Materialia, 135*, 141-147.

Jean, K. P., Froyen, L., Van Vaerenbergh, J., Mercelis, P., Rombouts, M., & Lauwers, B. (2004). Selective laser melting of iron-based powder. *Journal of Materials Processing Technology, 149*(1), 616-622.

Jean, K. P., Mercelis, P., Van Vaerenbergh, J., Froyen, L., & Rombouts, M. (2005). Binding mechanisms in selective laser sintering and selective laser melting. *Rapid Prototyping Journal, 11*(1), 26-36.

Jhabvala, J., Boillat, E., André, C., & Glardon, R. (2012). An innovative method to build support structures with a pulsed laser in the selective laser melting process. *The International Journal of Advanced Manufacturing Technology, 59*(1-4), 137-142.

Jia Ping, L., Li, S. H., De Groot, K., & Layrolle, P. (2002). *Preparation and characterization of porous titanium.* Paper presented at the Key Engineering Materials.

Jianyu, C., Zhang, Z., Chen, X., Zhang, C., Zhang, G., & Xu, Z. (2014). Design and manufacture of customized dental implants by using reverse engineering and selective laser melting technology. *The Journal of prosthetic dentistry, 112*(5), 1088-1095. e1081.

Jin, Z. M., Zheng, J., Li, W., & Zhou, Z. R. (2016). Tribology of medical devices. *Biosurface and Biotribology, 2*(4), 173-192.

Jo, Y. J., Lee, C. M., Jang, H. S., Lee, N. S., Suk, J. H., & Lee, W. H. (2007). Mechanical properties of fully porous and porous-surfaced Ti–6Al–4V implants fabricated by electro-discharge-sintering. *Journal of Materials Processing Technology, 194*(1–3), 121-125.

Jones, A. C., Arns, C. H., Hutmacher, D. W., Milthorpe, B. K., Sheppard, A. P., & Knackstedt, M. A. (2009). The correlation of pore morphology, interconnectivity and physical properties of 3D ceramic scaffolds with bone ingrowth. *Biomaterials, 30*(7), 1440-1451.

Kadkhodapour, J., Montazerian, H., Darabi, A. C., Zargarian, A., & Schmauder, S. (2016). The relationships between deformation mechanisms and mechanical properties of additively manufactured porous biomaterials. *Journal of the mechanical behavior of biomedical materials*.

Kaivosoja, E., Tiainen, V. M., Takakubo, Y., Rajchel, B., Sobiecki, J., Konttinen, Y. T., & Takagi, M. (2013). 7 - Materials used for hip and knee implants. In S. Affatato (Ed.), *Wear of Orthopaedic Implants and Artificial Joints* (pp. 178-218): Woodhead Publishing.

Kamath, A. F., Prieto, H., & Lewallen, D. G. (2013). Alternative Bearings in Total Hip Arthroplasty in the Young Patient. *Orthopedic Clinics of North America, 44*(4), 451-462.

Kante, B., Ourir, A., Burokur, S. N., Gadot, F., & de Lustrac, A. (2008). Metamaterials for optical and radio communications. *Comptes Rendus Physique, 9*(1), 31-40.

Katti, K. S. (2004). Biomaterials in total joint replacement. *Colloids and Surfaces B: Biointerfaces, 39*(3), 133-142.

Kennedy, F. E. (2013). 3 - Biomechanics of the hip and knee: implant wear A2 - Affatato, Saverio *Wear of Orthopaedic Implants and Artificial Joints* (pp. 56-92): Woodhead Publishing.

Kennedy, K. M., Bhaw-Luximon, A., & Jhurry, D. (2017). Cell-matrix mechanical interaction in electrospun polymeric scaffolds for tissue engineering: Implications for scaffold design and performance. *Acta Biomaterialia, 50*, 41-55.

Kienapfel, H., Sprey, C., Wilke, A., & Griss, P. (1999). Implant fixation by bone ingrowth. *The Journal of Arthroplasty, 14*(3), 355-368.

Kim, R. H., Dennis, D. A., & Carothers, J. T. (2008). Metal-on-Metal Total Hip Arthroplasty. *The Journal of Arthroplasty, 23*(7, Supplement), 44-46.

Kluess, D., Mittelmeier, W., & Bader, R. (2010). Intraoperative impaction of total knee replacements: An explicit finite-element-analysis of principal stresses in ceramic vs. cobalt–chromium femoral components. *Clinical Biomechanics, 25*(10), 1018-1024.

Kohtala, C. (2015). Addressing sustainability in research on distributed production: an integrated literature review. *Journal of Cleaner Production, 106*, 654-668.

Krishna, B. V., Xue, W., Bose, S., & Bandyopadhyay, A. (2008). Functionally graded Co–Cr–Mo coating on Ti–6Al–4V alloy structures. *Acta Biomaterialia, 4*(3), 697-706.

Kulinets, I. (2015). 1 - Biomaterials and their applications in medicine. In S. F. Amato & R. M. Ezzell (Eds.), *Regulatory Affairs for Biomaterials and Medical Devices* (pp. 1-10): Woodhead Publishing.

Kumar, A., Mandal, S., Barui, S., Vasireddi, R., Gbureck, U., Gelinsky, M., & Basu, B. (2016). Low temperature additive manufacturing of three dimensional scaffolds for bone-tissue engineering applications: Processing related challenges and property assessment. *Materials Science and Engineering: R: Reports, 103*, 1-39.

Kumar, N., Arora, N. C., & Datta, B. (2014). Bearing surfaces in hip replacement – Evolution and likely future. *Medical Journal Armed Forces India, 70*(4), 371-376.

Kumar, S. (2014). Selective laser sintering/melting. *Comprehensive Materials Processing, Editors: Hashmi S., Batalha G. F, Van Tyne C. J, Yilbas B, Elsevier, Oxford*, 93-134.

Kurtz, S. M., Lau, E., Ong, K., Zhao, K., Kelly, M., & Bozic, K. J. (2009). Future young patient demand for primary and revision joint replacement: national projections from 2010 to 2030. *Clinical Orthopaedics and Related Research®, 467*(10), 2606-2612.

Landgraeber, S., Putz, S., Schlattjan, M., Bechmann, L. P., Totsch, M., Grabellus, F., Canbay, A. (2014). Adiponectin attenuates osteolysis in aseptic loosening of total hip replacements. *Acta Biomaterialia, 10*(1), 384-393.

Lappalainen, R., Juvonen, T., & Selenius, M. (2014). 6 - Joint bearing surfaces and replacement joint design*. In P. A. Revell (Ed.), *Joint Replacement Technology (Second Edition)* (pp. 167-185): Woodhead Publishing.

Lawrence, M. E., Gaytan, S. M., Martinez, E., Medina, F., & Wicker, R. B. (2012). Next generation orthopaedic implants by additive manufacturing using electron beam melting. *International journal of biomaterials, 2012*.

Lee, C. S., Kim, S. G., Kim, H. J., & Ahn, S. H. (2007). Measurement of anisotropic compressive strength of rapid prototyping parts. *Journal of Materials Processing Technology, 187*, 627-630.

Lee, P. H., Chung, H., Lee, S. W., Yoo, J., & Ko, J. (2014). *Review: dimensional accuracy in additive manufacturing processes*. Paper presented at the ASME 2014 International Manufacturing Science and Engineering Conference collocated with the JSME 2014 International Conference on Materials and Processing and the 42nd North American Manufacturing Research Conference.

Lee, W. H., & Hyun, C. Y. (2007). Fabrication of fully porous and porous-surfaced Ti-6Al-4V implants by electro-discharge-sintering of spherical Ti-6Al-4V powders in an one-step process. *Journal of Materials Processing Technology, 189*(1), 219-223.

Lees, D., & Partington, P. (2016). Articular cartilage. *Orthopaedics and Trauma, 30*(3), 265-272.

Li, F., Li, J., Xu, G., Liu, G., Kou, H., & Zhou, L. (2015). Fabrication, pore structure and compressive behavior of anisotropic porous titanium for human trabecular bone implant applications. *Journal of the mechanical behavior of biomedical materials, 46*, 104-114.

Li, J. P., Li, S. H., Van Blitterswijk, C. A., & De Groot, K. (2006). Cancellous bone from porous Ti6Al4V by multiple coating technique. *Journal of Materials Science: Materials in Medicine, 17*(2), 179-185.

Li, W., Liu, J., Zhou, Y., Li, S., Wen, S., Wei, Q., & Yan, C. (2016). Effect of laser scanning speed on a Ti-45Al-2Cr-5Nb alloy processed by selective laser melting: Microstructure, phase and mechanical properties. *Journal of Alloys and Compounds, 688*, 626-636.

Li, X., Van Humbeeck, J., & Kruth, J. (2017). Selective laser melting of weak-textured commercially pure titanium with high strength and ductility: A study from laser power perspective. *Materials & Design, 116*, 352-358.

Liao, Y. F., Hoffman, E., Wimmer, M., Fischer, A., Jacobs, J., & Marks, L. (2013). CoCrMo metal-on-metal hip replacements. *Physical Chemistry Chemical Physics, 15*(3), 746-756.

Limmahakhun, S., Oloyede, A., Sitthiseripratip, K., Xiao, Y., & Yan, C. (2017). Stiffness and strength tailoring of cobalt chromium graded cellular structures for stress-shielding reduction. *Materials & Design, 114*, 633-641.

Liu, Y., Li, S., Wang, H., Hou, W., Hao, Y., Yang, R., & Sercombe, T. (2016). Microstructure, defects and mechanical behavior of beta-type titanium porous structures manufactured by electron beam melting and selective laser melting. *Acta Materialia, 113*, 56-67.

Long, M., & Rack, H. J. (1998). Titanium alloys in total joint replacement—a materials science perspective. *Biomaterials, 19*(18), 1621-1639.

Lourtioz, J.-M. (2008). Photonic crystals and metamaterials. *Comptes Rendus Physique, 9*(1), 4-15.

Louvis, E., Fox, P., & Sutcliffe, C. J. (2011). Selective laser melting of aluminium components. *Journal of Materials Processing Technology, 211*(2), 275-284.

Luiz, J. A., Larosa, M. A., Maciel Filho, R., de Carvalho Zavaglia, C. A., Bernardes, L. F., Lambert, C. S., & Calderoni, D. R. (2014). Cranial reconstruction: 3D biomodel and custom-built implant created using additive manufacturing. *Journal of Cranio-Maxillofacial Surgery, 42*(8), 1877-1884.

Lv, J., Jia, Z., Li, J., Wang, Y., Yang, J., Xiu, P., & Zhang, K. (2015). Electron beam melting fabrication of porous Ti6Al4V scaffolds: cytocompatibility and osteogenesis. *Advanced Engineering Materials, 17*(9), 1391-1398.

M. Talha, C. K. B. a. O. P. S. (2013). A review on nickel-free nitrogen containing austenitic stainless steels for biomedical applications. *Materials and Engineering: C, 33*, 3563-3575.

Maksimkin, A. V., Senatov, F. S., Anisimova, N. Y., Kiselevskiy, M. V., Zalepugin, D. Y., Chernyshova, I. V., Kaloshkin, S. D. (2017). Multilayer porous UHMWPE scaffolds for bone defects replacement. *Materials Science and Engineering: C, 73*, 366-372.

Malek, N. A., Mohamed, S., Ghani, S. C., & Harun, W. W. (2015). *Critical evaluation on structural stiffness of porous cellular structure of cobalt chromium alloy*. Paper presented at the IOP Conference Series: Materials Science and Engineering.

Manam, N. S., Harun, W. S. W., Shri, D. N. A., Ghani, S. A. C., Kurniawan, T., Ismail, M. H., & Ibrahim, M. H. I. (2017). Study of corrosion in biocompatible metals for implants: A review. *Journal of Alloys and Compounds, 701*, 698-715.

Markaki, A. E., & Clyne, T. W. (2004). Magneto-mechanical stimulation of bone growth in a bonded array of ferromagnetic fibres. *Biomaterials, 25*(19), 4805-4815.

Maskery, I., Aboulkhair, N., Aremu, A., Tuck, C., Ashcroft, I., Wildman, R. D., & Hague, R. J. (2016). A mechanical property evaluation of graded density Al-Si10-Mg lattice structures manufactured by selective laser melting. *Materials Science and Engineering: A, 670*, 264-274.

Masmoudi, A., Bolot, R., & Coddet, C. (2015). Investigation of the laser–powder–atmosphere interaction zone during the selective laser melting process. *Journal of Materials Processing Technology, 225*, 122-132.

Matassi, F., Botti, A., Sirleo, L., Carulli, C., & Innocenti, M. (2013). Porous metal for orthopedics implants. *Clinical Cases in Mineral and Bone Metabolism, 10*(2), 111-115.

Mattew, S. J., Hayes, W. C., & Gibson, L. J. (1995). The effects of non-periodic microstructure on the elastic properties of two-dimensional cellular solids. *International Journal of Mechanical Sciences, 37*(11), 1161-1177.

McEntire, B. J., Bal, B. S., Rahaman, M. N., Chevalier, J., & Pezzotti, G. (2015). Ceramics and ceramic coatings in orthopaedics. *Journal of the European Ceramic Society, 35*(16), 4327-4369.

McKown, S., Shen, Y., Brookes, W., Sutcliffe, C., Cantwell, W., Langdon, G., & Nurick, G. (2008). The quasi-static and blast loading response of lattice structures. *International Journal of Impact Engineering, 35*(8), 795-810.

Méjica, G. F., & Lantada, A. D. (2013). Comparative study of potential pentamodal metamaterials inspired by Bravais lattices. *Smart Materials and Structures, 22*(11), 115013.

Melican, M. C., Zimmerman, M. C., Dhillon, M. S., Ponnambalam, A. R., Curodeau, A., & Parsons, J. R. (2001). Three-dimensional printing and porous metallic surfaces: A new orthopedic application. *Journal of biomedical materials research, 55*(2), 194-202.

Milosevic, M. (2016). Polymerization Mechanics of Dental Composites – Advantages and Disadvantages. *Procedia Engineering, 149*, 313-320.

Mishra, R., Mukherjee, A., Yamazaki, K., & Shoda, K. (1996). Effect of TiO 2 doping on rapid densification of alumina by plasma activated sintering. *Journal of materials research, 11*(05), 1144-1148.

Miyao, R., Omori, M., Watari, F., Yokoyama, A., Matsuno, H., Hirai, T., & Kawasaki, T. (2000). Fabrication of functionally graded implants by spark plasma sintering and their properties. *Journal of the Japan Society of Powder and Powder Metallurgy, 47*(11), 1239-1242.

Molinari, R. W. (2007). Dynamic stabilization of the lumbar spine. *Current Opinion in Orthopaedics, 18*(3), 215-220.

Monroy, K., Delgado, J., & Ciurana, J. (2013). Study of the pore formation on CoCrMo alloys by selective laser melting manufacturing process. *Procedia Engineering, 63*, 361-369.

Montazerian, H., Davoodi, E., Asadi-Eydivand, M., Kadkhodapour, J., & Solati-Hashjin, M. (2017). Porous scaffold internal architecture design based on minimal surfaces: A compromise between permeability and elastic properties. *Materials & Design, 126*, 98-114.

Moodley, S., Koorbanally, N. A., Moodley, T., Ramjugernath, D., & Pillay, M. (2014). The 3-(4, 5-dimethylthiazol-2-yl)-2, 5-diphenyl tetrazolium bromide (MTT) assay is a rapid, cheap, screening test for the in vitro anti-tuberculous activity of chalcones. *Journal of microbiological methods, 104*, 72-78.

Mouthuy, P. A., Snelling, S. J. B., Dakin, S. G., Milković, L., Gašparović, A. Č., Carr, A. J., & Žarković, N. (2016). Biocompatibility of implantable materials: An oxidative stress viewpoint. *Biomaterials, 109*, 55-68.

Mroz, W., Budner, B., Syroka, R., Niedzielski, K., Golański, G., Slósarczyk, A., Douglas, T. E. (2015). In vivo implantation of porous titanium alloy implants coated with magnesium-doped octacalcium phosphate and hydroxyapatite thin films using pulsed laser depostion. *Journal of Biomedical Materials Research Part B: Applied Biomaterials, 103*(1), 151-158.

Mullen, L., Stamp, R. C., Brooks, W. K., Jones, E., & Sutcliffe, C. J. (2009). Selective Laser Melting: A regular unit cell approach for the manufacture of porous, titanium, bone in-growth constructs, suitable for orthopedic applications. *Journal of Biomedical Materials Research Part B: Applied Biomaterials, 89*(2), 325-334.

Mumtaz, K. A., Erasenthiran, P., & Hopkinson, N. (2008). High density selective laser melting of Waspaloy®. *Journal of Materials Processing Technology, 195*(1–3), 77-87.

Munsch, M. (2017). 15 - Laser additive manufacturing of customized prosthetics and implants for biomedical applications A2 - Brandt, Milan *Laser Additive Manufacturing* (pp. 399-420): Woodhead Publishing.

Murnaghan, J. M., & Hamer, A. J. (2010). Hip and knee replacement. *Surgery (Oxford), 28*(10), 508-513.

Murr, L. E. (2015). Metallurgy of additive manufacturing: Examples from electron beam melting. *Additive Manufacturing, 5*, 40-53.

Murr, L. E., Amato, K. N., Li, S. J., Tian, Y. X., Cheng, X. Y., Gaytan, S. M., & Martinez, E. (2011). Microstructure and mechanical properties of open-cellular biomaterials

prototypes for total knee replacement implants fabricated by electron beam melting. *Journal of the mechanical behavior of biomedical materials, 4*(7), 1396-1411.

Murr, L. E., Gaytan, S., Ceylan, A., Martinez, E., Martinez, J., Hernandez, D., & Machado, B. (2010). Characterization of titanium aluminide alloy components fabricated by additive manufacturing using electron beam melting. *Acta Materialia, 58*(5), 1887-1894.

Murr, L. E., Gaytan, S. M., Ramirez, D. A., Martinez, E., Hernandez, J., Amato, K. N., & Shindo, P. W. (2012). Metal Fabrication by Additive Manufacturing Using Laser and Electron Beam Melting Technologies. *Journal of Materials Science & Technology, 28*(1), 1-14.

Murray, P. M. (2006). Prosthetic Replacement of the Proximal Interphalangeal Joint. *Hand Clinics, 22*(2), 201-206.

Nakano, T. (2010). 3 - Mechanical properties of metallic biomaterials. In M. Niinomi (Ed.), *Metals for Biomedical Devices* (pp. 71-98): Woodhead Publishing.

Nakayama, B., Hasegawa, Y., Hyodo, I., Ogawa, T., Fujimoto, Y., Kitano, H., & Torii, S. (2004). Reconstruction using a three-dimensional orbitozygomatic skeletal model of titanium mesh plate and soft-tissue free flap transfer following total maxillectomy. *Plastic and reconstructive surgery, 114*(3), 631-639.

Narushima, T. (2010). 15 - New-generation metallic biomaterials. In M. Niinomi (Ed.), *Metals for Biomedical Devices* (pp. 355-378): Woodhead Publishing.

Nasab, M. B., Hassan, M. R., & Sahari, B. B. (2010). Metallic biomaterials of knee and hip-a review. *Trends Biomaterials & Artificial Organs, 24*(1), 69-82.

Nelaturi, S., Kim, W., & Kurtoglu, T. (2015). Manufacturability feedback and model correction for additive manufacturing. *Journal of Manufacturing Science and Engineering, 137*(2), 021015.

Niinomi, M. (2008). Mechanical biocompatibilities of titanium alloys for biomedical applications. *Journal of the Mechanical Behavior of Biomedical Materials, 1*(1), 30-42.

Niinomi, M., Nakai, M., & Hieda, J. (2012). Development of new metallic alloys for biomedical applications. *Acta Biomaterialia, 8*(11), 3888-3903.

Onck, P. R., Andrews, E. W., & Gibson, L. J. (2001). Size effects in ductile cellular solids. Part I: modeling. *International Journal of Mechanical Sciences, 43*(3), 681-699.

Park, J. B., & Bronzino, J. D. (2002). *Biomaterials: principles and applications*: crc press.

Park, J. H., Olivares Navarrete, R., Baier, R. E., Meyer, A. E., Tannenbaum, R., Boyan, B. D., & Schwartz, Z. (2012). Effect of cleaning and sterilization on titanium implant surface properties and cellular response. *Acta Biomaterialia, 8*(5), 1966-1975.

Parthasarathy, J., Starly, B., & Raman, S. (2011). A design for the additive manufacture of functionally graded porous structures with tailored mechanical properties for biomedical applications. *Journal of Manufacturing Processes, 13*(2), 160-170.

Pattanayak, D. K., Fukuda, A., Matsushita, T., Takemoto, M., Fujibayashi, S., Sasaki, K., Kokubo, T. (2011). Bioactive Ti metal analogous to human cancellous bone: fabrication

by selective laser melting and chemical treatments. *Acta Biomaterialia, 7*(3), 1398-1406.

Petit, C., Maire, E., Meille, S., Adrien, J., Kurosu, S., & Chiba, A. (2016). CoCrMo cellular structures made by Electron Beam Melting studied by local tomography and finite element modelling. *Materials Characterization, 116*, 48-54.

Pezzotti, G., & Yamamoto, K. (2014). Artificial hip joints: The biomaterials challenge. *Journal of the mechanical behavior of biomedical materials, 31*, 3-20.

Philip, H. L. (2008). Medical devices in orthopedic applications. *Toxicologic pathology, 36*(1), 85-91.

Planell, J. A., Best, S., Lacroix, D., & Merolli, A. (2009). *Bone repair biomaterials*: Elsevier.

Podshivalov, L., Gomes, C. M., Zocca, A., Guenster, J., Bar-Yoseph, P., & Fischer, A. (2013). Design, Analysis and Additive Manufacturing of Porous Structures for Biocompatible Micro-Scale Scaffolds. *Procedia CIRP, 5*, 247-252.

Prasad, S., Ehrensberger, M., Gibson, M. P., Kim, H., & Monaco, E. A. (2015). Biomaterial properties of titanium in dentistry. *Journal of Oral Biosciences, 57*(4), 192-199.

Pyka, G., Kerckhofs, G., Schrooten, J., & Wevers, M. (2014). The effect of spatial micro-CT image resolution and surface complexity on the morphological 3D analysis of open porous structures. *Materials Characterization, 87*, 104-115.

Qiu, C., Yue, S., Adkins, N. J., Ward, M., Hassanin, H., Lee, P. D., & Withers, P. J. (2015). Influence of processing conditions on strut structure and compressive properties of cellular lattice structures fabricated by selective laser melting. *Materials Science and Engineering: A, 628*, 188-197.

Rausch, G., & Banhart, J. (2002). Making cellular metals from metals other than aluminum. *Handbook of cellular metals. Weinheim: Wiley-VCH Verlag*, 21-28.

Ren, K., Dusad, A., Zhang, Y., & Wang, D. (2013). Therapeutic intervention for wear debris-induced aseptic implant loosening. *Acta Pharmaceutica Sinica B, 3*(2), 76-85.

Ren, X., Shao, H., Lin, T., & Zheng, H. (2016). 3D gel-printing—An additive manufacturing method for producing complex shape parts. *Materials & Design, 101*, 80-87.

Rezwan, K., Chen, Q., Blaker, J., & Boccaccini, A. R. (2006). Biodegradable and bioactive porous polymer/inorganic composite scaffolds for bone tissue engineering. *Biomaterials, 27*(18), 3413-3431.

Riza, S. H., Masood, S. H., Wen, C., Ruan, D., & Xu, S. (2014). Dynamic behaviour of high strength steel parts developed through laser assisted direct metal deposition. *Materials & Design, 64*(0), 650-659.

Rombouts, M., Kruth, J. P., Froyen, L., & Mercelis, P. (2006). Fundamentals of selective laser melting of alloyed steel powders. *CIRP Annals-Manufacturing Technology, 55*(1), 187-192.

Rosa, B., Mognol, P., & Hascoët, J. Y. (2015). Laser polishing of additive laser manufacturing surfaces. *Journal of Laser Applications, 27*(S2), S29102.

Roy, R., Agrawal, D., Cheng, J., & Gedevanishvili, S. (1999). Full sintering of powdered-metal bodies in a microwave field. *Nature, 399*(6737), 668-670.

Rumpler, M., Woesz, A., Dunlop, J. W., van Dongen, J. T., & Fratzl, P. (2008). The effect of geometry on three-dimensional tissue growth. *Journal of The Royal Society Interface, 5*(27), 1173-1180.

Ryan, G., Pandit, A., & Apatsidis, D. P. (2006). Fabrication methods of porous metals for use in orthopaedic applications. *Biomaterials, 27*(13), 2651-2670.

Saitou, K. (2006). Microwave sintering of iron, cobalt, nickel, copper and stainless steel powders. *Scripta Materialia, 54*(5), 875-879.

Salih, S., & Hamer, A. (2013). Hip and knee replacement. *Surgery (Oxford), 31*(9), 482-487.

Salmi, M., Paloheimo, K. 00dS., Tuomi, J., Wolff, J., & Mäkitie, A. (2013). Accuracy of medical models made by additive manufacturing (rapid manufacturing). *Journal of Cranio-Maxillofacial Surgery, 41*(7), 603-609.

Santorinaios, M., Brooks, W., Sutcliffe, C., & Mines, R. (2006). Crush behaviour of open cellular lattice structures manufactured using selective laser melting. *WIT Transactions on the Built Environment, 85*.

Schmidt, J., Sachs, M., Fanselow, S., Zhao, M., Romeis, S., Drummer, D., Peukert, W. (2016). Optimized polybutylene terephthalate powders for selective laser beam melting. *Chemical Engineering Science, 156*, 1-10.

Seitz, H., Rieder, W., Irsen, S., Leukers, B., & Tille, C. (2005). Three-dimensional printing of porous ceramic scaffolds for bone tissue engineering. *Journal of Biomedical Materials Research Part B: Applied Biomaterials, 74*(2), 782-788.

Shamonina, E., & Solymar, L. (2007). Metamaterials: How the subject started. *Metamaterials, 1*(1), 12-18.

Shi, L., Guo, Z., & Liu, W. (2015). The recent progress of tribological biomaterials. *Biosurface and Biotribology, 1*(2), 81-97.

Sihvola, A. (2007). Metamaterials in electromagnetics. *Metamaterials, 1*(1), 2-11.

Silva, D. N., De Oliveira, M. G., Meurer, E., Meurer, M. I., da Silva, J. V. L., & Santa-Bárbara, A. (2008). Dimensional error in selective laser sintering and 3D-printing of models for craniomaxillary anatomy reconstruction. *Journal of Cranio-Maxillofacial Surgery, 36*(8), 443-449.

Simchi, A. (2006). Direct laser sintering of metal powders: Mechanism, kinetics and microstructural features. *Materials Science and Engineering: A, 428*(1), 148-158.

Sing, S. L., An, J., Yeong, W. Y., & Wiria, F. E. (2016). Laser and electron-beam powder-bed additive manufacturing of metallic implants: A review on processes, materials and designs. *Journal of Orthopaedic Research, 34*(3), 369-385.

Singh, S., Ramakrishna, S., & Singh, R. (2017). Material issues in additive manufacturing: A review. *Journal of Manufacturing Processes, 25*, 185-200.

Song, B., Dong, S., Deng, S., Liao, H., & Coddet, C. (2014). Microstructure and tensile properties of iron parts fabricated by selective laser melting. *Optics & Laser Technology, 56*, 451-460.

Sonntag, R., Reinders, J., & Kretzer, J. (2012). What's next? Alternative materials for articulation in total joint replacement. *Acta Biomaterialia, 8*(7), 2434-2441.

Speirs, M., Van Hooreweder, B., Van Humbeeck, J., & Kruth, J. P. (2017). Fatigue behaviour of NiTi shape memory alloy scaffolds produced by SLM, a unit cell design comparison. *Journal of the Mechanical Behavior of Biomedical Materials, 70*, 53-59.

Spoerke, E. D., Murray, N. G., Li, H., Brinson, L. C., Dunand, D. C., & Stupp, S. I. (2005). A bioactive titanium foam scaffold for bone repair. *Acta Biomaterialia, 1*(5), 523-533.

Stamp, R., Fox, P., O'neill, W., Jones, E., & Sutcliffe, C. (2009). The development of a scanning strategy for the manufacture of porous biomaterials by selective laser melting. *Journal of Materials Science: Materials in Medicine, 20*(9), 1839-1848.

Stampfl, J., & Hatzenbichler, M. (2014). Additive Manufacturing Technologies *CIRP Encyclopedia of Production Engineering* (pp. 20-27): Springer.

Starodubtsev, E. G. (2010). Characteristic properties of electromagnetic wave interaction with uniaxial absorbing metamaterials: A case of the near-zero axial parameter. *Metamaterials, 4*(1), 32-43.

Stoor, P., Suomalainen, A., Lindqvist, C., Mesimäki, K., Danielsson, D., Westermark, A., & Kontio, R. K. (2014). Rapid prototyped patient specific implants for reconstruction of orbital wall defects. *Journal of Cranio-Maxillofacial Surgery, 42*(8), 1644-1649.

Street, B. D., & Gage, W. (2017). After total knee replacement younger patients demonstrate superior balance control compared to older patients when recovering from a forward fall. *Clinical Biomechanics, 44*, 59-66.

Su, X. B., Yang, Y. Q., Yu, P., & Sun, J. F. (2012). Development of porous medical implant scaffolds via laser additive manufacturing. *Transactions of Nonferrous Metals Society of China, 22, Supplement 1*, s181-s187.

Sufiiarov, V. S., Popovich, A., Borisov, E., Polozov, I., Masaylo, D., & Orlov, A. (2017). The Effect of Layer Thickness at Selective Laser Melting. *Procedia Engineering, 174*, 126-134.

Sumner, D. R. (2015). Long-term implant fixation and stress-shielding in total hip replacement. *Journal of Biomechanics, 48*(5), 797-800.

Taheri Andani, M., Dehghani, R., Karamooz-Ravari, M. R., Mirzaeifar, R., & Ni, J. (2017). Spatter formation in selective laser melting process using multi-laser technology. *Materials & Design, 131*, 460-469.

Taib, Z. A. M., Harun, W. S. W., Ghani, S. A. C., Rashid, M. F. F. A., Omar, M. A., & Ramli, H. (2016). Dimensional Accuracy Study of Open Cellular Structure CoCrMo Alloy Fabricated by Selective Laser Melting Process. *Advanced Materials Research, 1133*, 280.

Taljanovic, M. S., Jones, M. D., Ruth, J. T., Benjamin, J. B., Sheppard, J. E., & Hunter, T. B. (2003). Fracture Fixation *Radiographics, 23*(6), 1569-1590.

Tan, X. P., Tan, Y. J., Chow, C. S. L., Tor, S. B., & Yeong, W. Y. (2017). Metallic powder-bed based 3D printing of cellular scaffolds for orthopaedic implants: A state-of-the-art review on manufacturing, topological design, mechanical properties and biocompatibility. *Materials Science and Engineering: C, 76*, 1328-1343.

Tang, H. P., Wang, J., & Qian, M. (2015). 28 - Porous titanium structures and applications. In M. Q. H. Froes (Ed.), *Titanium Powder Metallurgy* (pp. 533-554). Boston: Butterworth-Heinemann.

Taniguchi, N., Fujibayashi, S., Takemoto, M., Sasaki, K., Otsuki, B., Nakamura, T.,. Matsuda, S. (2016). Effect of pore size on bone ingrowth into porous titanium implants fabricated by additive manufacturing: An in vivo experiment. *Materials Science and Engineering: C, 59*, 690-701.

Ten Broeke, R. H. M., Tarala, M., Arts, J. J., Janssen, D. W., Verdonschot, N., & Geesink, R. G. T. (2014). Improving peri-prosthetic bone adaptation around cementless hip stems: A clinical and finite element study. *Medical Engineering & Physics, 36*(3), 345-353.

Thijs, L., Verhaeghe, F., Craeghs, T., Van Humbeeck, J., & Kruth, J.-P. (2010). A study of the microstructural evolution during selective laser melting of Ti–6Al–4V. *Acta Materialia, 58*(9), 3303-3312.

Tigani, D., Fosco, M., Ben Ayad, R., & Fantasia, R. (2013). 6 - Orthopaedic implant materials and design. In S. Affatato (Ed.), *Wear of Orthopaedic Implants and Artificial Joints* (pp. 133-177): Woodhead Publishing.

Torres, Y., Pavón, J., & Rodríguez, J. (2012). Processing and characterization of porous titanium for implants by using NaCl as space holder. *Journal of Materials Processing Technology, 212*(5), 1061-1069.

Vaezi, M., Seitz, H., & Yang, S. (2013). A review on 3D micro-additive manufacturing technologies. *The International Journal of Advanced Manufacturing Technology, 67*(5-8), 1721-1754.

Van Bael, S., Chai, Y. C., Truscello, S., Moesen, M., Kerckhofs, G., Van Oosterwyck, H., . . . Schrooten, J. (2012). The effect of pore geometry on the in vitro biological behavior of human periosteum-derived cells seeded on selective laser-melted Ti6Al4V bone scaffolds. *Acta Biomaterialia, 8*(7), 2824-2834.

Van Bael, S., Kerckhofs, G., Moesen, M., Pyka, G., Schrooten, J., & Kruth, J. P. (2011). Micro-CT-based improvement of geometrical and mechanical controllability of selective laser melted Ti6Al4V porous structures. *Materials Science and Engineering: A, 528*(24), 7423-7431.

Van der Stok, J., Van der Jagt, O. P., Amin Yavari, S., De Haas, M. F., Waarsing, J. H., Jahr, H., Zadpoor, A. A. (2013). Selective laser melting-produced porous titanium scaffolds regenerate bone in critical size cortical bone defects. *Journal of Orthopaedic Research, 31*(5), 792-799.

Van Hooreweder, B., Apers, Y., Lietaert, K., & Kruth, J.-P. (2017). Improving the fatigue performance of porous metallic biomaterials produced by Selective Laser Melting. *Acta Biomaterialia, 47*, 193-202.

Vollmer, N., & Ayers, R. (2012). Decomposition combustion synthesis of calcium phosphate powders for bone tissue engineering. *International Journal of Self-Propagating High-Temperature Synthesis, 21*(4), 189-201.

Wang, K., Wu, C., Qian, Z., Zhang, C., Wang, B., & Vannan, M. A. (2016). Dual-material 3D printed metamaterials with tunable mechanical properties for patient-specific tissue-mimicking phantoms. *Additive Manufacturing, 12, Part A*, 31-37.

Wang, Y., Yan, Y., Su, Y., & Qiao, L. (2017). Release of metal ions from nano CoCrMo wear debris generated from tribo-corrosion processes in artificial hip implants. *Journal of the Mechanical Behavior of Biomedical Materials, 68*, 124-133.

Warnke, P. H., Douglas, T., Wollny, P., Sherry, E., Steiner, M., Galonska, S., Sivananthan, S. (2008). Rapid prototyping: porous titanium alloy scaffolds produced by selective laser melting for bone tissue engineering. *Tissue engineering part c: Methods, 15*(2), 115-124.

Watari, F., Kondo, H., Miyao, R., Omori, M., Okubo, A., Hirai, T., Kawasaki, T. (2002). Effect of Spark Plasma Sintering Pressure on the Properties of Functionally Graded Implant and its Biocompatibility. *Journal of the Japan Society of Powder and Powder Metallurgy, 49*(12), 1063-1069.

Wauthle, R., van der Stok, J., Amin Yavari, S., Van Humbeeck, J., Kruth, J.-P., Zadpoor, A. A., & Weinans, H. (2015). Additively manufactured porous tantalum implants. *Acta Biomaterialia, 14*, 217-225.

Weber, J. N., & White, E. W. (1972). Carbon-metal graded composites for permanent osseous attachment of non-porous metals. *Materials Research Bulletin, 7*(9), 1005-1016.

Wehmöller, M., Warnke, P., Zilian, C., & Eufinger, H. (2005). *Implant design and production—a new approach by selective laser melting.* Paper presented at the International Congress Series.

Weißmann, V., Bader, R., Hansmann, H., & Laufer, N. (2016). Influence of the structural orientation on the mechanical properties of selective laser melted Ti6Al4V open-porous scaffolds. *Materials & Design, 95*, 188-197.

Weller, C., Kleer, R., & Piller, F. T. (2015). Economic implications of 3D printing: Market structure models in light of additive manufacturing revisited. *International Journal of Production Economics, 164*, 43-56.

Wits, W. W., Bruins, R., Terpstra, L., Huls, R. A., & Geijselaers, H. (2016). Single scan vector prediction in selective laser melting. *Additive Manufacturing, 9*, 1-6.

Xia, M., Gu, D., Yu, G., Dai, D., Chen, H., & Shi, Q. (2016). Influence of hatch spacing on heat and mass transfer, thermodynamics and laser processability during additive manufacturing of Inconel 718 alloy. *International Journal of Machine Tools and Manufacture, 109*, 147-157.

Xia, X., Yang, H., Wang, Z., Li, Y., Cui, Z., Chen, Y., & Gu, C. (2007). Fabrication of near-infrared and optical meta-materials on insulating substrates by lift-off using PMMA/Al stack. *Microelectronic Engineering, 84*(5–8), 1144-1147.

Xiao, L., Song, W., Wang, C., Tang, H., Fan, Q., Liu, N., & Wang, J. (2017). Mechanical properties of open-cell rhombic dodecahedron titanium alloy lattice structure

manufactured using electron beam melting under dynamic loading. *International Journal of Impact Engineering, 100*, 75-89.

Yadroitsev, I., Gusarov, A., Yadroitsava, I., & Smurov, I. (2010). Single track formation in selective laser melting of metal powders. *Journal of Materials Processing Technology, 210*(12), 1624-1631.

Yamako, G., Chosa, E., Totoribe, K., Hanada, S., Masahashi, N., Yamada, N., & Itoi, E. (2014). In-vitro biomechanical evaluation of stress shielding and initial stability of a low-modulus hip stem made of β type Ti-33.6Nb-4Sn alloy. *Medical Engineering & Physics, 36*(12), 1665-1671.

Yan, C., Hao, L., Hussein, A., & Raymont, D. (2012). Evaluations of cellular lattice structures manufactured using selective laser melting. *International Journal of Machine Tools and Manufacture, 62*, 32-38.

Yan, C., Hao, L., Hussein, A., Young, P., Huang, J., & Zhu, W. (2015). Microstructure and mechanical properties of aluminium alloy cellular lattice structures manufactured by direct metal laser sintering. *Materials Science and Engineering: A, 628*, 238-246.

Yan, C., Hao, L., Hussein, A., Young, P., & Raymont, D. (2014). Advanced lightweight 316L stainless steel cellular lattice structures fabricated via selective laser melting. *Materials & Design, 55*, 533-541.

Yánez, A., Herrera, A., Martel, O., Monopoli, D., & Afonso, H. (2016). Compressive behaviour of gyroid lattice structures for human cancellous bone implant applications. *Materials Science and Engineering: C, 68*, 445-448.

Ye, X. X., Yang, Y. Y., & Tang, G. Y. (2014). Microhardness and corrosion behavior of surface gradient oxide coating on the titanium alloy strips under high energy electro-pulsing treatment. *Surface and Coatings Technology, 258*, 467-484.

Zadpoor, A. A. (2017). Mechanics of additively manufactured biomaterials. *Journal of the Mechanical Behavior of Biomedical Materials, 70*, 1-6.

Zhang, S., Wei, Q., Cheng, L., Li, S., & Shi, Y. (2014). Effects of scan line spacing on pore characteristics and mechanical properties of porous Ti6Al4V implants fabricated by selective laser melting. *Materials & Design, 63*, 185-193.

Zhang, X., Ayers, R., Thorne, K., Moore, J., & Schowengerdt, F. (2000). Combustion synthesis of porous materials for bone replacement. *Biomedical sciences instrumentation, 37*, 463-468.

Zhou, X., Liu, X., Zhang, D., Shen, Z., & Liu, W. (2015). Balling phenomena in selective laser melted tungsten. *Journal of Materials Processing Technology, 222*, 33-42.

APPENDIX A
PAPER PUBLICATIONS

PAPER PUBLICATION

[1] Malek, N.A., Mohamed, S.R., Ghani, S.C., & Harun, W.W. (2015). Critical evaluation on structural stiffness of porous cellular structure of cobalt chromium alloy. *IOP Conference Series: Materials Science and Engineering, 100 (1)*, p. 012019.

[2] Zakaria M.F., Che Ghani S.A., Wan Harun W.S., Zaulkafilai Z., Mohamed S.R. (2017). Fabrication of Aluminium Internally Cooled Cutting Tool by Means of Selective Laser Melting (SLM). *Journal of Mechanical Engineering, 3 (1)*, 187-200.

CONFERENCE PROCEEDING

[1] Siti Rohaida Mohamed, Saiful Anwar Che Ghani, Wan Sharuzi Wan Harun, Nor Aida Zuraimi Md Noar, Evaluations of Co-Cr-Mo Metabiomaterials Manufactured by Selective Laser Melting for Orthopaedic Application. Symposium & Exhibition on Additive Manufacturing (SEAM2016)

[2] Siti Rohaida Mohamed, Saiful Anwar Che Ghani, Wan Sharuzi Wan Harun, Nor Aida Zuraimi Md Noar , Evaluations of Geometrical Accuracy, Density, Top Surface and Side Roughness of Co-Cr-Mo Parts Processed using Different Additive Manufacturing Techniques. Advanced Materials Conference (AMC2016)

APPENDIX B1
ADDITIONAL TABLE AND FIGURES OF METHODOLOGY

Instruments	Description
SLM125HL	To fabricate metabiomaterials
Dino-lite optical microscope	To evaluate morphology, to measure dimension and metabiomaterials geometries
Vacuum furnace	To stress relieved by heat treatment
Shimadzu AutoGraph AG-X100kN	To perform compression test
Density apparatus	To measure the density of metabiomaterials
Incubator	To incubate the cell culture
Tabletop Hitachi Scanning Electron Microscope	To scan the image with higher magnification
ELISA plate reader	To measure the absorbance of MTT solution

APPENDIX B2
METABIOMATERIALS CAD MODELS

Square		Diamond	
SL15T04	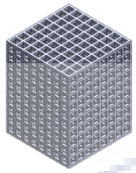	DL15T04	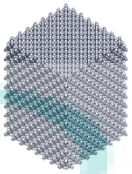
SL15T06	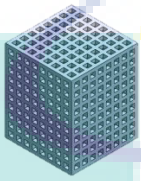	DL15T06	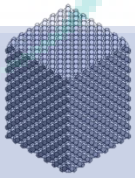
SL20T05	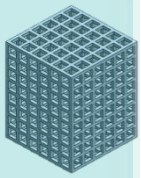	DL20T05	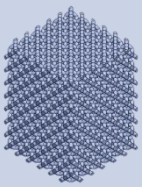
SL25T04	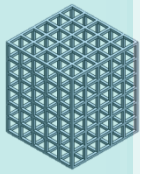	DL25T04	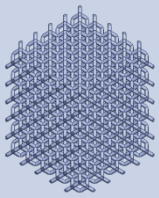
SL25T06	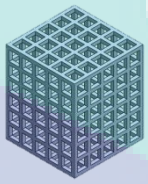	DL25T06	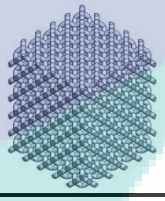
			5mm

APPENDIX B3
DETAILS OF METABIOMATERIAL FOR UNIAXIAL COMPRESSION TEST

Sample	Original length (mm)	Area (mm^2)	Expected results
SL15T04	15.296	158.0464	
SL15T06	15.430	162.4767	
SL20T05	16.536	115.7093	
SL25T04	15.593	176.0973	Elastic modulus Compression strength
SL25T06	15.593	176.9793	
DL15T04	14.993	146.7653	
DL15T06	14.893	145.2973	
DL20T05	15.910	147.7267	
DL25T04	14.936	158.7755	
DL25T06	15.013	158.6467	

APPENDIX B4
FIGURES OF CELL CULTURE METHODOLOGY

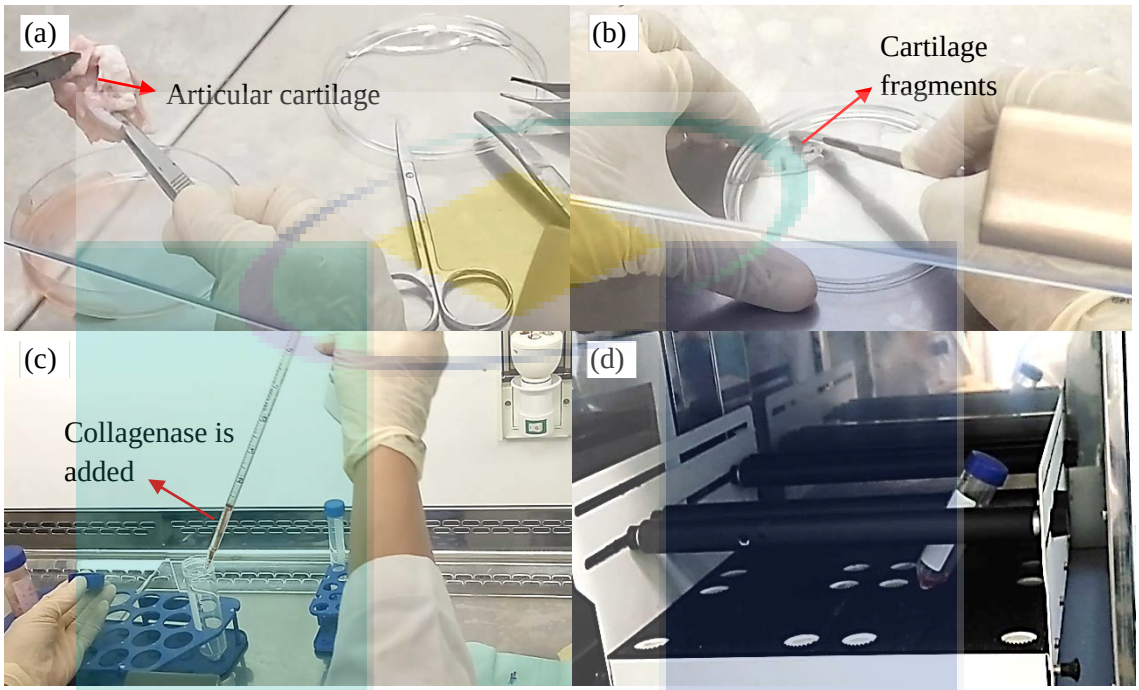

(a) Articular cartilage from an adult rabbit was dissected and washed with PBS solution, (b) Harvested cartilage was minced into small fragments, (c) 2 ml collagenase was added to digest the cartilage and (d) Condrocyte isolation was taken in orbital incubator for 4 hours

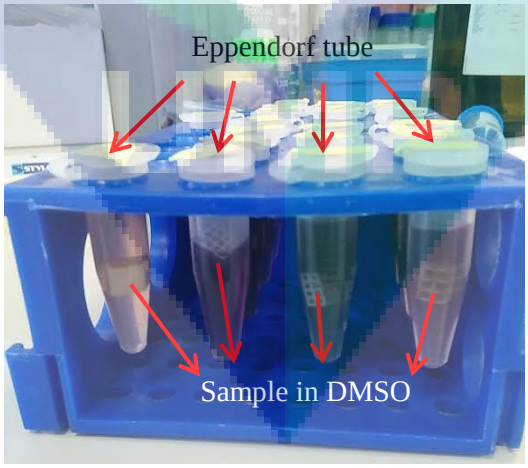

Samples were placed in Eppendorf tube for solubilisation

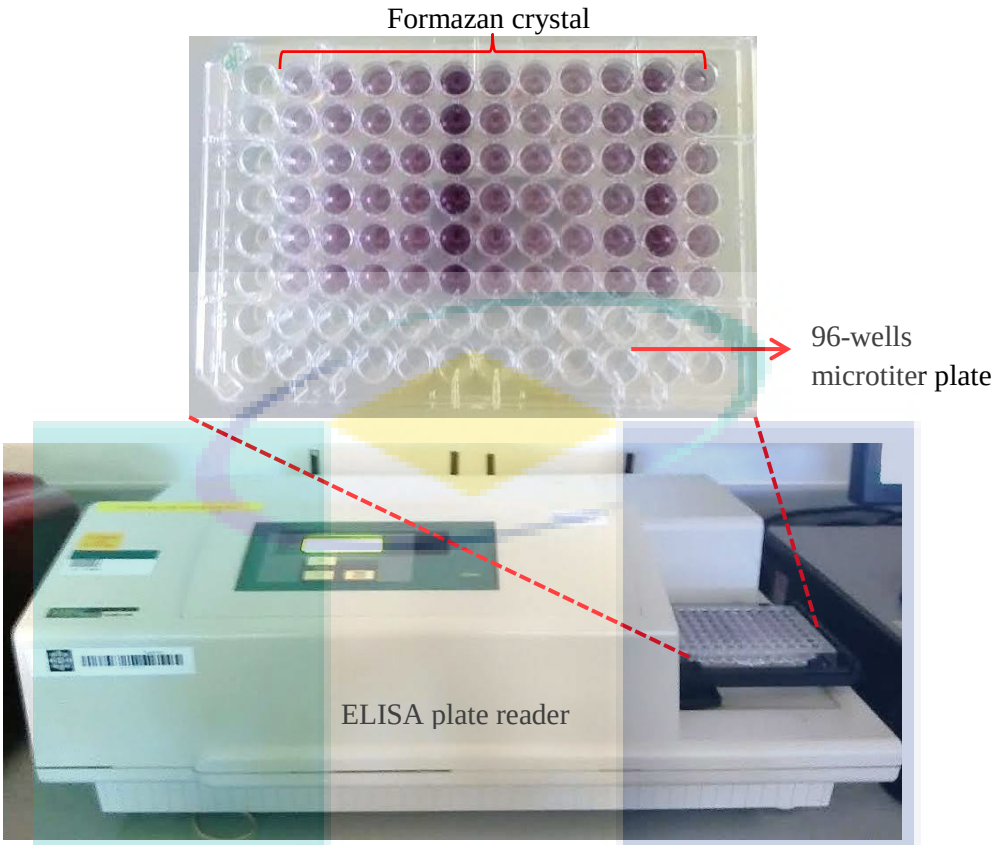

Absorption intensity of formazon MTT reductions was read spectrophotometry using ELISA plate reader at the 570 nm

APPENDIX C
METABIOMATERIALS CATALOGUE

Type	Unit cell length, L_{cell} (mm)	Strut size, Φ_S (mm)	Porosity (%)	Density (g/mm^3)	Relative density (%)	Elastic modulus (GPa)	0.2 % yield strength (MPa)	Ultimate compressive strength (MPa)	Compression strength (MPa)	MTT absorbance Gamma ray	MTT absorbance Autoclave
Square	1.5	0.4	79.8	8.09	97.58	4.467	47.676	79.017	59.696	0.23	0.26
Square	1.5	0.6	60.9	7.67	92.49	8.749	154.932	276.542	245.030	0.22	0.20
Square	2.0	0.5	81.2	7.92	95.52	2.914	54.304	64.570	46.673	0.27	0.10
Square	2.5	0.4	91.0	7.75	93.48	0.919	12.076	14.229	11.805	0.66	0.73
Square	2.5	0.6	81.7	7.99	96.37	2.100	46.877	52.257	41.104	0.28	0.26
Diamond	1.5	0.4	70.7	7.02	84.68	2.826	73.853	85.158	62.929	0.17	0.22
Diamond	1.5	0.6	44.8	7.69	92.71	7.473	247.675	302.775	240.078	0.15	0.25
Diamond	2.0	0.5	73.8	7.40	89.29	2.289	54.457	63.211	44.591	0.22	0.20
Diamond	2.5	0.4	88.1	8.07	97.29	0.445	11.397	16.864	10.766	0.45	0.37
Diamond	2.5	0.6	75.6	7.67	92.57	1.926	44.534	55.133	40.042	0.21	0.15
Full dense	-	-	-	8.23	99.30	224.63	NA	NA	NA	0.21	0.15

Type	Design L_{cell} (mm)	Measured L_{cell} (mm)	Error (%)	Design Φ_S (mm)	Measured Φ_S (mm)	Error (%)	Design pore (mm)	Measured pore (mm)	Error (%)
Square	1.5	1.519	1.23	0.4	0.407	1.82	1.1	1.111	1.02
Square	1.5	1.448	3.46	0.6	0.6165	2.75	0.9	0.8316	7.60
Square	2.0	2.009	0.47	0.5	0.5106	2.10	1.5	0.8316	0.07
Square	2.5	2.513	0.52	0.4	0.406	1.40	12.076	14.229	11.805
Square	2.5	2.533	1.30	0.6	0.6113	1.88	46.877	52.257	41.104
Diamond	1.5	0.515	0.98	0.4	0.405	1.12	0.8	0.749	6.36
Diamond	1.5	1.513	0.87	0.6	0.605	0.78	0.6	0.538	10.27
Diamond	2.0	2.076	3.78	0.5	0.501	0.12	1.1	1.017	7.54
Diamond	2.5	2.519	0.75	0.4	0.405	1.15	1.5	1.438	4.15
Diamond	2.5	2.538	1.51	0.6	0.604	0.60	1.2	1.249	4.06